İZMİR KÂTİP ÇELEBİ ÜNİVERSİTESİ
2010
GRADUATE SCHOOL OF NATURAL AND APPLIED SCIENCES

Manufacturing and Characterization of Peptide Coated Polylactic Acid Based Composites for Various Medical Applications

Doctor of Philosophy in Department of Material Science and Engineering

by

Metehan ATAGÜR

ORCID 0000-0002-1916-457X

December, 2022

This is to certify that we have read the thesis **Manufacturing and characterization of peptide coated polylactic acid based composites for various medical applications** submitted by **Metehan ATAGÜR**, and it has been judged to be successful, in scope and in quality, at the defense exam and accepted by our jury as a DOCTORAL THESIS.

APPROVED BY:

Advisor: **Prof. Dr. Mehmet Özgür SEYDİBEYOĞLU**
İzmir Kâtip Çelebi University

Committee Members:

Prof. Dr. Mücahit SÜTÇÜ
İzmir Kâtip Çelebi University

Assoc. Prof. Dr. Ozan KARAMAN
İzmir Kâtip Çelebi University

Prof. Dr. Ümit Halis ERDOĞAN
Dokuz Eylül University

Assoc. Prof. Dr. Mehmet SARIKANAT
EGE University

Date of Defense: December 29, 2022

Declaration of Authorship

I, **Metehan ATAGÜR**, declare that this thesis titled **Manufacturing and characterization of peptide coated polylactic acid based composites for various medical applications** and the work presented in it are my own. I confirm that:

- This work was done wholly or mainly while in candidature for the Master's degree at this university.
- Where any part of this thesis has previously been submitted for a degree or any other qualification at this university or any other institution, this has been clearly stated.
- Where I have consulted the published work of others, this is always clearly attributed.
- Where I have quoted from the work of others, the source is always given. This thesis is entirely my own work, with the exception of such quotations.
- I have acknowledged all major sources of assistance.
- Where the thesis is based on work done by myself jointly with others, I have made clear exactly what was done by others and what I have contributed myself.

Date: 29.12.2022

Manufacturing and characterization of peptide coated Polylactic acid based composites for various medical applications

Abstract

Within the scope of this thesis, PLA-based composites have been developed and coated with peptide to increase biocompatibility for temporary implant applications and PLA biocomposite materials have been produced. HA and β-TCP were used as additive materials, and PLLA and PDLA polymers were used as polymer matrix. The main purpose is to obtain the composite with the best mechanical properties and to improve the biocompatibility properties as a result of coating this final material with peptide. In the first stage, 10% HA (PLA-10 HA), 10% β-TCP (PLA-10TCP) and 5% HA + 5% β-TCP (PLA-5TCP-5HA) are added into the PLLA matrix material and the composite materials are mechanical, thermal and thermal, crystallographic, morphological and toxicological properties were investigated. As a result of the mechanical analysis, the highest value was obtained in PLA-10HA, and similar results were obtained with the mechanical properties of the PLA-5TCP-5HA hybrid composite. In the results of the cytotoxicity test, the viability was obtained in the PLA-

5TCP-5HA hybrid composite with an increase of approximately 60% compared to the extruded undoped polymer. 5% HA + 5% β-TCP was chosen as the additive ratio, since it has mechanically similar properties to PLA-10HA and shows the highest increase in viability. In the second stage, PLLA/PDLA blends containing varying proportions of PDLA were produced in order to further improve the mechanical properties. In the mechanical analysis results, it was seen that the blend (2.5PDLA) containing 2.5% PDLA had the best properties. 2.5PDLA increased the tensile strength of pure PLLA by about 5%. Addition of 5TCP-5HA decreased the T_c, T_{m1} and T_{m2} values by 2 to 5 °C. Highest tensile strength was obtained at 2.5PDLA-5HA-5TCP. An approximately 27% increase in tensile strength of PLLA was obtained with the final composition, 2.5PDLA-5HA-5TCP. PLLA-based composite material functionalized with EEEEEE peptide possessed more potential on triggering osteogenesis of hMSCs.

Keywords: PLLA, PDLA, HA, β-TCP, Tensile Strength, Peptides, biocompatibility

Çeşitli Medikal Uygulamalara Yönelik Peptit Kaplı Polilaktik Asit Tabanlı Kompozitlerin Üretimi ve Karakterizasyonu

Öz

Bu tez kapsamında PLA bazlı kompozitler geliştirilip peptit ile kaplanarak geçici implant uygulamalarına yönelik biyouyumluluğu arttırılmış ve PLA biyokompozit malzemeler üretilmiştir. Katkı malzemesi olarak HA ve β-TCP, polimer matris olarak ise PLLA ve PDLA polimerleri kullanılmıştır. Ana amaç en iyi mekanik özelliklere sahip kompozitin elde edilmesi ve bu nihai malzemenin peptit ile kaplanması sonucunda biyouyumluluk özelliklerinin geliştirilmesidir. İlk aşamada PLLA matris malzemesi içerisine %10 HA (PLA-10 HA), %10 β-TCP (PLA-10TCP) ve %5 HA+%5 β-TCP (PLA-5TCP-5HA) eklenerek elde edilen kompozit malzemelerin mekanik, termal, kristalografik, morfolojik ve toksikolojik özellikleri incelenmiştir. Mekanik analizler sonucunda en yüksek değer PLA-10HA'da elde edilmiş, PLA-5TCP-5HA hibrit kompozitinin mekanik özellikleri ile benzer seviyede sonuçlar elde edilmiştir. Sitotoksisite testi sonuçlarında ise canlılık ekstrüde edilmiş katkısız polimere kıyasla yaklaşık %60 artış ile PLA-5TCP-5HA hibrit kompozitinde elde edilmiştir. Mekanik açıdan PLA-10HA ile benzer özelliklere sahip olduğundan ve canlılıkta en yüksek artışı göstermesinden dolayı katkı oranı olarak %5 HA+%5 β-TCP seçilmiştir. İkinci aşamada mekanik özellikleri de daha da geliştirmek amacıyla değişen oranlarda PDLA içeren PLLA/PDLA blendlerinin üretimleri

gerçekleştirilmiştir. Mekanik analiz sonuçlarında %2,5 PDLA içeren blend (2.5PDLA) oranının en iyi özelliklere sahip olduğu görülmüştür. 2.5PDLA saf PLLA'nın çekme mukavemetini yaklaşık %5 oranında artırmıştır. 5TCP-5HA eklenmesi T_c, T_{m1} ve T_{m2} değerlerini 2 ila 5 ^oC azaltmıştır. En yüksek çekme mukavemeti 2.5PDLA-5HA-5TCP'de elde edilmiştir. Nihai bileşim olan 2.5PDLA-5HA-5TCP ile PLLA'nın çekme mukavemetinde yaklaşık %27'lik bir artış elde edilmiştir. EEEEEE peptidi ile işlevselleştirilmiş PLLA bazlı kompozit malzeme, hMSC'lerin osteogenezini tetikleme konusunda daha fazla potansiyele sahiptir.

Anahtar Kelimeler: PLLA, PDLA, HA, B-TCP, Çekme Mukavemeti, Peptit, Biyouyumluluk

Acknowledgment

First and foremost, I would like to express my sincere gratitude to my supervisor Prof. Dr. M. Özgür SEYDİBEYOĞLU for his support, immense knowledge, encouragement, invaluable guidance and patience throughout this thesis. Also, I would like to thank the members of my thesis supervising committee, Prof. Dr. Mücahit SÜTÇÜ and Assoc. Prof. Dr. Ozan KARAMAN for their encouragement, technical support and comments. And also, I would like to thank you Prof. Dr.Ümit Halis ERDOĞAN and Assoc. Prof. Dr. Mehmet SARIKANAT for their participation in my PhD thesis defense.

I would like to thank Bonegraft Biological Materials Industry and Trade Inc. for their financial and moral support throughout my thesis. I would like to thank Res. Assist. Dr. Günnur PULAT and Gülşah UYSAL for their great help both theoretically and practically in the medical part of my thesis.

Last but not the least; I am especially grateful to my dear wife Tuğçe Büşra ATAGÜR for his support and motivation. I am also thankful to my father Mehmet ATAGÜR and my mother Makbule ATAGÜR and my sister Özge YILMAZ for their support.

Table of Contents

List of Figures

List of Tables

List of Abbreviations

PLA	Polylactic acid
PLLA	Poly (L-lactic acid)
PDLA	Poly (D-lactic acid)
HA	Hydroxyapatite
β-TCP	Beta tricalcium phosphate
Ca $(NO_3)_2.4H_2O$	Calcium nitrate tetrahydrate
$(NH_4)2HPO_4$	Ammonium phosphate dibasic
HNO_3	Nitric acid solution
SEM	Scanning electron microscopy
XRD	X-ray diffraction
TGA	Thermal gravimetry analysis
DSC	Differential Scanning Calorimetry
FTIR-ATR	Fourier Transform Infrared - Attenuated Total Reflectance
ICP-MS	Inductively Coupled Plasma Mass Spectrometry
DMA	Dynamic Mechanical Analysis
CA	Contact Angle
JCPDS	Joint Committee on Powder Diffraction Standards
MPa	Megapascal
ASTM	American Society for Testing and Materials

List of Symbols

℃	Celcius degree
μ	Micro
β	Beta Phase
%	Percent
θ	Theta
ρ	Density
kN	Kilonewton

Chapter 1

1 Introduction

The use of biomaterials may be traced back to ancient cultures. As a consequence of the examinations, prosthetic eyes, ears, and teeth were discovered in Egyptian mummies, while wax and glue were employed to fix missing or injured body parts in China and India. For millennia, the rise in biological applications has resulted in an increase in biomaterials utilization [1,2]. Today's medical practice makes extensive use of implants. Implantable biomaterials (ligaments, vascular grafts, heart valves, intraocular lenses, dental implants, etc.) are frequently utilized to replace and/or restore the function of injured or degraded tissues or organs, therefore improving patients' quality of life [3]. As biomaterials, a wide range of materials, including all traditional materials such as metals, ceramics, and polymers, have been investigated [3].

1.1 Metallic Materials

Metals have almost entirely been utilized for load-bearing implants such as hip and knee prostheses and fracture fixation wires, pins, screws, and plates. Although pure metals are used on occasion, alloys usually increase material qualities such as strength and corrosion resistance. Stainless steel, cobalt-chromium-molybdenum alloys, and titanium and titanium alloys are the most common biomedical metals.

Metals and alloys for biomedical applications are chosen for their good electrical and thermal conductivity, biocompatibility, acceptable mechanical qualities, corrosion resistance, and low cost. It is critical to understand the physical and chemical characteristics of the many metallic materials utilized in surgery, as well as their interactions with human body host tissue. Application of metal implants are shown in Table 1.1 and Figure 1.1.

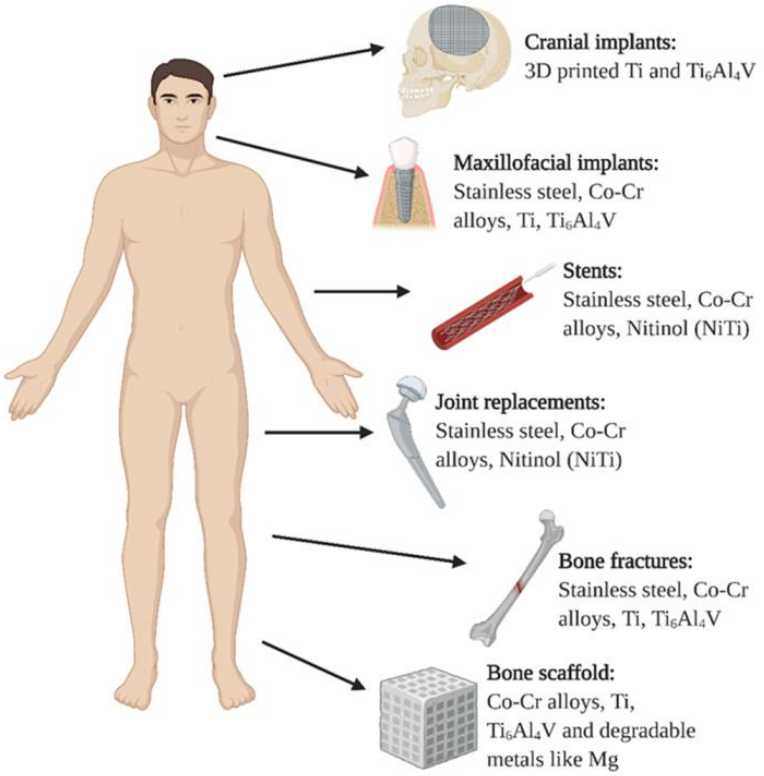

Figure 1.1: Types of metal implants used in the human body [4].

Table 1.1: Application of Metals as Implants Used in Human Body [3].

Types of Materials	Applications
Stainless steel	Replacement of joints, a bone plate for fracture repair, Dental implants, heart valves, spinal instruments, surgical instruments, screws, and shoulder prostheses are all examples of medical devices.
Cobalt-chromium alloy	Screws, dental root implant, pacer, and suture for fracture repair, dentistry, orthopedic prosthetic Bone and joint replacements, as well as mini plates
Titanium and its Alloys	Cochlear implants, bone and joint replacements, dental implants, screws, sutures, orthodontic surgery components, bone fixation devices, screws and plates, artificial heart valves and surgical equipment, cardiac pacemakers

1.2 Ceramic Materials

Ceramics are polycrystalline materials. Ceramic materials are distinguished by their hardness and brittleness, high strength and stiffness, resistance to corrosion and wear, and low density. They function well with compression pressures and perform poorly with tension forces. Ceramics are commonly used as electrical and thermal insulators. Ceramics are employed in a variety of applications, including dentistry, orthopedics, and medical sensors [5]. Overall, however, these biomaterials have been employed less widely than either metals or polymers. Ceramics fail with little to no plastic

deformation and are susceptible to the existence of fractures or other flaws. Application of ceramic implants are shown in

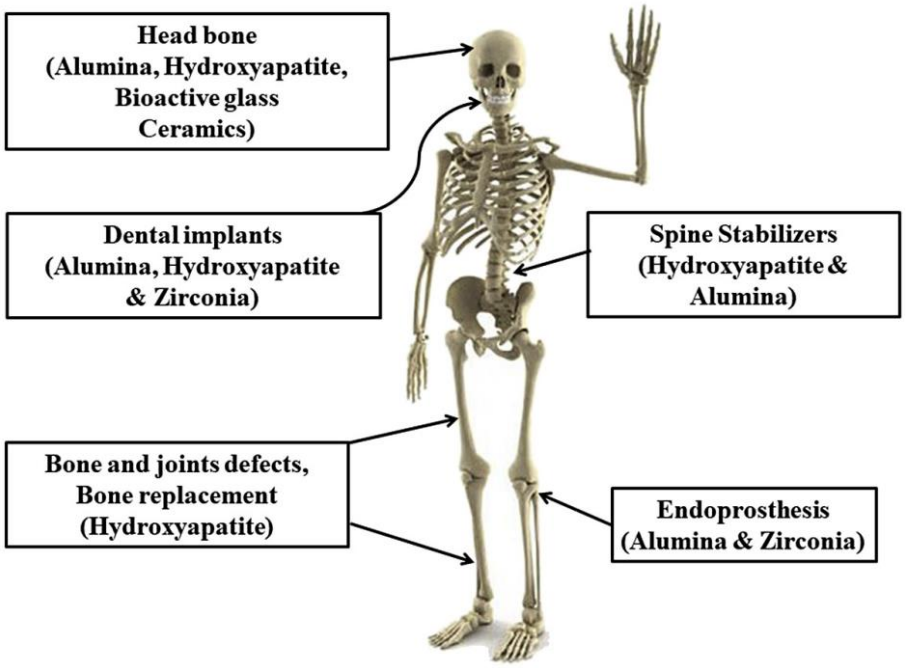

Figure 1.2: Application of ceramics as ımplants used in human body[6].

Table 1.2 and Figure 1.2.

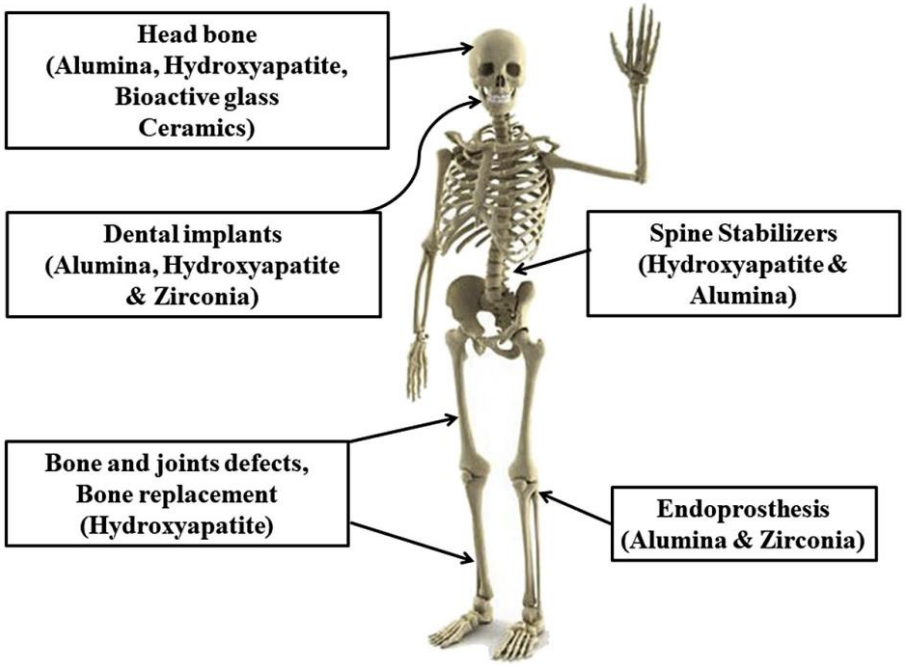

Figure 1.2: Application of ceramics as ımplants used in human body[6].

Table 1.2: Application of Ceramics as Implants Used in Human Body [3].

Types of Materials	**Applications**

Alumina	Orthodontic anchors, Artificial total joint replacement, vertebral spacers and extensors, acetabular and femoral components, and dental implants for tooth fixation are all examples of artificial complete joint replacement.
Zirconia	Replacement of tendons, and ligaments, hips, teeth, knees, periodontal disease treatment, and bone fillers following tumor surgery
Pyrolytic carbon	Artificial heart valves, end osseous dental implant implants, and prosthetic limbs that are permanently installed
Bioglass-ceramics	Prosthetics, soft tissue implants, pericardium, artificial complete hip replacement, plates and screws, wires, intra - medullary nails, lumbar fusion, and dental implant implants are all examples of surgical procedures.
Calcium phosphates	Skin care, dentistry implantation, jawbone replacement, orthopedics, face surgery, and ear, nose, and throat repair are all available.

1.3 Polymeric Materials

The evolution of polymeric biomaterials may be regarded as a process of evolution. Natural polymers have been used as biomaterials for thousands of years, according to reports [7]. Polymers are the most common materials utilized in biomedical applications. Polymers are biological molecules that create long chains of repeating units. Polymeric materials have a wider range of applications than metallic implants, although their interchangeability is limited. Polymers have almost no opposition from other kinds of materials in the majority of applications. Their distinguishing characteristics are as follows:

- Good flexibility and processibility,
- Chemical resistance,
- Biocompatibility,
- Lightweight,
- Formulations with sufficient physical and mechanical qualities are available in a wide range of compositions.

For biomedical composite production, there are many fillers and reinforcement materials used with polymeric matrix in the literature. Table 1.3 summarizes generally the materials used in the studies [3].

Table 1.3: Fillers, fibers and polymer matrix studied generally in the literature [3].

Filler	Fiber	Polymer
Inorganic	***Polymers***	***Thermosets***
Glass	Aromatic Polyamides	Epoxy
Alumina	UHMWPE	Polyacrylates
Organic	Polyesters	Polymethacrylates
Polyacrylate	Polyolefins	Polyesters
Polymethacrylate	PTFE	Silicones
	Resorbable polymers	***Thermoplastics***
	Polylactide, and its copolymers with polyglyocolide	Polyolefins (PP, PE)
	Silk	UHMWPE
	Collagen	Polysulfones
		Poly (ether ketones)
	Inorganic	Polyesters
	Carbon	***Inorganic***
	Glass	Hydroxyapatite
	Hydroxyapatite	Glass ceramics
	Tricalcium phosphate	Calcium carbonate ceramics
		Calcium phosphate ceramics
		Carbon Steel
		Titanium
		Resorbable polymers
		Polylactide, polyglycolide, and their copolymers
		Polydioxanone

Polymeric materials have highly configurable mechanical characteristics that fall somewhere in the middle among biological polymeric materials and metal [8]. In the production of scaffolds for tissue engineering (primarily bone, skin, and cartilage; arteries; and ligaments), they have significant benefits over natural polymers:

(1) They can be manufactured on a large scale, at a low cost, and in a repeatable way;

(2) They are simple to process;

(3) They contain no immunological risk;

(4) Their characteristics and degradation rates can be easily modified for the particular application.

The main disadvantages of synthetic bioresorbable polymers are;

(1) they are much less biocompatible than biopolymers,

(2) They often lack cell recognition sites.

(3) Many of their breakdown products are not natural compounds and may create difficulties if accumulated.

Aliphatic polyesters or polymers are an important type of synthetic bioresorbable polymers (a-hydroxy acids). Poly(a-hydroxy acids) such as PGA, poly(lactic acid) (PLA) stereoisomers poly(L-lactic acid) (PLLA) and poly(D-lactic acid), and poly(lactic-co-glycolic acid) (PLGA) copolymers are the most widely used and popular bioresorbable polymers since they were approved for clinical use in humans in various forms by the Food and Drug Administration (FDA) (eg, fibers for sutures, injectable forms) [9] Table 1.4 shows some biomedical studies made by using several synthetic bioresorbable polymers. Polymeric and copolymeric synthetic bioresorbable polymers are available in a variety of molecular weights and compositional ratios. Furthermore, these polyesters are particularly adaptable in processing, resulting in fibers, sponges, and bulk devices. There are other commercial products based on trimethylene carbonate and polydioxanone copolymers.

Table 1.4: Biomedical studies made by using several synthetic bioresorbable polymers.

Biomedical Application	Synthetic bioresorbable polymer type	References
X-Repair high tensile strength surgical mesh	PLLA (sutured over degenerative tissues as a reinforcement)	[10]
Porous scaffolds (cardiac TE)	Random copolymers of lactic acid and trimethylene carbonate (PLA-co-TMC)	[11]
Suture materials	Other copolymers of polycarbonates (with glycolides and other cyclic lactones)	[12]
Bone fixation devices	Other copolymers of polycarbonates (with glycolides and other cyclic lactones)	[12]
Electrospun meniscus scaffolds	polylactic acid (PLA)	[13]
Electrospun meniscus scaffolds	PCL	[14]

Orthopedic (bulk) devices made of biodegradable synthetic polymers have thus found widespread use in anatomical settings requiring lower strength, such as the ankle, knee, and hand; as interference screws, tacks, and pins for ligament attachment and meniscal repair; suture anchors; and rods and pins for fracture fixation [8]. Various resorbable polymeric implants used in the human body were shown in Figure 1.3.

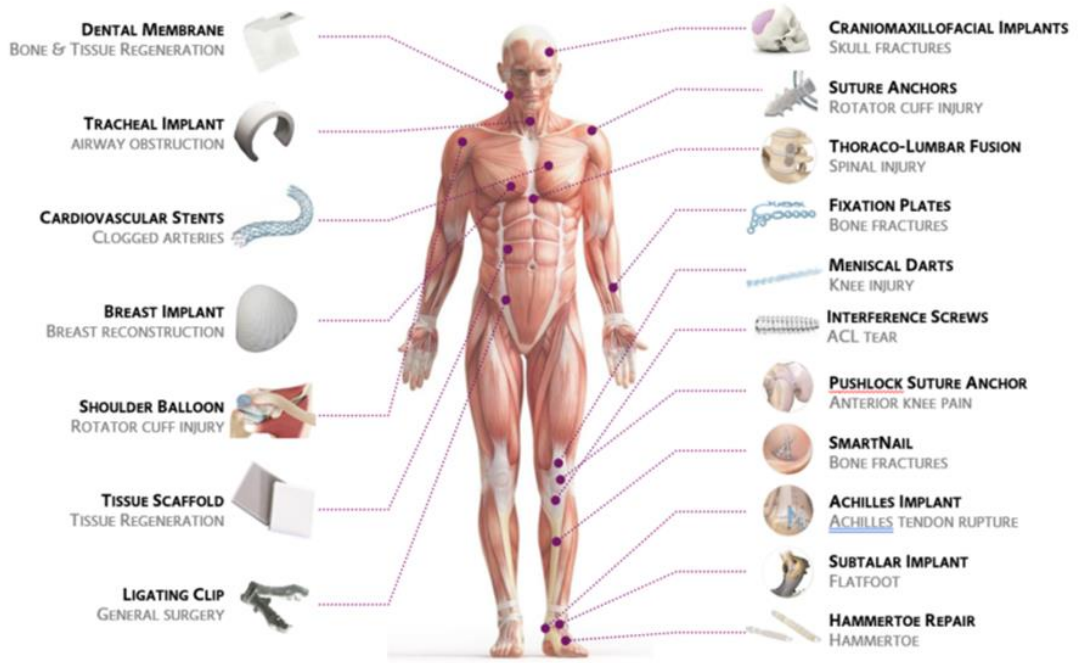

Figure 1.3: Various resorbable polymeric implants used in the human body [15].

1.4 PLA, its blends and composites

PLA, a hard and semicrystalline, high-molecular-weight polymer with thermoplastic properties, was introduced in 1955 [16]. Poly (lactic acid) (PLA) is a bioresorbable polymer authorized by the FDA that is a linear aliphatic polyester. Because ester groups have weak hydrolytic stability in aqueous conditions, PLA undergoes minimal erosion inside the body, resulting in the production of lactic acids. Lactic acid is a prominent actor in the citric acid biosynthetic cycle, which is found in practically every creature; hence, it can be totally destroyed within the body. As a result, PLA is an excellent synthetic polymer for use in medical applications.

The ring-polymerization process produces two enantiomeric forms of PLA, poly-L-lactide (PLLA) and poly-D-lactide (PDLA), with opposing configurational structures. Because PDLA is amorphous, it is weaker and degrades more quickly. [17]. PLLA is an aliphatic polyester with strong biodegradability and biocompatibility, as well as reasonable mechanical characteristics and fiber processability. PLLA has been widely explored and used as a biological material in tissue engineering and medication delivery during the last 60 years. Understanding the pace and mechanism(s) of biodegradation of a biodegradable polymer material is critical for practical applications. Several variables influence the degradation rate, including molecular

weight, polymer enantiomeric content, implant size and form, environmental aspects, processing techniques, and sterilization [18]. PLLA degrades the slower of the two enantiomeric forms. The primary breakdown process for PLLA is widely assumed to be simple hydrolysis [19]. PLLA is one of the most common biomaterials used for medical devices (e.g., bioabsorbable screws for fixation of tendon to bone and bone to bone) [20], and it is also used in compounding with other materials for sutures and bone fillings. There are many studies made by using PLA polymer in the literature. Table 1.5 shows these studies with their references, including polymer matrix, filler or reinforcement materials, production process, coating type and application area. As it is seen from the literature, PLA based blends and bio composites were studied for general purpose or specific applications.

Table 1.5: Polymer matrix, filler or reinforcement materials, production process, coating type and application area of the studies with given references.

Polymer Matrix	**Filler/ Reinforcement**	**Production Process**	**Coating Type**	**Application Area**	**Ref.**
PLA- and PGA-based (co)polymers	HA and β-TCP	-	Peptide sequences	General Purpose	[21]
PLLA	β-TCP	Solution casting	Gelatin/ hydroxyapatite (Gel/HAp)	Scaffolds	[22]
PLLA	-	-	-	Mesh and autologous bone chips	[23]
PLGA-(PEG)	-	-	-	For dexamethasone acetate (DXA) delivery in rabbits	[24]
PLGA films	-	-	-	glaucoma treatment in rabbits	[25]
PLLA	Mg nanoparticles	Compression molding	-	General Purpose	[26]
PLGA/PLLA	-	Phase inversion and phase separation technique	-	Scaffolds	[27]
Biodegradable polyesters	-	-	-	Jawbone	[28]
PLA	HA	Electrospinning		General Purpose	[29]

PDLLA	HA	Electrospinning	-	General Purpose	[30]
PLA	Bioactive glass	Electrospinning	-	General Purpose	[31]
PLA	TCP	Electrospinning	-	General Purpose	[32]
PLLA	HA	Phase separation	-	General Purpose	[33]
PLLA	bioactive glass	Phase separation	-	General Purpose	[34]
PLA	HA	Solvent casting	-	General Purpose	[35]
PDLLA	bioactive glass	Solvent casting	-	General Purpose	[36]
PLA	CaP glass	3D printing	-	General Purpose	[37]

Chapter 2

2 Literature Survey

Poly(lactide) or poly (lactic acid) (PLA) is a type of polyester which is used in various areas such as hygiene products, indoor and outdoor furnishings, textiles such as apparel and especially in medical industry because PLA is non-toxic, biocompatible and biodegradable which can be produced from renewable resources [38,39]. In medical area PLA has been used as a matrix for the controlled-release of drugs and as scaffolds on which living tissue can regenerate itself [38]. Although PLA is a strong candidate for use in the medical field, it must meet certain requirements to meet its intended use.

Conditions such as high compressive strength in bone screws, flexibility in suture applications, and increased cell adhesion capacity in tissue engineering applications can be given as examples of these requirements. Therefore, if independent control of the bioactivity, degradation rate and mechanical properties of PLA can be achieved, specific applications of PLA become feasible. The low tensile and compressive strength and Young's modulus should be increased for increased bio-mechanical performance of PLA [40]. General studies about bioabsorbable polymer composites were given in Table 2.1. In addition, some research results of in vitro and in vivo experiments using different PLA-CaP/PLGA-CaP composites were tabulated in Table 2.2. PLA and Some of the studies carried out to improve the mechanical properties and biocompatibility of PLA are summarized below for a more detailed review.

Huang et al. (2020) produced nanoplate-like hydroxyapatite (HA)/polylactide (PLA) composites for biomimetic nanocomposites via direct melt intercalation and investigated properties of composites. They indicated that the compressive and tensile strengths of composites increased with increasing HA content until 10 wt.%, above 10 wt.% reinforcement strength values decreased because of HA aggregation in PLA matrix [41]. Gendviliene et al. (2020) produced hydroxyapatite (HA)/PLA composites for the use of scaffolds. Researchers indicated that approximately 10% concentration of HA improves osteogenic potential, with no measurable changes to cellular compatibility or the mechanical shear strength of the composite [42].

Orozco-Díaz et al. (2020) produced HA/PLA composites for biomedical applications. They revealed that HAp composites containing 10 wt.% HA exhibited better cell attachment than composite containing 20 wt.% HA [43].

Liu et al. (2018) produced laminated HA/PLA composites. They indicated that when the HA content exceeded 10%, tensile strength of composite tended to decrease because of agglomeration [44].

Custodio et al. (2021) produced PLA composites containing 5-15 wt.% HA and investigated physicochemical and mechanical behavior of incorporation of HAp with PLA matrix. They indicated that tensile strength of composites decreased at incorporation of 15% HA into PLA matrix [45].

Ferri et al. (2017) incorporated HA bioceramics particles into PLA matrix at varying ratios of 5-20 wt.%. They indicated the PLA-HA composites containing 10–20 wt.% HA represent a good balance between overall mechanical responses [46].

PLA is enantiomeric polyester including poly(l-lactide) (PLLA) and poly(d-lactide) (PDLA); two types of three-dimensional helical structures that twist in counter-clockwise (L-configured) and clockwise (D-configured) directions [47]. And another method to improve the properties of PLA such as hydrolysis resistance, mechanical performance, thermal stability and heating resistance is the formation of stereo complex between enantiomeric constituents [48].

Park et al. (2021) investigated PLLA and PDLA blends in different ratios from 9/1 to 5/5. They indicated increasing PDLA content increased the crystallinity of resultant blend and the tensile strength of blends increased with increasing content of PDLA, while elongation at break values did not chance [49].

Yu et al. (2017) prepared stereo complex PLA films by melt blowing. The dried PLLA and PDLA pellets were melt mixed by using high speed mixer. PDLA content of blends were 0.1, 0.2, 0.3, 0.4, 0.5, 1, 3 and 5 wt.%. They indicated that addition of PDLA improved the toughness of the PLLA/PDLA blends [50].

Jumat et al. (2021) prepared melt mixed and 3D printed PLLA/PDLA blends for the use of scaffold. The ratio of PDLA in blends were 0, 10, 20 and 30 wt.%. They stated that The blending of PDLA into PLLA has improved the hydrophobicity, mechanical, and degradation properties of the scaffolds. Increasing PDLA content until 20 wt.% increased mechanical performance. Tensile properties decreased above the addition of 20 wt.% [51].

Saeidlou et al (2012) prepared PLLA/PDLA blends by using twin-screw extruder containing 1,3 and 5 wt.% PDLA. Stereo complex spherulitic structures were found to act as particulates inside the PLLA matrix. This resulted in increasing viscosity and a modification in morphology and melt enthalpy [52].

As a result, the PDLA and PLLA percentage in the blends affect the glass-transition, melting point, crystal structure and degradation rate of PLA [53–56].

HA possesses superior biocompatibility and poor biodegradation, while TCP possesses less excellent biocompatibility and time-dependent biodegradation. Nevertheless, using HA or TCP alone cannot achieve the ideal mechanical properties required for bone repair. Synthetic polymers have been very attractive candidates since their mechanical and chemical properties can be controlled [57].

In the light of literature studies, PLA bioceramics composites were prepared in this thesis study. Different ratios of HA/TCP mixtures were used as bioceramics additives. Since the optimization between mechanical properties and biocompatibility is achieved in the case of 10% reinforcement, the reinforcement rate was fixed as 10% in this study. In order to improve the properties of PLA matrix, PLLA/PDLA mixtures were prepared in different ratios and HA/TCP mixed powders were added to these mixtures at different ratios. Moreover, pectin coating process was applied to improve the biocompatibility of the prepared composites. With regard to our best knowledge on related literature review, PLA/bioceramics (HA or TCP), formation of PLLA/PDLA stereo complex and PLLA/bioceramics (HA or TCP) were well studied but there is no study on stereo complex composites formed with different ratios of PLLA/PDLA mixture containing varying proportions of HA/TCP mixture and their coating with peptide. In this context, this thesis study presents different perspective for bioceramics reinforced PLLA/PDLA composite studies.

Table 2.1: Some research on bioabsorbable polymer composites.

Polymer Matrix	Filler/Reinforcement	Aim to produce	Production Process	Results	Reference
PLGA	β-TCP (0–60 wt. %)	Scaffold with porosity 83.5%-91.4%	Phase separation	Compressive modulus: up to 6.64±1.03 MPa (30 wt.% β-TCP)	[58]
PLA	HA (0–30% wt. %)	Fibrous scaffold with porosity up to 90% to make synthetic bone-like materials	Phase separation	Compressive modulus: up to 0.63 MPa (20 wt.% HA)	[33]
PLA, PCL, PG	HA		Adhesion experiments	-	[59]
PLA	Amorphous-TCP (0–30 wt. %)	film	Solvent casting	Young's modulus: up to 2800 MPa (30 wt.% amorphous-TCP)	[60]
PLA	HA (0–50 wt. %)	Scaffold with porosity 86–92%	Solvent casting	Compressive modulus: up to 9.87 ±1.8 MPa (50 wt.% HA)	[61]
PLGA	HA (0–15 wt. %)	Film	Solvent casting	Tensile strength: up to 3.9±0.37 MPa (10 wt.% HA)	[62]
PLA	CDHA (0–10.5 vol. %)	Film	Solvent casting	Tensile modulus: up to 2.47 GPa (10.5 vol.% CDHA)	[63]
PLA	HA (0 to 16.7 wt. %)	Fibers	Electrospinning	Young's modulus: up to 4.711± 0.019 MPa (16.7 wt.% HA) Tensile strength: up to 0.262±0.007 MPa (16.7 wt.% HA)	[64]
PLA	HA (N/A)	Fibers	Electrospinning	Young's modulus: up to 118±10 MPa (with HA) Tensile strength: up to 2.86±0.24 MPa (with HA)	[29]
PLA	CDHA	Scaffold with porosity up to 95%	CaP coating	Compressive modulus: approximately 10 MPa (with CDHA)	[5]
PLA/PLGA	HA/β-TCP (0-30 wt. %)	Rod-like profiles with a diameter of 2-2.5 mm	Melt extrusion	Young's modulus: up to 4.5±0.2 GPa (30 wt.% HA and 70 wt.% PLA) Flexural strength: up to 136 ±5 MPa (10 wt.% HA and 90 wt.% PLGA)	[65]
PLA	HA (0–50 wt. %)	Billet	Forging	Flexural strength: up to 270±4.1 MPa (40 wt.% HA) Flexural modulus: up to 12.3±0.2 GPa (50 wt.% HA) Tensile strength: 154.1±0.8 MPa (PLA) Young's modulus: up to 2.4±0.9 GPa (50 wt.% HA) Compressive strength: up to 115.3±3.9 MPa (PLA) Compressive modulus: up to 6.5± 0.2 GPa (50 wt.% HA)	[66]

PLGA	HA (50 wt. %)	Scaffold with porosity 91±3%	Supercritical gas foaming	Compressive modulus: 4.5±0.3 MPa Young's modulus: 26.9±0.2 MPa	[67,68]
PLA	HA (N/A)	3-D block	Cold/Hot Pressing	Compressive strength: up to 140 MPa Compressive modulus: up to 10 GPa	[68]
PLA	TCP (50 wt. %)	Scaffold with porosity up to 89.6%	(Solid Free Fabrication) SFF	Compressive modulus: 60.11 MPa	[69]
PLGA	TCP (23-33.3 wt. %)	Scaffold with porosity from 50% to 90% in different regions	SFF	Tensile strength: up to 5.7±1 MPa (33.3 wt.% TCP) Young's modulus: up to 233±27 MPa (23 wt.% TCP) Compressive strength: up to 13.7±0.8 MPa (23 wt.% TCP) Compressive modulus: up to 450±79 MPa (23 wt.% TCP)	[70]

Table 2.2: Results of in vitro and in vivo experiments using different PLA-CaP/PLGA-CaP composites.

Composites	Method	Cell culturing or implantation	Period
In vitro experiment			
PLGA/HA [62]	Solvent casting	Chondrocytes isolated from joint of porcine rear leg	6 days (cell number is 1.3 times higher than control group)
PLGA/HA [71]	Phase seperation	Mesenchymal stem cells from rabbit tibia	2 weeks (significantly higher cell growth and alkaline phosphatast (ALP) activity)
PLA/β-TCP [72]	Electrospinning	Human adipose stem cells	2 weeks (high DNA content and ALP activity)
PLGA-HA [73]	Sintering	Human mesenchymal stem cells	3 weeks (enhance cell proliferation at early point, but differentiation and mineralization were promoted at later point)
In vivo experiment			
PLGA/BCP [74]	Emulsion	Implantation in alveolar bones	24 weeks (significantly higher bone density as compared to control group)
PLA/β-TCP [75]	Emulsion	Implantation in rabbit femur	4 weeks (mineralized bone with repairing of soft tissue)
PLGA/TCP [76]	Electrospinning	Implantation in rabbit calvarial bone	4 weeks (mineralized bone)
PLGA/HA [67]	Supercritical gas foaming with salt leaching	Implantation in rat skulls	8 weeks (mineralized bone with lamellar structures and osteoid formation)
PLA/β-TCP [77]	Supercritical gas foaming	Implantation in sheep femur and tibia	12 months (mineralized bone)
PLA/HA [78]	Cold/hot pressing	Implantation in mice femur	12 weeks (good growth in surrounding connective tissue)
PLGA/β-TCP [79]	SFF	Implantation in rabbit calvarial bone	8 weeks (mineralized bone)

Chapter 3

3 Purpose, Importance, and Outline of Thesis Study

This thesis focuses on the development of PLA-based absorbable composites with enhanced bioactivity for biomedical applications. In this context, two main objectives have been determined in general. The first is to improve the mechanical properties of the polymer composite to be produced. Secondly, the bioactivity of the mechanically cured final composite material is increased as a result of coating with peptide. Based on this situation, which formed the basis of the study, the most important motivation source for the study was to produce more durable and higher-bioactivity implants for use in temporary implantation applications.

The outline and steps of the thesis study are shown in the Figure 3.1.

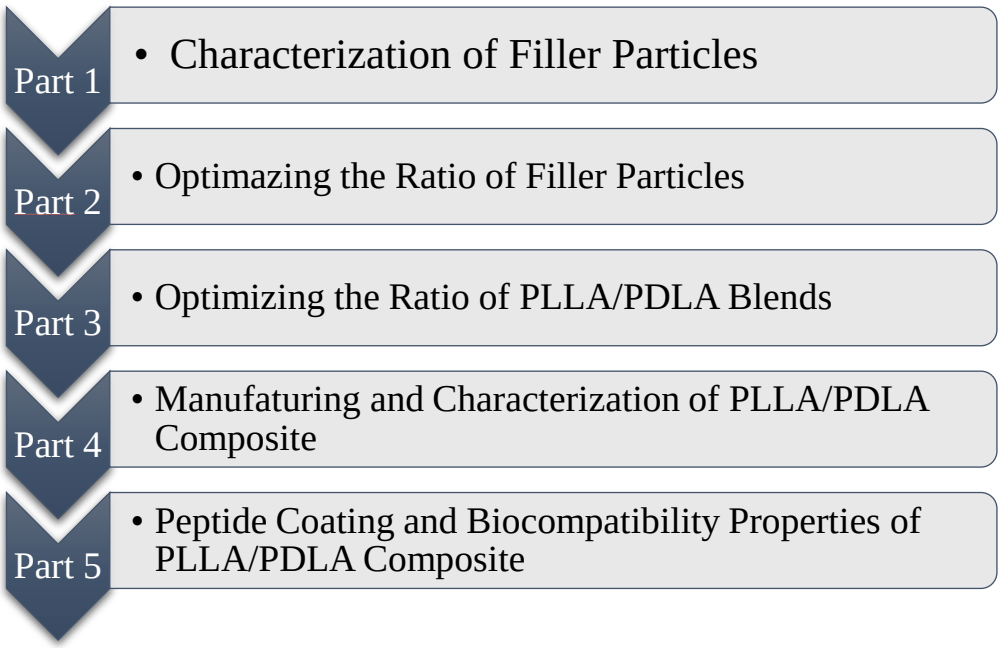

Figure 3.1: The outline and steps of the thesis study.

Chapter 4

4 Powder Characterizations

4.1 Introduction

Ceramics are hard and brittle due to the presence of bonding and few slip mechanisms in their structures. Because of these characteristics, while having various applications throughout history, their usage as a biomaterial did not become common until the last century. Ceramics have begun to be employed as biomaterials thanks to newly discovered manufacturing processes [80]. Ceramics are strong, brittle, porous, resistant to corrosion and body fluids, have a high compressive strength, and are biocompatible. They are utilized in orthopedic, dental, and cardiac applications because of these characteristics. A ceramic material must be non-toxic, non-carcinogenic, non-allergenic, biocompatible, and have an effective function in the application area in order to be used as a biomaterial [80].

Today, tissue transplantation applications for the repair of damaged hard tissue are widely used in the treatment of bone cancer, bone loss due to skeletal trauma and infection, bone fractures, and congenital deformities of the facial and skull bones. Although autografts are the gold standard, interest in synthetic bone grafts produced by tissue engineering techniques is growing due to limitations such as tissue damage and limited graft availability [81], as well as the risk of an immune system response in allografts [82].

Many bioceramics materials are used as bone substitutes, including β-tricalcium phosphate (β-TCP), hydroxyapatite (HA), and calcium sulfate. Bio ceramic implants can be made from mixtures of HA and TCP. During biodegradability, TCP can occur at the best time of dissolution and production of bones with appropriate Ca and P ions. Since hydroxyapatite is the inorganic component of bone, it has been widely used in

wet ceramic coating forms and in medical applications. It has also been used as a catalyst for the hydrogenation and dehydration of HA primary alcohols. HA is the most popular among many apatite-structured materials [83]. Hydroxyapatite (HA), β-tricalcium phosphate (β-TCP), and their composites are widely used due to their excellent biocompatibility [84,85] . Their chemical composition is similar to that of bone mineral, leading to excellent compatibility in ossification [86,87]. The main difference between sintered hydroxyapatite and bone mineral is the high crystallinity and absence of carbonate [88].

In this chapter, the production of β-TCP powders by chemical precipitation method and the characterization of both HA and β-TCP powders were carried out.

4.2 Production of β-TCP powder

The flow chart of the production of β-TCP by the precipitation method is shown in Figure 4.1.

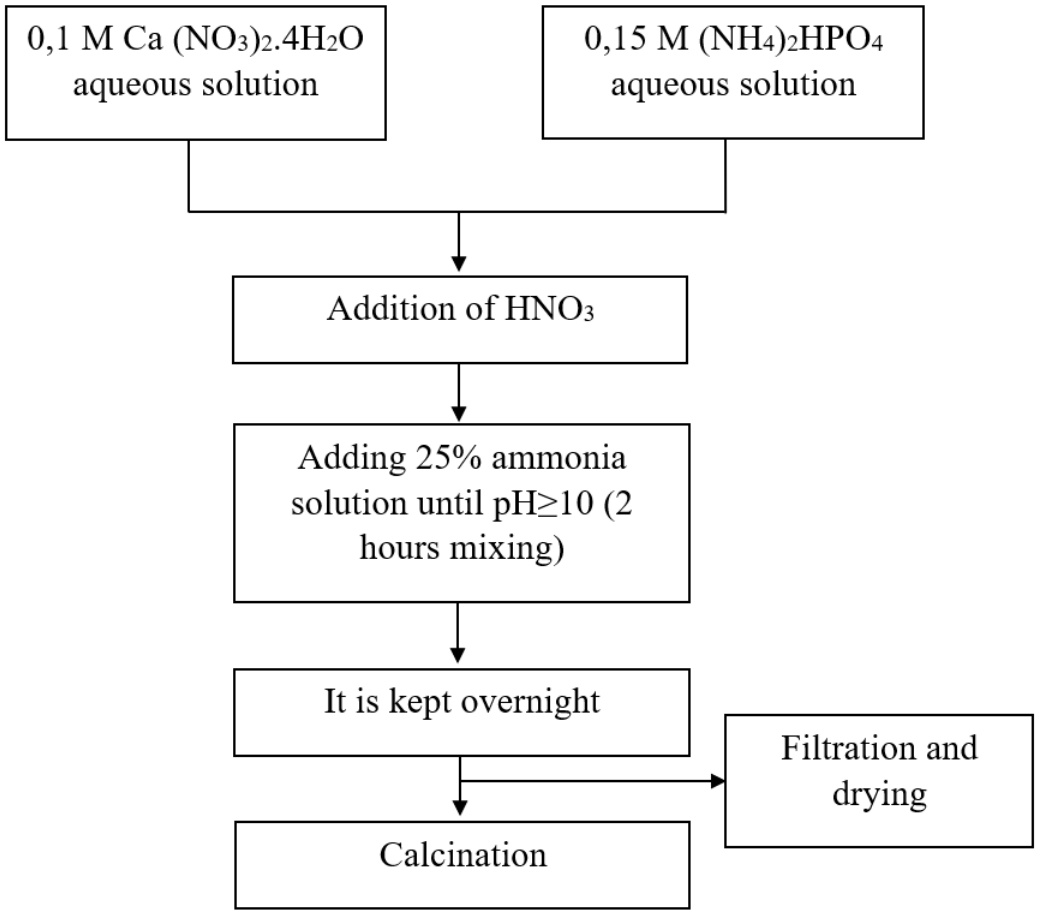

Figure 4.1: Flow chart of the synthesis of β-TCP powders by precipitation method.

The production of β-TCP powders was carried out as follows;

- Preparation of 100 ml 0.15M Ca $(NO_3)_2.4H_2O$ and 0.1 M $(NH_4)2HPO_4$ solution.
- The solution was made transparent by adding nitric acid.
- A 25% ammonia solution was added dropwise into the prepared solution and the pH was brought to 10 and stirred for 2 hours.
- The crystals formed were allowed to precipitate by keeping the solution overnight.
- The precipitate was filtered and dried.
- The resulting powder was calcined by removing it from 20 °C to 1000 °C with a heating rate of 5 °C/min using a box furnace.

4.3 Experimental Details

4.3.1 Particle Size Distribution

The particle size distribution of β-TCP and HA powders were analyzed by a laser particle size analyzer (Mastersizer hydro 3000, Malvern) in water as a dispersant. Sonic pulse was applied to dispersant in the course of measurement.

4.3.2 Zeta Potential Measurement

The surface charges of β-TCP and HA powders were measured by using a Zetasizer Nano series (Malvern Nano ZS 90) from pieces of the aqueous suspensions under the following conditions: 0.8872 cP viscosity, 25 °C and dispersant dielectric constant of 78.5.

4.3.3 Contact Angle Measurement

The wettability of β-TCP and HA powders was examined using Attension Theta contact angle measurement. Using a micro syringe, one drop of 4 µl DW was placed on the surface of the pelleted samples. The image of the droplet shape was recorded by a CCD video camera, and analyzed to determine the contact angle evolution.

4.3.4 X-Ray Diffractometry (XRD)

X-ray diffraction (XRD) analysis of β-TCP and HA powders sample were performed using a Panalytical Emperian model (with CuKa radiation at 45 kV and 40 mA) to determine the characteristic peaks of the raw materials.

4.3.5 Thermogravimetric Analysis (TGA)

Thermal stabilities of β-TCP and HA powders were investigated by Thermogravimetric analysis (TGA) using a TA Q600 instrument from TA Instruments. The samples were heated from room temperature to 1000 ºC at a heating rate of 10 ºC/min under nitrogen atmosphere.

4.3.6 Scanning Electron Microscopy (SEM)

SEM observations β-TCP and HA powders were performed by using a scanning electron microscope (SEM) (Carl Zeiss 300VP, Germany) operated at 2.5 kV. A thin layer of gold was coated on the surface of the sample by using an automatic sputter coater (Emitech K550X) to reduce the extent of sample arcing during SEM observation.

4.3.7 Inductively Coupled Plasma Mass Spectrometry (ICP-MS)

ICP-MS analysis of granule and putty were performed by using Agilent 7800 ICP-MS Spectrometer. Measurement parameters were shown as follows:

Analysis Modes: Analysis Type: Quantitative, Acquisition Mode: Steady State, Scan Mode: Peak Hopping, Spacing: Coarse, Points/Peak: 1, Scans/Replicate: 10, Replicates/Sample: 10

Plasma: Plasma flow: 18.00 L/min Auxiliary flow: 1.80 L/min Sheath Gas Flow: 0.20 L/min Nebulizer flow: 1.01 L/min, Sampling depth: 6.50 mm, Power: 1.40 kW Pump rate: 4 rpm Stabilization delay 10 sec.

Ion Optics (volt): Version Number: 0, First Extraction Lens: -42.00 Second Extraction Lens: -166.00 Third Extraction Lens: -240.00, Left Mirror Lens: 31.00 Right Mirror Lens: 21.00 Bottom Mirror Lens: 29.00, Corner Lens: -208.00 Entrance Lens: 1.00, Fringe Bias: -4.50 Entrance Plate: -10.00, Detector Focus: True Pole Bias: -0.50

CRI (mL/min): Skimmer Cone: H2 CRI Skimmer Gas Flow: 68 mL/min, Sampler Cone: OFF CRI Sampler Gas Flow: 0 mL/min

Sampling: Aerosol generation: Nebulizer, Source: Autosampler, Fast pump during sample delay/rinse: On, enable device control: Off, Probe height: 0 mm, Premix: Off, Rinse time: 20 sec, Spray Chamber Cooling: On Spray Chamber Temp: 3.00 Degrees Celsius, Sample uptake delay: 80 sec, Smart Rinse: Yes, Switch Delay: OFF, Scan time: 1458 msec, Replicate time: 14.58 sec

4.4 Result and Discussions

4.4.1 Particle Size Distribution

Particle size distribution of β-TCP and HA powders were shown in Figure 4.2 and Figure 4.3, respectively. The mean size of β-TCP powders was 19.80 µm (D50) based on a volume distribution and 50% of the particles are smaller than 19.80 µm. Besides, D10 and D90 were obtained to be 3.39 µm and 71.30 µm, respectively. The graph also shows the presence of some particles smaller than 1 µm and larger than 100 µm.

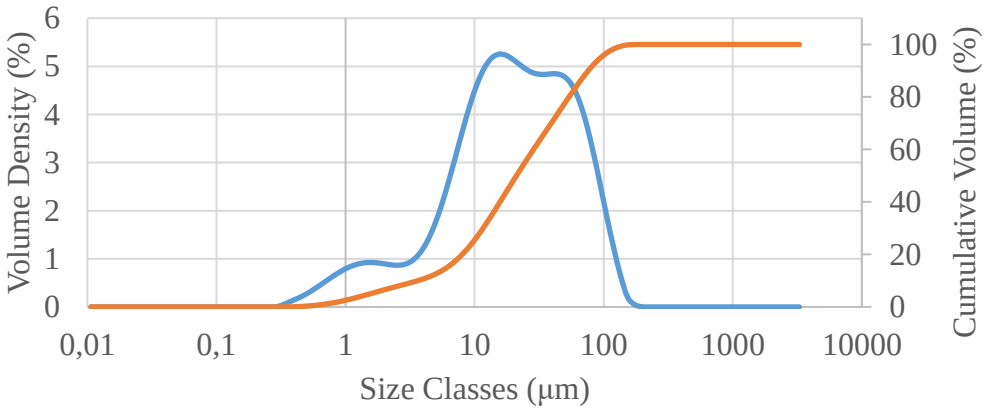

Figure 4.2: Particle size distribution of B-TCP powder.

In addition, the mean size of HA powders was obtained 4.55 umm (D 50). Further, D10 and D90 were obtained as 1.08 µm and 10.10 µm, respectively. The graph also shows the presence of some particles smaller than 1 µm and greater than 10 µm.

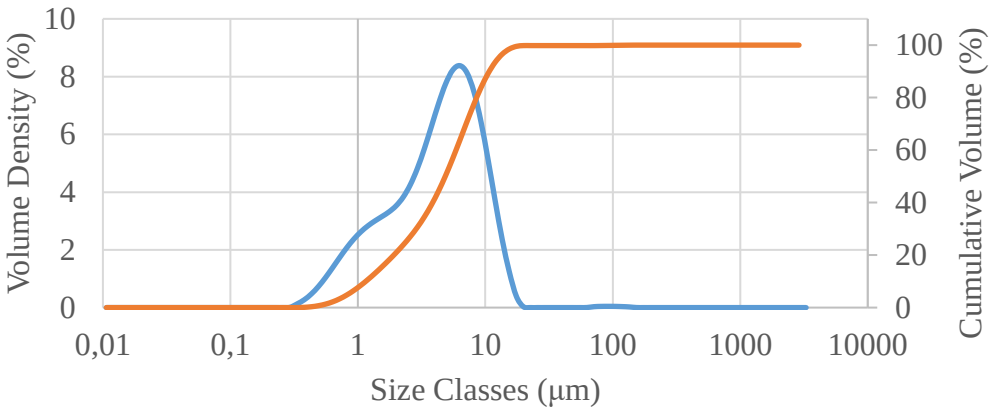

Figure 4.3: Particle size distribution of HA powder.

4.4.2 Zeta Potential Measurement

The zeta potential of β-TCP and HA powder were shown in Figure 4.4 and Figure 4.5, respectively. The zeta potential is a measure of the stability of the particles on the surfaces [89,90]. The results are presented in Table 4.1.

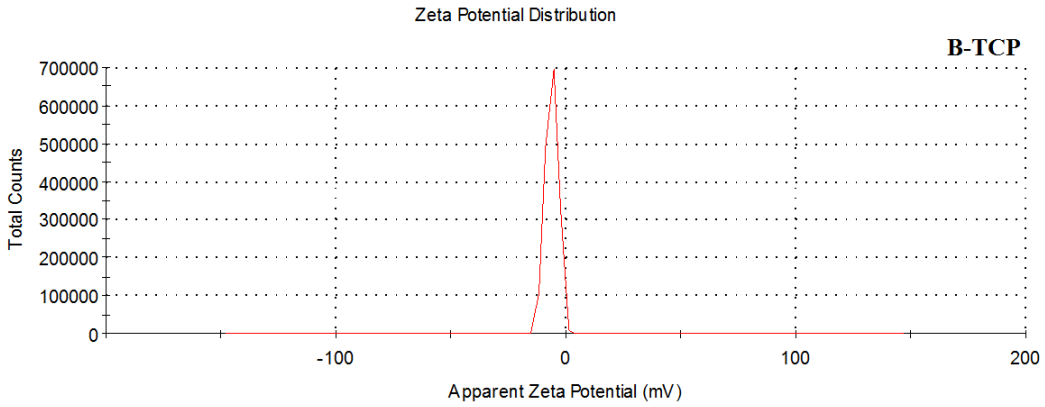

Figure 4.4: Zeta potential of β-TCP powder.

It has been shown in the literature that particles with little or no repulsive force exhibit a greater zeta potential associated with a greater electrostatic repulsion between the particles [91]. From this information, it can be said that the gravitational force between the particles of β-TCP and HA powders is high and similar. The zeta potential of powders can be better understood during the production and characterization of composite materials.

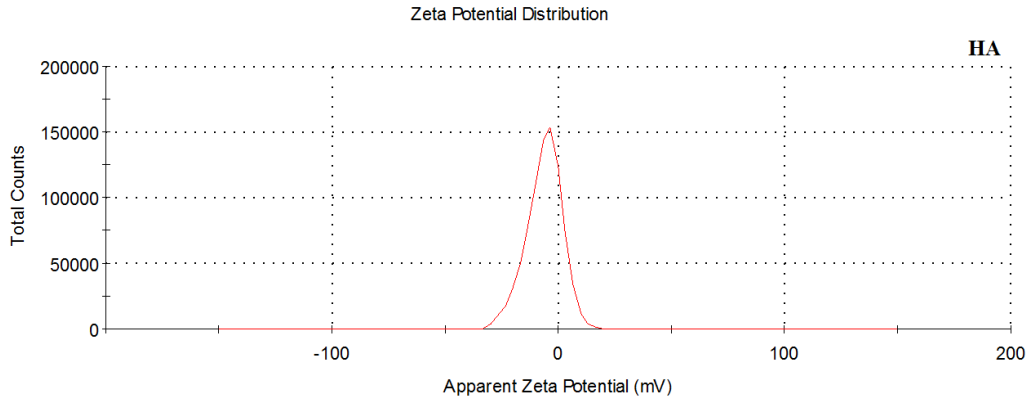

Figure 4.5: Zeta potential of HA powder.

Table 4.1: Zeta potential results of β-TCP and HA powders.

Sample	**Average (mV)**	**Area (%)**	**Standard Deviation (mV)**
B-TCP	-6.05	100	2.86
HA	-6.20	100	7.83

4.4.3 Contact Angle Measurement

Contact angle measurement results of β-TCP and HA were tabulated in Table 4.2 As can be seen from Table 4.2, average contact angles of β-TCP and HA were found as 21.33 and 25.03, respectively. This result shows that wettability of β-TCP is higher than that of HA. Difference between the wettability of β-TCP and HA may be related to their microstructure. Besides, this result also may be attributed that cell adhesion on β-TCP may be higher than that of HA.

Table 4.2: Contact angle measurement results of β-TCP and HA powders.

Samples	Statistics	CA left [°]	CA right [°]	CA mean [°]
B-TCP	Mean	23.74	18.91	21.33
	Std deviation	6.08	5.31	5.69
HA	Mean	25.4	24.66	25.03
	Std deviation	2.68	2.5	2.59

4.4.4 X-Ray Diffractometry (XRD)

The XRD graph of β-TCP and HA powders were shown in Figure 4.6 and Figure 4.7, respectively. 2θ values at which the phases are peaked maximum were defined by matching them to the JCPDS (Joint Committee on Powder Diffraction Standards) database. When XRD data of β-TCP powders was analyzed, it was seen that the maximum peak values which is 27.77 (214), 31.03 (2010), and 34.37 (220),

respectively were compatible with whitlockite with JCPDS 090169 card number. In the literature, β-TCP and whitlockite have been shown to have similar XRD profiles [92,93]

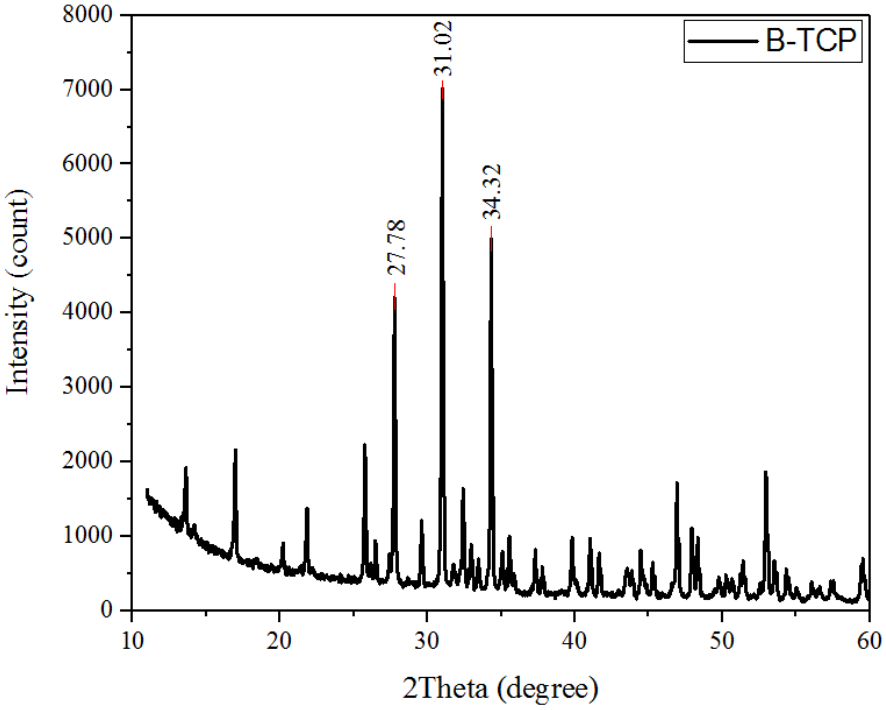

Figure 4.6: XRD pattern of B-TCP powder.

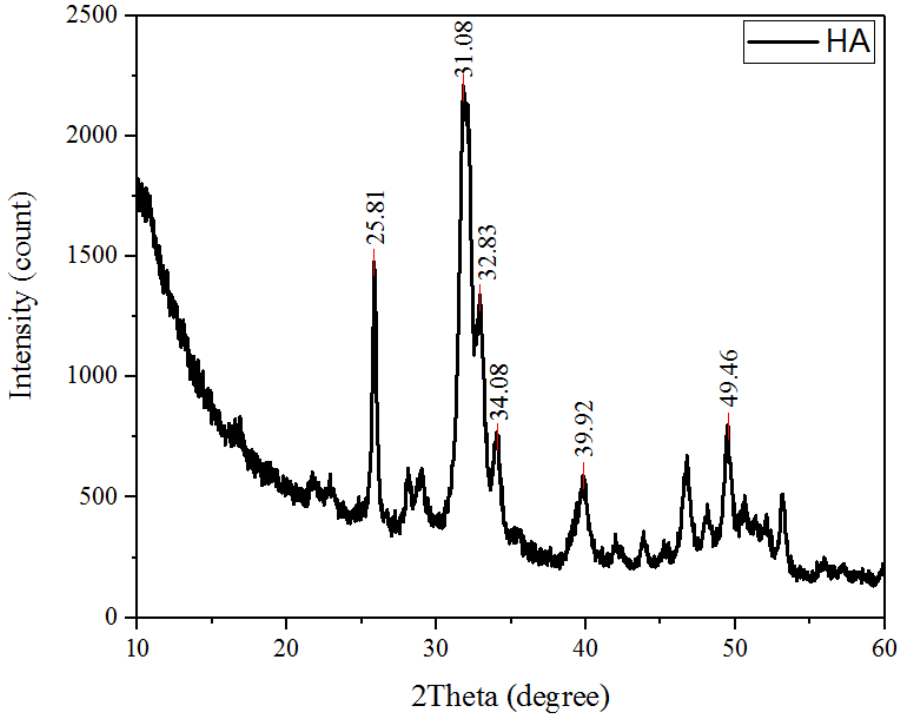

Figure 4.7: XRD pattern of HA powder.

The 2θ peak values of HA powders were obtained to be at 25.81, 31.08, 32.83, 34.08, 39.92, and 49.46, respectively. In the literature, many studies on HA characterization were realized, and similar results were obtained [94–96] When XRD data was analyzed, it was seen that the maximum peak values which is 25.77 (002) and 31.77 (211) respectively were compatible with JCPDS 009-0432 card number [94].

4.4.5 Thermogravimetric Analysis (TGA)

TGA curves of β-TCP and HA powders were given in Figure 4.8 and Figure 4.9, respectively. As shown in figures from 25 °C to 1000 °C, β-TCP and HA were degraded about 0.88 wt. % and 7.75 wt.%. These results showed that thermal stability of β-TCP was higher than the thermal stability of HA [97]. This is also revealed that using β-TCP in polymer, shows a greater thermal stability than that of using HA in polymer.

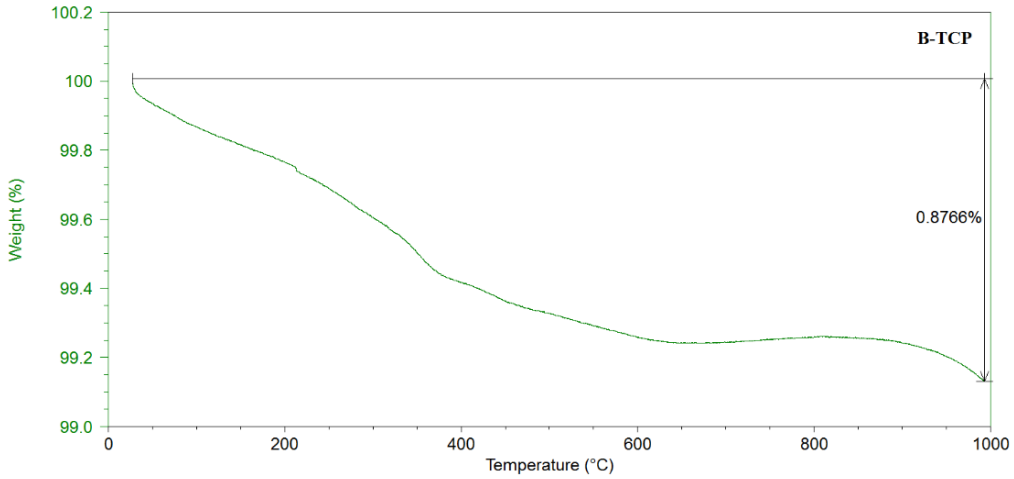

Figure 4.8: TGA curve of B-TCP powder.

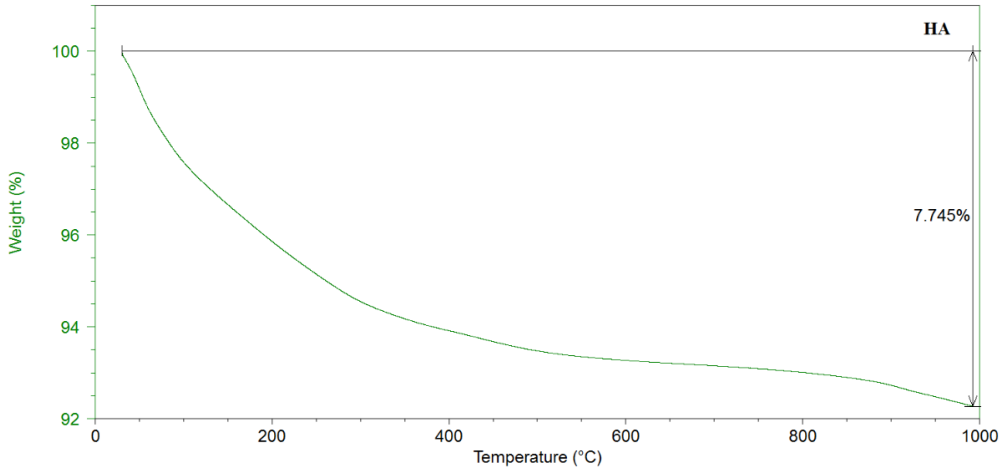

Figure 4.9: TGA curve of HA powder.

4.4.6 Scanning Electron Microscopy

SEM images of β-TCP and HA powders were shown in Figure 4.10. It can be seen from the SEM images the particle size of HA is smaller than the particle size of TCP which is similar to the result of particle size analysis.

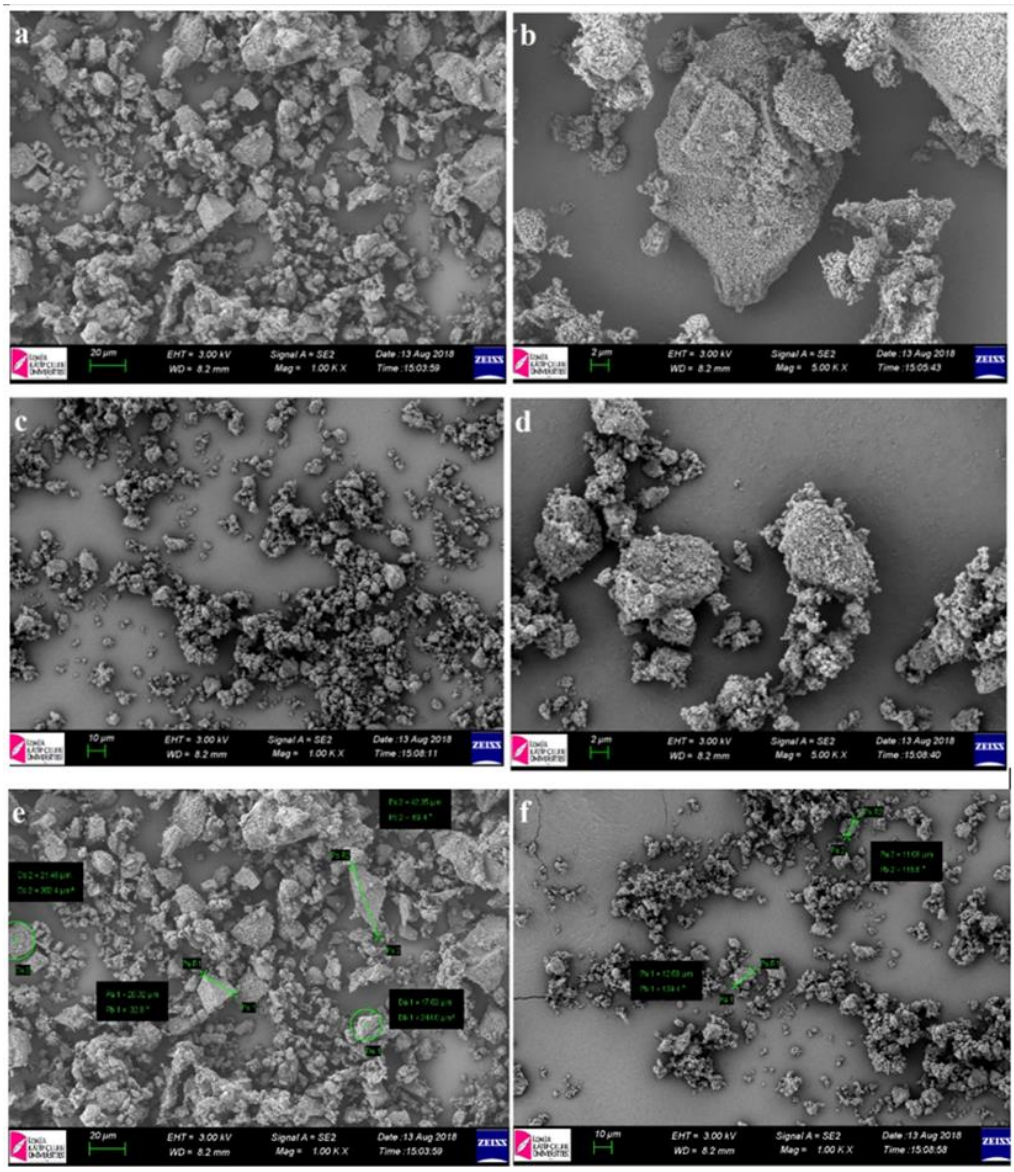

Figure 4.10: SEM images of β-TCP particles (a, b, e) and HA particles (c, d, f).

Furthermore, SEM images shows that the microstructure of β-TCP was more porous than that of HA. This result can be explaining the difference between the wettability of β-TCP and HA. When the SEM images of both materials were observed, it is observed that they have a heterogeneous size distribution, which is similar to the results obtained from the particle size distribution analysis. Furthermore, when the

SEM images of β-TCP and HA were examined, the change in dimensional difference was found to be larger in β-TCP, comparable to the particle size distribution. This dimensional difference in β-TCP can be interpreted as the fact that some particles have a higher aspect ratio. Due to its large aspect ratio, β-TCP is expected to contribute positively to mechanical properties [98,99].

4.4.7 Inductively Coupled Plasma Mass Spectrometry (ICP-MS)

The chemical constitutions of β-TCP and HA powders were examined by inductively coupled plasma mass spectrometer (ICP-MS). Chemical contents of β-TCP and HA powders were tabulated on Table 4.3 These results showed that both β-TCP and HA powders were provided standard specification of for β-TCP for Surgical Implantation which was shown in Table 4.4 [100]. These results also indicated that these powders were suitable for using biomedical applications.

Table 4.3: ICP_MS results of β-TCP and HA powder.

Parameter	Unit	β-TCP	HA
Al	ppm	33.0	212.3
P	%	25.7	19.9
Ca	%	51.0	45.0
Fe	ppm	20.5	74.1
Cu	ppm	1.1	0.5
Zn	ppm	3.1	2.9
As	ppm	0.5	0.6
Cd	ppm	0.001	0.4
Hg	ppm	0.043	0.042
Pb	ppm	8.3	0.5

Table 4.4: Standard Specification for Beta-Tricalcium Phosphate for Surgical Implantation [101]

Element	Content (ppm, max)
Pb	30
Hg	5
As	3
Cd	5

4.5 Conclusion

The results obtained in this chapter where the synthesis and characterization of the powder additives to be utilized within the scope of the thesis are presented below.

- When XRD results were examined, it was concluded that β-TCP synthesis was successful. In addition, it was seen that the XRD results of HA particles showed similar properties with the literature.
- When the ICP-MS results were evaluated, it was found that both β-TCP and HA met the requirements of ASTM F1088 - 18.
- According to the results of zeta potential and contact angle analysis, HA and β-TCP exhibit similar properties and both show hydrophilic characteristics.
- When the particle size analysis and SEM analysis results were examined, it was observed that HA had a smaller particle size than β-TCP and that β-TCP had a more porous structure than HA.

Chapter 5

5 Production and Characterization of PLLA Based Composites

5.1 Introduction

For many healthcare applications natural biodegradable polymers, such as collagen, gelatin, chitosan, and hyaluronic acid etc., have been used for many years. They are more suitable materials for medical applications because they have a promising advantage than natural polymers. These advantages are good biocompatibility, biodegradability, bioresorbability, mechanical and proliferation properties and their cost. With a few modifications their chemical and physical properties can reach desirable mechanical and degradation characteristics. On the other hand, because of their high cost and suspicious purity, their applications are limited [102].

In the last three decades, as alternatives of metallic implantable materials, biodegradable synthetic polymers have been studied. Aliphatic polyesters, such as poly (glycolic acid) (PGA), poly (lactic acid) (PLA) and their copolymer, poly(lactide-co-glycolide) (PLGA) are extensively investigated and used as biodegradable polymers [103]. For aliphatic polyester, there are many usage areas in medical applications. For example, tissue fixation (i.e., bone screws, bone plates, and pins), drug delivery systems (i.e., diffusion control), wound dressing (i.e., artificial skin), and wound closure (i.e., sutures and surgical staples). Polylactic acid (PLA) and poly-di-lactic-co-glycolic acid (PLGA) are used for production of bone screws, bone plates and pin structures [104]. The ease of processing PLA-based biomaterials by extrusion, injection molding, stretch blow molding, film casting, thermoforming, foaming, fiber spinning, electrospinning, melt electrospinning, and micro- and nano-fabrication

techniques into various shapes and sizes has played a critical role in expanding the applications of these materials [105–107].

Lactic acid-based polymers are densely researched and proven to be a safe biomaterial for the clinical applications such as sutures, implants for bone fixation, drug delivery vehicles, and tissue engineering scaffolds [108]. However, the scientific researches for PLA-based composites are limited. So, in this field, many scientists go on the researches on PLA-based composites. Different types of ceramics are widely used as substitutes and fillers for bone applications. The one of the most important ceramics is hydroxyapatite (HA). HA has mineral components that are similar to those of human bone and which are, thus, more compatible with the human body than other types of ceramic. On the other hand, mechanical limitations of artificial bone-based HA materials will be an issue when comparing with metallic or ceramic based materials [109]. Besides, the beta-tricalcium phosphate (β-TCP) is used as filler for PLA in recent years. In addition, β-TCP filled PLA composites are widely observed in tissue engineering for regeneration because of its improved biocompatibility and biodegradability. Despite its brittleness, this composite having good mechanical, dynamic mechanical and thermal properties were reported for biomedical applications [110].

In this study, HA and β-TCP are used as a filler material for PLLA based composites which are produced by using twin screw extruder. The physical, thermal, and crystallographic properties of neat PLLA, extruded PLLA, and PLLA based composites are investigated.

5.2 Materials and Methods

5.2.1 Materials

5.2.1.1 HA and β-TCP

Two different inorganic fillers which is Hydroxyapatite (HA) and beta-tricalcium phosphate (β-TCP), are used in this study. HA was obtained by Sigma Aldrich and β-TCP was produced in Bonegraft Biyolojik Malzemeler San. ve Tic. A.Ş. laboratory during my thesis study.

5.2.1.2 PLLA polymer

PLA homopolymer Luminy L175 (Tm=175 ^{o}C, ρ=1.24 g/cm3, melt flow rate (210 ^{o}C/2.16 kg) = 8 g/10 min) produced by Total Corbion, was used as the matrix material. Physical and mechanical properties of PLLA matrix material were shown in Table 5.1

Table 5.1: Properties of PLLA matrix material (Datasheet of Luminy L175).

Typical Resin Properties	**Standard**	**Unit**	**Value**
Melt Flow Rate (210 °C, 2.16 kg)	ISO 1133	g/10min	8
Density	ISO 1183	g/cm³	1.24
Tensile Modulus	ISO 527-1	MPa	3500
Tensile strength	ISO 527-1	MPa	50
Elongation at yield	ISO 527-1	%	≤5

5.2.2 Methods

5.2.2.1 Compound Preparation

Melt mixing method was used for the preparation of HA and β-TCP composites. All the composites were prepared by using Gülnar Makine corotating twin screw extruder with a screw speed of 100 rpm and barrel temperatures of about 170–190 °C. L/D ratio of the extruder is selected as 16:1. After passing through the extruder, the polymer strands (3 mm in diameter) entered a water bath and then a pelletizer that produced nominally 3 mm pellets. At the exit of the pelletizer, composite pellets produced had moist due to cooling process after extrusion. The oven was used to eliminate the moisture of the composite pellets. After extrusion, composite pellets were dried in oven for 1 hour at 80 °C. Sample codes of neat PLA, extruded PLA, and PLLA based composites were shown in Table 5.2.

Table 5.2: Sample codes of PLA, extruded PLA, and PLA based composites.

Materials	**Sample Codes**
PLLA Neat	PLA Neat
PLLA Extruded	PLA Ext.
PLLA+10% B-TCP	PLA-10TCP
PLLA+10% HA	PLA-10HA
PLLA+5%B-TCP+5%HA	PLA-5TCP-5HA

5.2.2.2 Manufacturing of Composite Plates

Composite plates (200x200x2 mm) were prepared by compression molding technique (Gülnar Hot Press with controlled heating, cooling and pressure, Turkey). The composites were produced by pressing the blends between the hot plates of a compression press at 170 °C for 4 min at 70–120 bar pressure.

5.3 Characterization of PLLA Based Composites

5.3.1 X-Ray Diffractometry (XRD) Analysis

X-ray diffraction (XRD) analysis of PLA and PLA based composites were performed using a Panalytical Emperian model (with CuKa radiation at 45 kV and 40 mA) to determine the characteristic peaks of the raw materials.

5.3.2 Thermogravimetric Analysis (TGA)

Thermogravimetric analyses of the PLA and PLA based composites were conducted by using thermogravimetric analyzer (TA Instruments, TGAQ500) at a heating rate of 10 °C/min in the range of 30–600 °C under nitrogen atmosphere.

5.3.3 Differential Scanning Calorimeter (DSC) Analysis

Differential scanning calorimetry (DSC) analysis (DSC Q2000; TA Instruments Inc., USA) was carried out to investigate the crystallization and melting behaviors of PLLA and PLLA-based composites. To eliminate any thermal history from processing, samples were heated from 20 °C to 200 °C at a rate of 10 °C/min in a nitrogen environment. This temperature was held for 5 min. After that, the samples were cooled to ambient temperature under a nitrogen atmosphere at a rate of 10 °C/min.

5.3.4 FTIR-ATR Analysis

FTIR-ATR analyses of the PLLA and PLLA based composites were carried out by using Bruker Alpha spectrometer. The analyses were performed in the range of 400–4000 cm^{-1}, with a resolution of 4 cm^{-1} and with an accumulation of 16 scans.

5.3.5 Contact Angle Measurement

The wettability of PLLA and PLLA based composites was examined using Attension Theta contact angle measurement. Using a micro syringe, one drop of 4 µl DW was placed on the surface of the pelleted samples. The image of the droplet shape was recorded by a CCD video camera and analyzed to determine the contact angle evolution.

5.3.6 Mechanical Analysis

Tensile tests were conducted in accordance with ASTM D638-10 standard, with specimen type IV. and the crosshead speed of 50 mm/min. Three-point bending test was performed by using ASTM D790 standard with a support span of 32 mm and a deformation rate of 1 mm/min. All tests were performed on universal testing machine having a 5 kN load cell (Shimadzu AGS-X).

5.3.7 Rheological Analysis

Rheological properties of PLLA and PLLA based composites were determined by using Discovery HR-2 (TA Instruments) rheometer at the testing temperature of 200 ºC. Complex viscosity of neat PLA and composites were determined in shear ramp mode with an increasing shear rate from 0.1 s^{-1} to 1000 s^{-1}. Storage (G') and loss (G'') modulus of neat PLA and composites were determined by oscillatory shear test in which ω was increased from 0.02 to 600 rad/s at 200 ºC.

5.3.8 SEM Analysis

The surface of HA and β-TCP particles and the fractured surfaces of PLLA and PLLA based composites were coated with a thin layer of gold via a plasma sputtering system.

Then, SEM analyses of samples were observed using a scanning electron microscope (300 VP FE-SEM, Carl Zeiss AG, Germany) operated at an acceleration voltage of 5 to 15 kV.

5.3.9 Inductively Coupled Plasma Mass Spectrometry (ICP-MS)

ICP-MS analysis of the samples were performed by using Agilent 7800 ICP-MS Spectrometer. Measurement parameters were shown as follows:

Analysis Modes: Analysis Type: Quantitative, Acquisition Mode: Steady State, Scan Mode: Peak Hopping, Spacing: Coarse, Points/Peak: 1, Scans/Replicate: 10, Replicates/Sample: 10

Plasma: Plasma flow: 18.00 L/min Auxiliary flow: 1.80 L/min Sheath Gas Flow: 0.20 L/min Nebulizer flow: 1.01 L/min, Sampling depth: 6.50 mm, Power: 1.40 kW Pump rate: 4 rpm Stabilization delay 10 sec.

Ion Optics (volt): Version Number: 0, First Extraction Lens: -42.00 Second Extraction Lens: -166.00 Third Extraction Lens: -240.00, Left Mirror Lens: 31.00 Right Mirror Lens: 21.00 Bottom Mirror Lens: 29.00, Corner Lens: -208.00 Entrance Lens: 1.00, Fringe Bias: -4.50 Entrance Plate: -10.00, Detector Focus: True Pole Bias: -0.50

CRI (mL/min): Skimmer Cone: H2 CRI Skimmer Gas Flow: 68 mL/min, Sampler Cone: OFF CRI Sampler Gas Flow: 0 mL/min

Sampling: Aerosol generation: Nebulizer, Source: Autosampler, Premix: Off, Rinse time: 20 sec, Spray Chamber Cooling: On Spray Chamber Temp: 3.00 Degrees Celsius, Sample uptake delay: 80 sec, Scan time: 1458 msec, Replicate time: 14.58 sec

5.3.10 Cytotoxicity Tests

The cytotoxicity test of PLA, HA and TCP were performed according to ISO 10993-5 standards. PLA, HA and TCP were incubated in serum free Dulbecco's Modified Eagle Medium (DMEM) cell culture medium for 24 hours (h) at %5 CO2 37 °C. After 24 hours, the extracts were taken from the media for cell proliferation analysis.

Keratinocyte cells (HS2) were seeded on 24 well plates and incubated in DMEM medium supplemented by 10% Fetal Bovine Serum (FBS), 1% Penicillin Streptomycin for 24 hours. The extract of material was added on the cells. MTT (3-(4,5-dimethyl-2-thiazolyl)-2,5-diphenyl-2Htetrazolium bromide) assay was applied for evaluating the cell proliferation of sutures. Briefly, the MTT solution was added on the each well and incubated for 2 hours at %5 CO2 37 °C. After 2 hours, the MTT solution was removed from the cells and 500 µl Dimethyl Sulfoxide (DMSO) was put on the cells. The cell numbers were obtained by absorbance reading at 570 nm by using plate reader.

5.4 Results and Discussions

5.4.1 X-Ray Diffractometry (XRD) Analysis

XRD patterns of PLA neat, PLA ext., and PLLA based composites were shown in Figure 5.1 and Figure 5.2. PLA exhibits a small and broad peak at 2θ = 16.6 with one less prominent peak and can be considered as semicrystalline in nature.

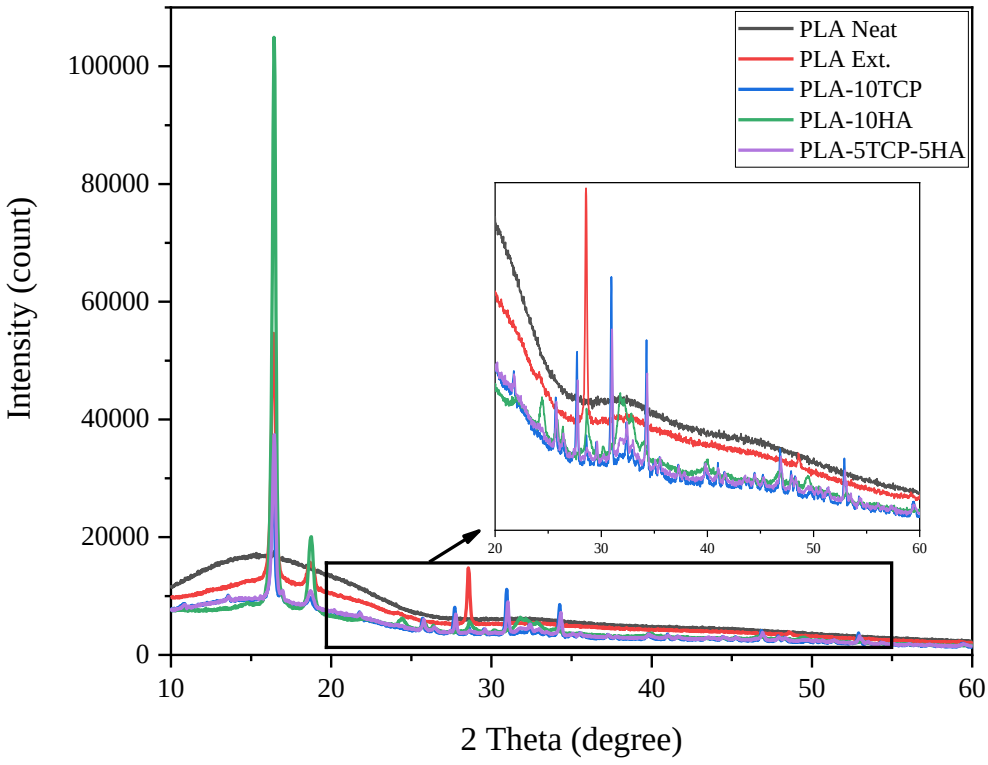

Figure 5.1: Normal XRD patterns of PLA neat, PLA ext., and PLLA based composites.

It was observed that the crystalline structure of PLLA was formed during the extrusion process. It is thought that a significant increase in crystallinity as compared to the raw material results from the thermal effect during the extrusion process. Similar conclusions have been obtained for injected materials [111]. The peaks around 2θ = 16° and 19° correspond to the crystalline structure of PLA, and the peak positions are in accordance with those reported by Mathew et al. [112].

As it can be seen from Figure 5.1 and Figure 5.2, peak values which is 27.77 (214), 31.03 (2010), 34.37 (220), respectively were compatible with whitlockite with JCPDS 090169 card number. In the literature, β-TCP and whitlockite have been shown to have similar XRD profiles [3-4]. And also, peak values which is 25.77, 31.77 and 34.08, respectively were compatible with HA patterns which card number is JCPDS 009-0432 [95].

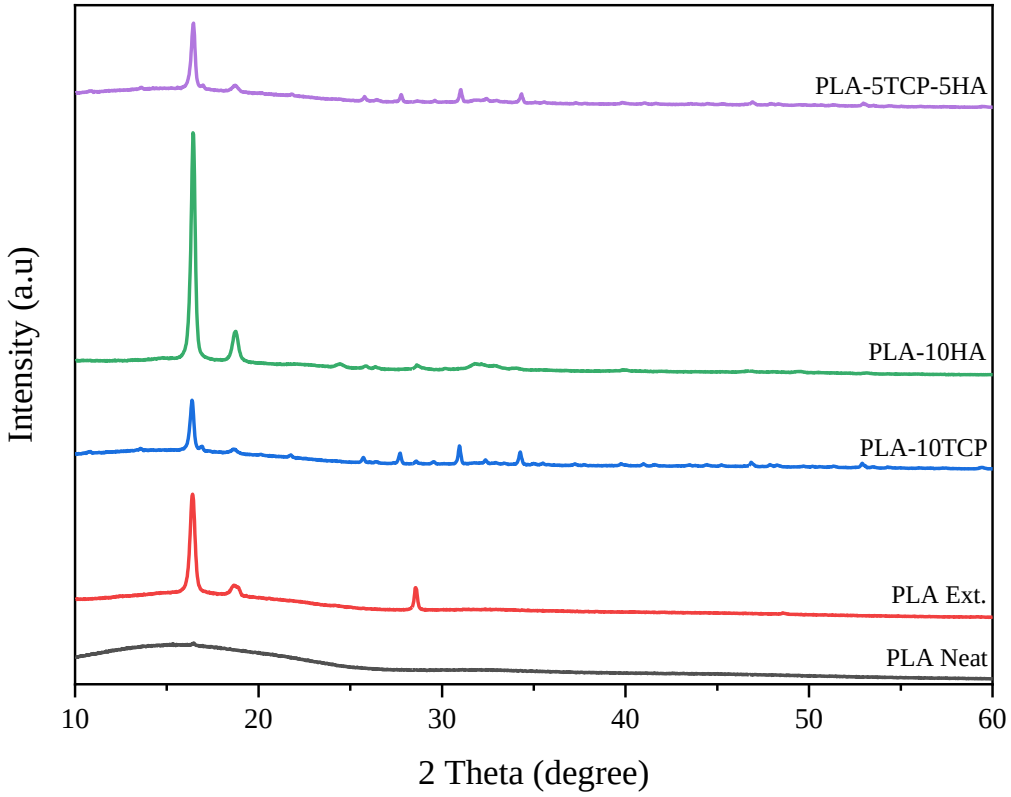

Figure 5.2: Stacked XRD patterns of PLA neat, PLA ext., and PLLA based composites.

5.4.2 Thermogravimetric Analysis (TGA)

TGA data of PLA neat, PLA ext., and PLLA based composites were shown in Table 5.3. According to Table 5.3, decomposition temperature of pure PLLA was decreased around 10 ºC after melt extrusion, because breakage of long molecules of PLLA results in fragments with shorter chain length. The percentage of these short-length macromolecules rises as the decomposition process continues, which causes the initial degradation temperature to decrease [113].

Table 5.3: TGA data of PLA neat, PLA ext., and PLLA based composites.

Samples	**T_{onset} (at 5% degradation) (°C)**	**T_{max} (°C)**	**Degraded Weight (%)**
PLA Neat	342.00	370.91	99.46
PLA Ext.	332.33	367.27	98.91
PLA-10TCP	312.99	368.07	92.91
PLA-10HA	301.51	366.58	93.33
PLA-5TCP-5HA	322.61	367.79	90.21

PLLA is rather stable to temperature; nevertheless, PLA-TCP and PLA-HA composites show a slight decrease in the degradation onset due to hydrolysis processes [46]. In a similar work, Liu et al. showed that the onset degradation temperature decreased when HA or talc was added to PLLA [114]. Siqueira et al. found a remarkable decrease in the onset and the maximum degradation temperature of PLLA/β-TCP fiber composites obtained by electrospinning processes [115]. This is more pronounced with an increase in the β-TCP content. As it has been reported in literature, HA is a highly hydrophilic inorganic compound and its tendency to moisture gain can affect PLLA as this polyester-type polymer is highly sensitive to hydrolysis. The percentage residue is directly related to the total inorganic content (HA and β-TCP). As it can be observed, although the onset degradation temperature is lower for PLLA based composites with regard to neat PLLA, maximum degradation temperature of PLLA composites was higher than that of neat PLLA. This may be due to the higher thermal stability of inorganic additives (HA and β-TCP) compared to PLA.

5.4.3 Differential Scanning Calorimeter (DSC) Analysis

DSC curves of PLA neat, PLA ext., and PLLA based composites were shown in Figure 5.3. DSC melting and crystallization parameters for PLA neat, PLA ext. and PLLA based composites such as glass transition temperature (T_g), melting temperature (T_m), crystallization temperature (T_c), crystallization enthalpy (ΔH_c), and melting enthalpy (ΔH_m) are presented in Table 5.4. The degree of crystallinity (X_c) of PP composites was estimated using equation (1) [116].

$$\%Xc \frac{\Delta Hm/_{\phi PLA}}{\Delta Hm^0} x\ 100 \quad (1)$$

where $\Delta Hm^0$is the melting enthalpy of 100% crystalline PLLA assumed to be (93 J/g) and ϕPLA is PLLA weight fractions in the composite.

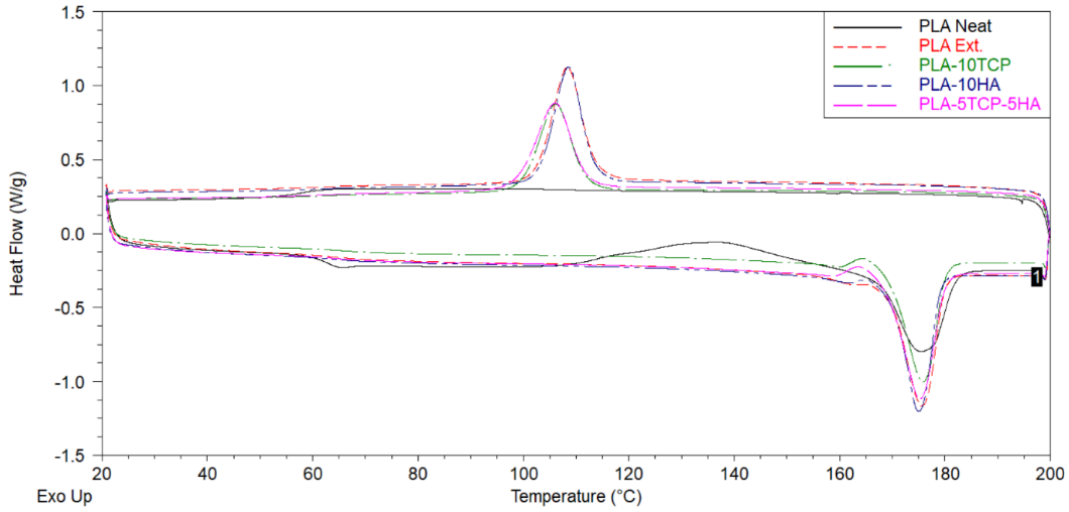

Figure 5.3: DSC curves of PLA neat, PLA ext., and PLLA based composites.

The thermogram of neat PLLA showed the glass transition temperature (T_g) and melt temperature (T_m), which are typical of amorphous polymer. Similar to XRD results, after extrusion process PLLA was gained crystal structure because of thermal effect of extrusion process. Only slight changes were observed for the melting temperatures of neat PLA, PLA ext., and PLLA based composites.

As it is seen from the table that the addition of HA and β-TCP fillers caused slight decrease in T_c and T_m points. Ferri et al. (2017) indicated that HA particles promote formation of stable spherulites at lower temperatures and on the other hand hydrophilic nature of HA could contribute to hydrolyze some PLA chains and promote a

plasticization process with the formed lactic acid oligomers which causes decrease of T_c towards lower temperatures [117]. Damadzadeh et al. (2010) indicated that the decrease in T_m could be ascribed to the stress release of molecular chains [118].

Table 5.4: DSC data of PLA neat, PLA ext., and PLLA based composites.

Samples	**T_g(°C)**	**T_c(°C)**	**ΔH_c(j/g)**	**T_m (°C)**	**ΔH_m(j/g)**	**X_c (%)**
PLA Neat	61.37	-	-	175.53	32.95	-
PLA Ext.	-	108.47	34.27	175.55	40.81	43.88
PLA-10TCP	-	106.08	27.69	175.90	37.62	44.94
PLA-10HA	-	108.47	32.37	175.03	37.48	44.78
PLA-5TCP-5HA	-	105.93	30.26	175.25	39.03	46.63

The observed crystallization behavior shows that the presence of HA and β-TCP in PLLA matrix effects thermal behavior and causes a slightly increase on the crystallinity of PLLA from 43.88% to 46.63% which can be attributed to additives facilitate organizing of the polymer structure, and – acting as crystallization seeds – leads to the increase on the rate of nucleation and mobility of the PLLA chains [119]. An interesting result was obtained by PLA-5TCP-5HA. Although the crystallinity degree of HA and TCP filled composites were similar, the crystallinity degree of PLA-5TCP-5HA was higher than both composites. This may indicate that the combined use of HA and β-TCP has a synergistic effect. Further studies are needed on this subject.

5.4.4 FTIR-ATR Analysis

FTIR spectra of PLA neat, PLA ext., and PLLA based composites was shown in Figure 5.4. PLA shows characteristic stretching frequencies for C=O, –CH3 asymmetric, –CH3 symmetric, and C–O, at 1746, 2995, 2946 and 1080 cm^{-1}, respectively. Bending frequencies for –CH3 asymmetric and –CH3 symmetric have been identified at 1452 and 1361 cm^{-1}, respectively. The peaks at about 1750 and 1180 cm^{1}, which belong to the C=O stretching and the C–O–C stretching of PLLA, are clearly visible in Figure 5.4. The presence of phosphate group PO_4^{-3} which is stem from the HA and β-TCP, is highlighted by the bands 600 cm^{-1} associated to the V_4 vibration mode [114,115].

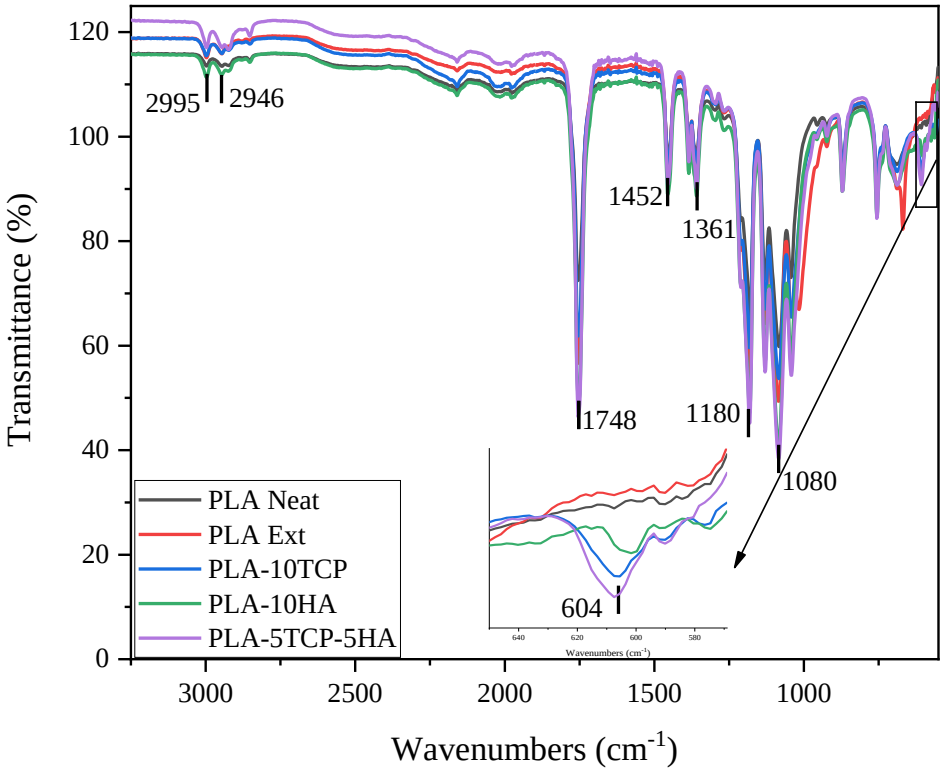

Figure 5.4: FTIR spectra of PLA neat, PLA ext., and PLLA based composites.

5.4.5 Contact Angle Measurement

Contact angle measurement results of PLA neat, PLA ext., and PLLA based composites were shown in Figure 5.5. As can be seen from the figure, average contact angles (°) of PLA neat, PLA ext., PLA-10TCP, PLA-10HA, and PLA-5TCP-5HA were found as 95.82, 79.54, 81.45, 87.43, and 81.42, respectively. The results showed that wettability of PLLA was increased by extrusion process.

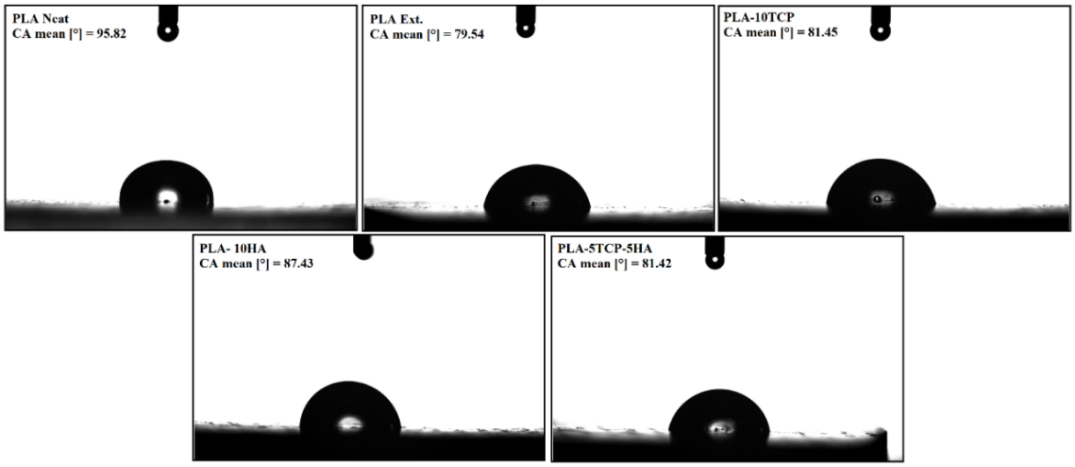

Figure 5.5: Contact angle measurement results of PLA neat, PLA ext., and PLLA based composites.

5.4.6 Mechanical Analysis

4.4.7.1 Tensile Test

Tensile testing results of PLA neat, PLA ext., and PLLA based composites were shown in Figure 5.6 and Figure 5.7. According the test results, tensile strengths (MPa) of neat PLA, PLA Ext., PLA-10HA, PLA-10TCP, PLA-5HA-5TCP were obtained to be 36.6, 35.5, 38.3, 49.6, and 48.2, respectively. When the tensile test results are examined, it is seen that the tensile strength of extruded PLA decreases a little compared to that of neat PLLA. This situation is thought to be a result of the weakening of the polymer chains by thermal and mechanical effects during the extrusion process [120].

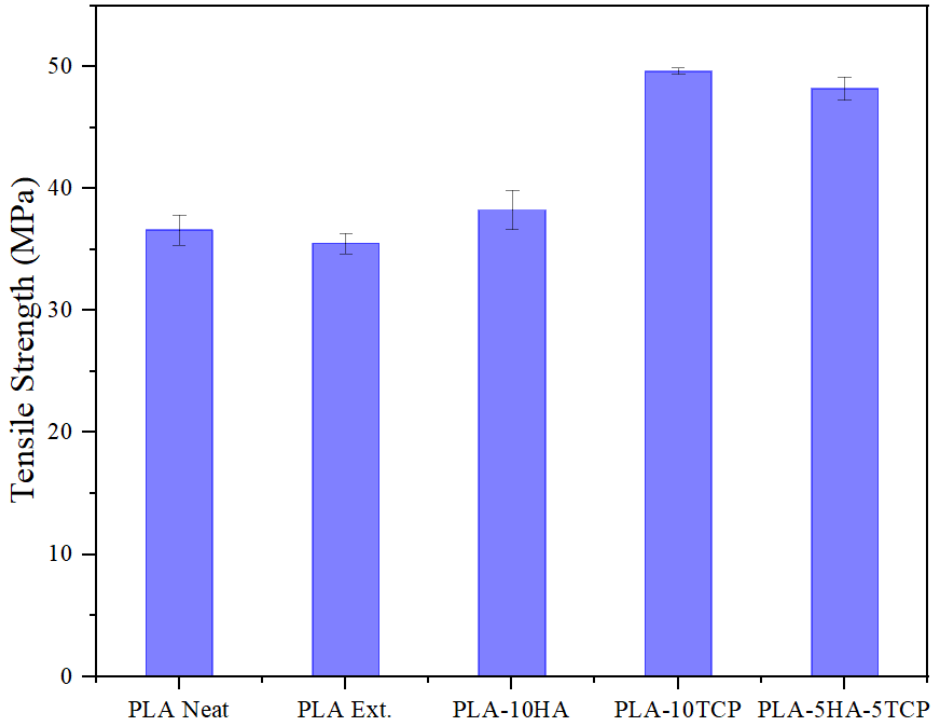

Figure 5.6: Tensile strength results of neat PLA, PLA Ext., and PLLA based composites.

The results indicated that the tensile strength and Young's modulus of PLLA based composites were higher than those of PLA. Maximum tensile strength and maximum Young's modulus were obtained at PLA-10TCP. The increase in tensile strength is thought to be due to the homogeneous distribution of filler in PLLA matrix. It was seen that similar results were found in the literature [121].

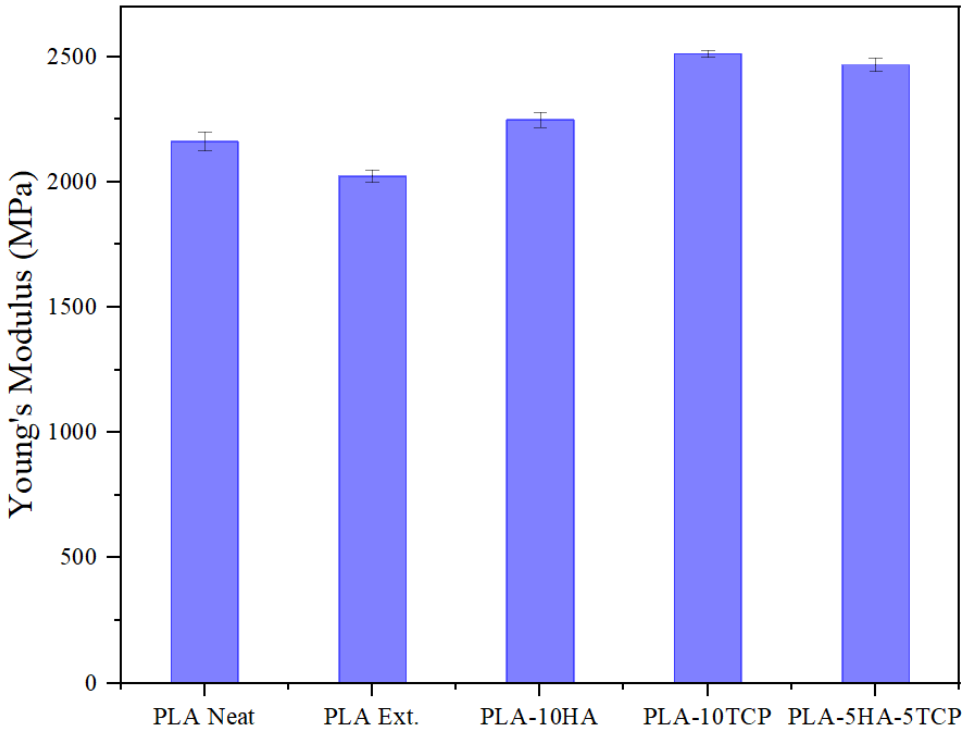

Figure 5.7: Young's modulus results of neat PLA, PLA Ext., and PLLA based composites.

According to the literature, the uniform distribution of fillers in the microstructure of polymer composites is one of the most important factors in enhancing their mechanical properties [122,123]. When 10% β-TCP was added into the PLLA matrix, the Young's modulus of PLA Ext. increased by approximately 25%. As hard particles have considerably higher stiffness values than the matrix, adding nano- and micro-particles into a polymer matrix improves it significantly [124]. The tensile strength and Young's modulus values of the hybrid composite are higher than the HA filled composite and almost the same as the TCP filled PLLA composite

4.4.7.2 Three Point Bending Test

Three-point bending test results of PLA neat, PLA ext., and PLLA based composites were shown in Figure 5.8 and Figure 5.9. The three-point bending results show that the flexural strength of extruded PLLA is about 27% less than that of neat PLLA. Similar to the tensile strength results, it has been observed that the extrusion process reduces the mechanical properties of the material [120].

Like the tensile strength results due to the homogeneous distribution of the filler material [122,123], the highest flexural strength was obtained in PLA-10TCP. Among

the composite materials while the lowest elastic modulus was observed in HA-PLA composite, the highest modulus was determined in TCP-PLA composite. In all composites, the elasticity of the composite reduces (elastic modulus value increases) with the addition of filler material. This alignment of the studied materials according to the values of elastic modulus may be due to the average filler size and stiffer nature of filler [121,125,126].

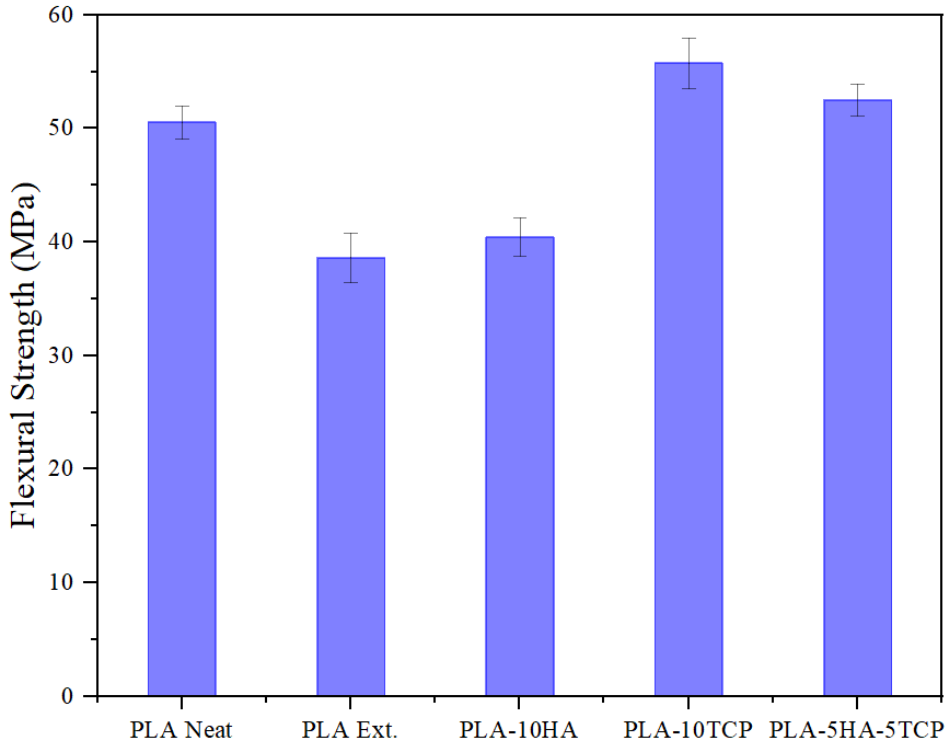

Figure 5.8: Flexural strength results of PLA neat, PLA ext., and PLLA based composites.

Among the materials lowest values of elastic modulus show HA-composite while the highest: TCP-composite. It has been observed that the elasticity of the composite material decreases with the addition of filling material in all composites. (increase in elastic modulus value). This alignment of the studied materials according to the values of elastic modulus may be due to the average filler size [121].

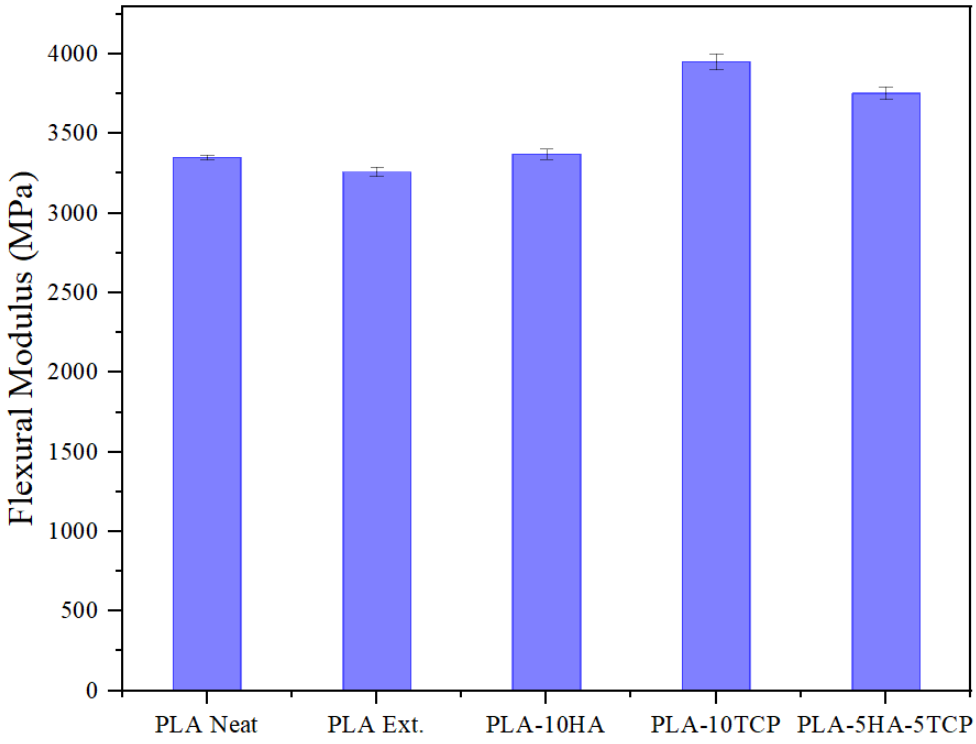

Figure 5.9: Flexural modulus results of PLA neat, PLA ext., and PLLA based composites.

5.4.7 Rheological Analysis

Figure 5.10 shows the rheological behavior of PLA and HA/PLA composite with different HA content of at 200 °C. Based on the result, all HA/PLA composites have pseudoplastic behavior. As it is seen viscosity values of all samples; PLA and PLA/HA composites decreased with increasing shear rate which indicates shear thinning (pseudoplastic) non-Newtonian behavior. Sitticharoen et al. (2017) indicated that polymer chains become oriented and thus reduced entanglement causes decreasing of viscosity [127]. The highest pseudoplastic behavior occurred of PLA-10TCP and the lowest pseudoplastic behavior occurred for PLA-10HA and PLA-5HA-5TCP placed in the middle of those two. Although all composites have the same reinforcement ratio by weight, they have different viscosity values. The reason for this behavior can be explained by the particle size. HA had smaller particle size than β-TCP and it is seen that the viscosity decreases with decreasing particle size.

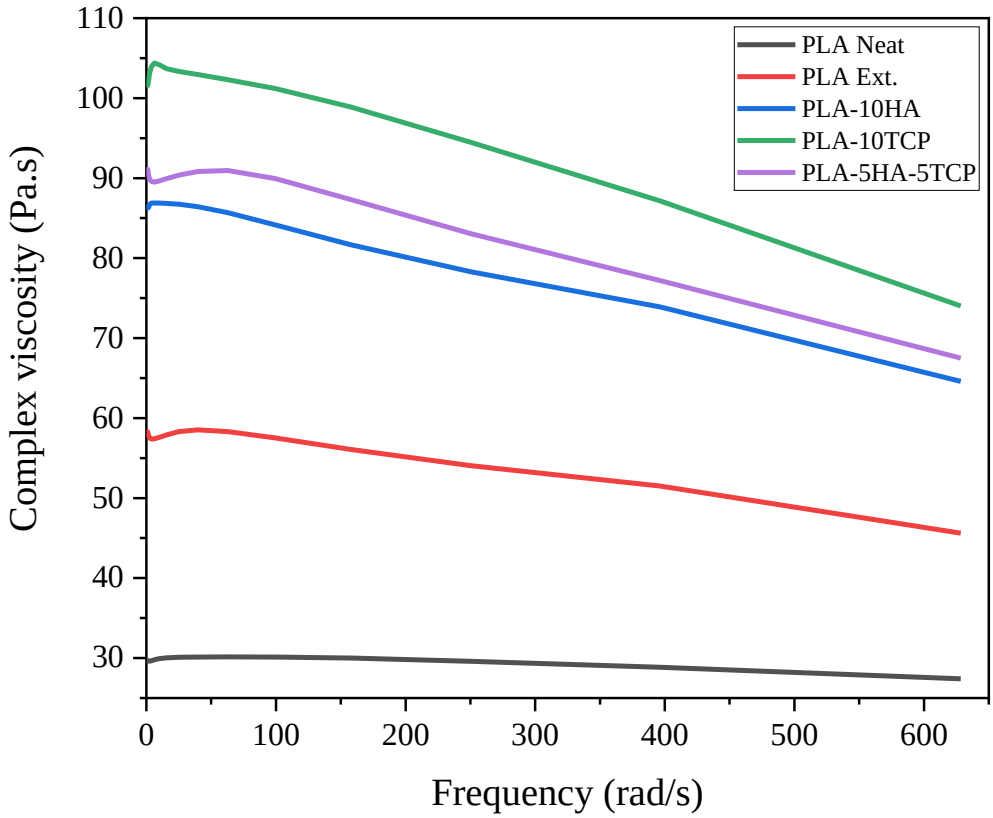

Figure 5.10: Complex viscosity- frequency curves of PLA neat, PLA ext., and PLLA based composites.

Particles increase the viscosity by creating an obstacle to the movement of the chains in the molten polymer mixture. In the case of spherical shaped particles, the increased surface area due to the decreasing particle size causes an increase in viscosity and a decrease in fluidity due to the increase in particle interaction and inter-particle friction [128]. However, Hausnerova et al. (2017) stated that the trend of increasing viscosity due to decreasing particle size is not valid for systems consisting of irregularly shaped particles, viscosity of irregular shaped powder filled composites decreases with decreasing particle size [129].

Storage (G') and loss (G'') modulus- frequency curves of neat PLA and composites are shown in Figure 5.11 and Figure 5.12, respectively. As it is seen from the figure that regardless of incorporation of HA and β-TCP particles and particle size, G' and G'' values of composites increased with increasing frequency. And also, PLA-10TCP presents the highest values of G' and G'' which indicates G' and G'' increased with increasing particle size incorporation.

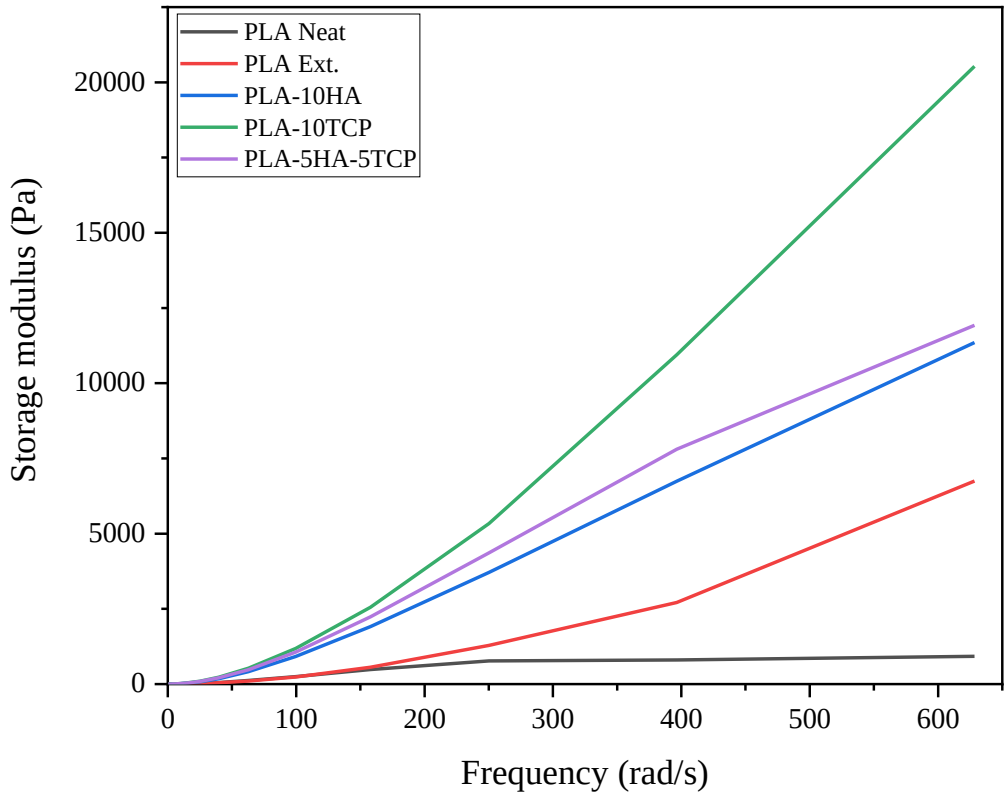

Figure 5.11: Storage modulus (G') modulus-frequency curves of PLA neat, PLA ext., and PLLA based composites

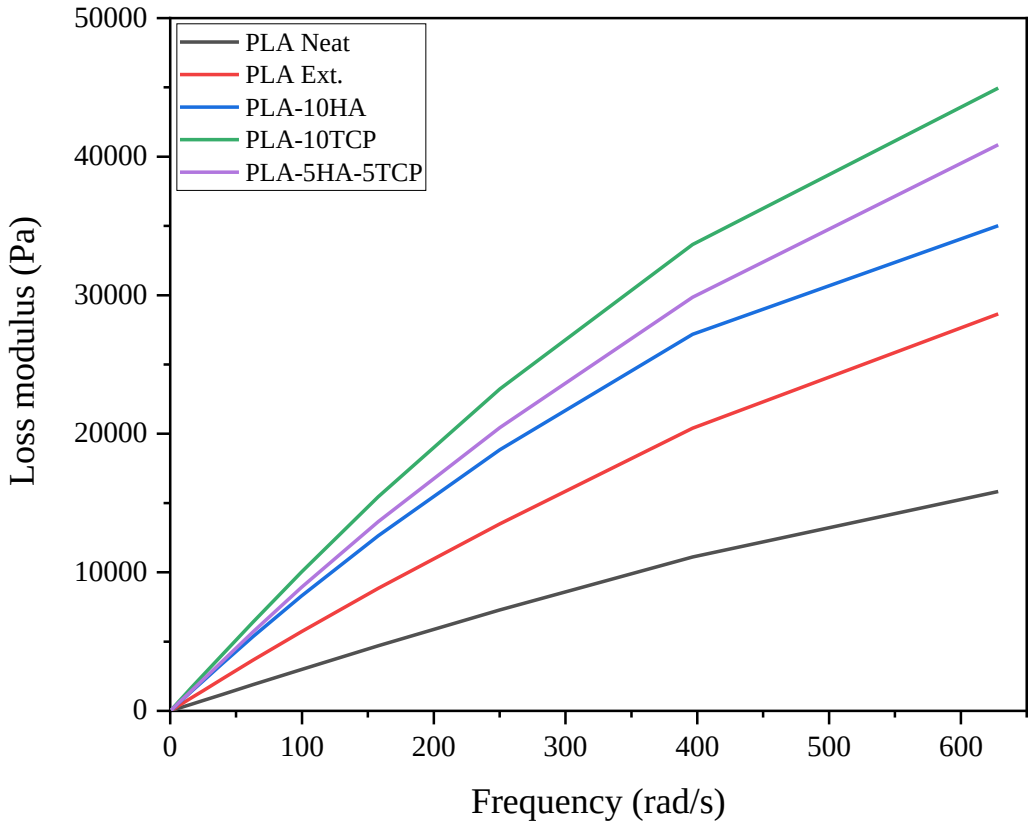

Figure 5.12: Loss (G'') modulus-frequency curves of PLA neat, PLA ext., and PLLA based composites.

5.4.8 SEM Observations

SEM images of fractured surface of PLA neat, PLA ext., and PLLA based composites were shown in Figure 5.13 a-e. As can be seen in Figure 5.13 a and b, it is seen that there is orientation in the internal structure of the material after the extrusion process. In addition, it was observed that the fracture surface of neat PLLA was sharp, while the fracture surface of extruded PLLA was observed to be spongy. This result supports the slight decrease of tensile strength obtained with the tensile test.

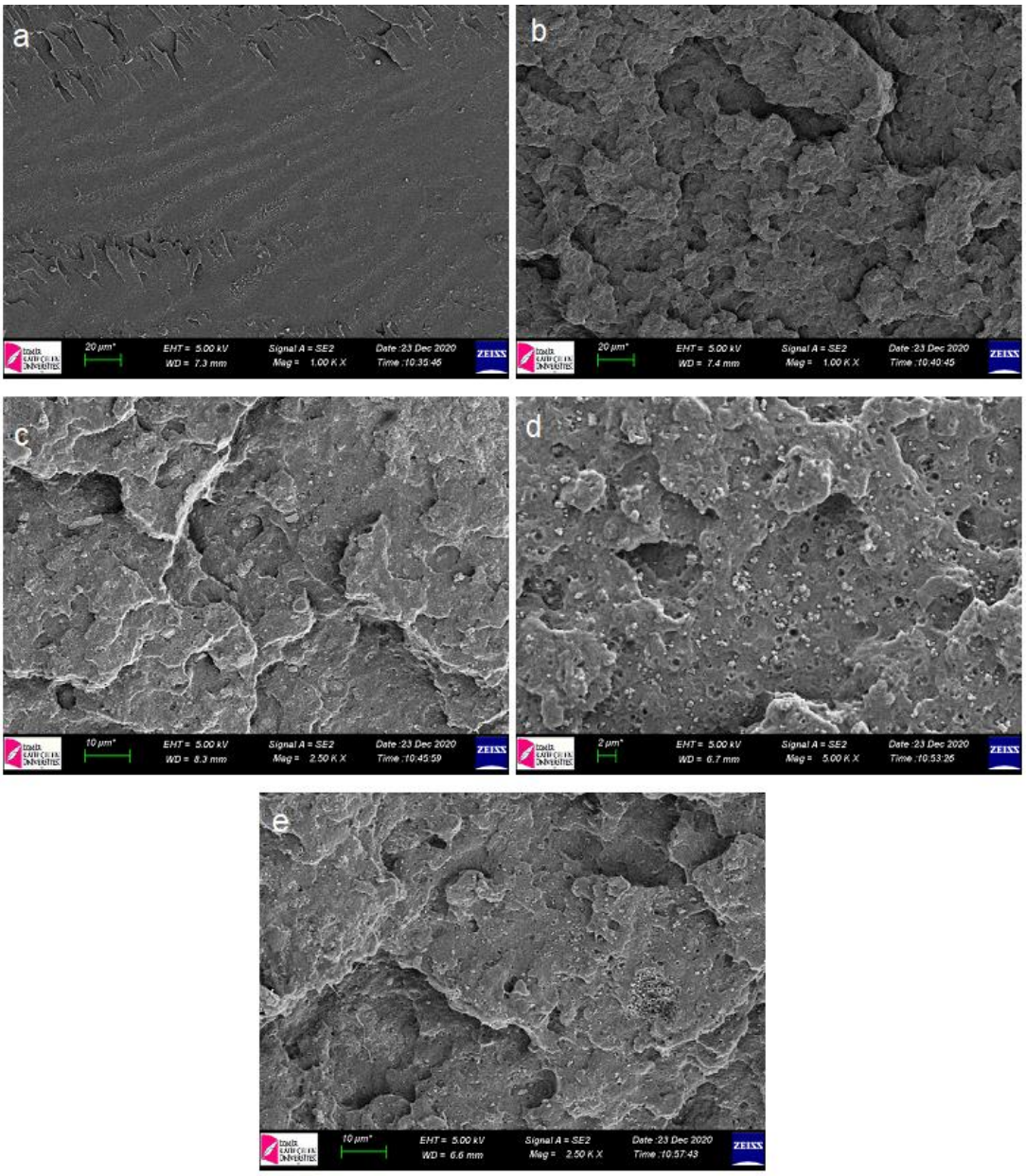

Figure 5.13: SEM images of fractured surface of a) neat PLA, b) PLA Ext., c) PLA-10 HA, d) PLA-10TCP, e) PLA-5HA-5TCP.

When Figure 5.13 c-e is examined, it is seen that HA and TCP particles in PLA-10HA, PLA-10TCP and PLA-5HA-5TCP composites are homogeneously distributed. However, it has been observed that the HA particles in the PLA-10 HA composite are larger than the particles in the other two composites. The difference in mechanical test results is thought to be due to the negative effect of large particles on mechanical properties [130,131].

5.4.9 Inductively Coupled Plasma Mass Spectrometry (ICP-MS)

The chemical constitutions of PLA neat, PLA ext., and PLLA based composites were examined by inductively coupled plasma mass spectrometer (ICP-MS). Chemical contents of PLA neat, PLA ext., and PLLA based composites were tabulated on Table 5.5.

Table 5.5: Chemical constitutions PLA neat, PLA ext., and PLLA based composites.

Elemets	**Unit**	**PLA Neat**	**PLA Ext.**	**PLA-10TCP**	**PLA-10HA**	**PLA-5TCP-5HA**
As	ppm	0.0122	0.0171	0.2620	0.0098	0.0158
Cd	ppm	0.0030	0.0031	0.0066	0.0042	0.0063
Hg	ppm	<0.0001	<0.0001	<0.0001	<0.0001	<0.0001
Pb	ppm	<0.0001	<0.0001	<0.0001	<0.0001	<0.0001

These results showed that both PLA neat, PLA ext. and, PLLA based composites were provide standard specification of for β-TCP for Surgical Implantation which was shown in Table 5.6 [132]. These results also indicated that PLA neat, PLA ext., and PLLA based composites were suitable for using biomedical applications.

Table 5.6: Standard Specification for Beta-Tricalcium Phosphate for Surgical Implantation (ASTM F1088 - 04a (2010)).

Element	**Content (ppm, max)**
Pb	30
Hg	5
As	3
Cd	5

5.4.10 Cytotoxicity Results

The cell viability of Keratinocyte cells exposed of HA, TCP, neat PLA, PLA Ext., and PLA based composites were monitored within 24 h of culturing. As shown in Figure 5.14, viability was not observed below 70% in any experimental group. Materials in all experimental groups are biocompatible.

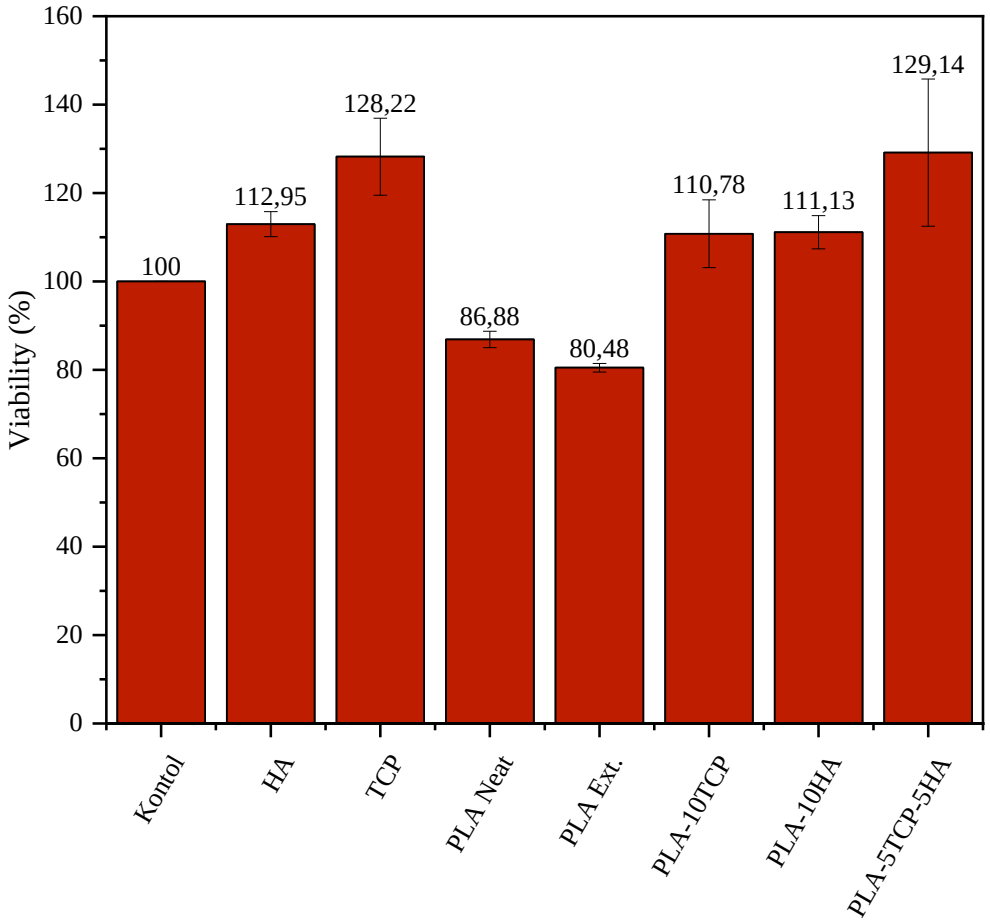

Figure 5.14: Cytotoxicity results of PLA neat, PLA ext., and PLA based composites.

It is thought that the decrease in the viability of PLLA after extrusion process is caused by impurities in the device. The addition of TCP and HA increased the viability of PLA ext. by about 37% and 38%, respectively. This may be related to the nucleating effects of TCP and HA surfaces which provide nucleating sites for the precipitation of calcium phosphate crystals. These crystals potentially have favorable biological effects by providing trace ions [133,134]. The highest increase in viability was observed in PLA-5TCP-5HA and was approximately 60%. This result directly related to the results of DSC analysis. In summary, results seem to indicate that increasing the inorganic content increases the bioactivity characteristics of the PLLA matrix.

5.5 Conclusion

The production and characterization of PLLA and PLLA based composites were carried out in this study. The main conclusions obtained from this study are as follows:

- While neat PLLA showed amorphous behavior, it was observed that extruded PLA and HA / TCP filled composites showed crystalline behavior. The highest crystallinity value was obtained in PLA-5HA-5TCP composite.
- From the contact angle measurements, it was seen that the extrusion process and HA/TCP additive increased the wettability properties of PLLA.
- Addition of TCP and HA increased the viability of PLLA, and the highest cell viability was obtained in composite PLA-5HA-5TCP.
- The extrusion process reduced the tensile and flexural strength of neat PLLA, while the HA / TCP additive increased both the tensile and flexural strength.

Chapter 6

6 Production and Characterization of PLLA/PDLA Blends

6.1 Introduction

Poly (L-lactic acid) (PLLA) is a popular biodegradable and biocompatible polymer derived from renewable resources [135–138], and as such, it has gained increased research in order to improve its reducibility and eco-friendliness. Furthermore, because it is biocompatible and non-toxic, it is regarded as a promising material for widespread usage in biomedical applications such as blood vessel engineering, drug delivery, and scaffolding, and tissue engineering. The usage of PLLA is restricted because of its low melt strength, low service temperature, poor processability, slow crystallization rate, brittleness, and low toughness. The low crystallinity of PLLA applications is a significant disadvantage. Blending PLLA with other polymers is a low-cost and effective method of eliminating these restrictions and modifying the characteristics of the final PLLA-based products for applications [139–142].

The degree of crystallinity of PLLA is known to have a considerable effect on its degradation rate [143,144]. So, understanding the crystallinity of PLLA is very critical [145]. The most successful and promising technology for creating PLLA engineering thermoplastics with better physicochemical qualities is stereo complex crystallization (SC) between PLLA and its enantiomer poly (D-lactic acid) (PDLA), which was initially described in 1987 by Ikaca et al. [146–149]. The melting temperature (Tm) of the stereo complex PLLA/PDLA mix was 230 °C, which was 50 °C higher than that of pure PLLA or PDLA, indicating that SC PLA may have better thermal and mechanical capabilities than pure PLLA [138]. In addition, Tsuji and Ikada found that

stereo complex PLLA/PDLA mixes had significantly higher strength, stiffness, and heat resistance than pure PLLA or PDLA. Tan et al. highlighted recent advances in the application of stereo complexation to improve PLA's thermal and mechanical characteristics [150]. Furthermore, polymer blends play a significant role in the development of novel materials with superior qualities to net polymers. They are also significant from an environmental and economic standpoint [151].

In this chapter, PLLA/PDLA blends were produced in varying proportions, and the most suitable blend ratio was determined mechanically and economically. In addition, thermal properties, crystallographic structures, and bond structures were investigated.

6.2 Materials and Methods

6.2.1 Materials

5.2.1.1 PLLA and PDLA Polymers

PLA homoploymer Luminy L175 (Tm=175^{o}C, ρ=1.24 g/cm3, Melt flow rate (210 ^{o}C/2.16 kg) = 8 g/10 min) and PDLA Luminy D070 (Tm=175 ^{o}C, ρ=1.24 g/cm^{3}, Melt flow rate (210 ^{o}C/2.16 kg) = 20 g/10 min) produced by Total Corbion, were used for blending. Physical and mechanical properties of polymers were shown in Table 6.1.

Table 6.1: Properties of PLLA and PDLA.

Properties			**Luminy D175**	**Luminy D070**
Typical Resin Properties	**Standard**	**Unit**	**Value**	
Melt Flow Rate (210°C, 2.16 kg)	ISO 1133	g/10min	8	20
Density	ISO 1183	g/cm³	1.24	1.24
Tensile Modulus	ISO 527-1	MPa	3500	3500
Tensile strength	ISO 527-1	MPa	50	40
Elongation at yield	ISO 527-1	%	≤5	≤5

6.2.2 Methods

5.2.2.1 Blend Preparation

Melt mixing method was used for the preparation of PLLA/PDLA blends. All blends were prepared by using Lab tech corotating twin screw extruder with a screw speed of 100 rpm and barrel temperatures of about 170–190 °C. L/D ratio of the extruder is selected as 25:1. After passing through the extruder, the polymer strands (3 mm in diameter) entered a water bath and then a pelletizer that produced nominally 3 mm pellets. At the exit of the pelletizer, blend pellets produced had moist due to cooling process after extrusion. The oven was used to eliminate the moisture of the composite pellets. After extrusion, blend pellets were dried in oven for 1 hour at 80 °C. Sample codes of PLLA and blends were shown in Table 6.2.

Table 6.2: Sample codes of PLLA and blends.

Materials	**Sample Codes**
PLLA Extruded	PLLA
PLLA+2.5% PDLA	2.5PDLA
PLLA+5% PDLA	5PDLA
PLLA+7.5% PDLA	7.5PDLA
PLLA+10% PDLA	10PDLA

5.2.2.2 Manufacturing of Composite Plates

The pellets obtained by the extrusion process were molded in a Bole 100 EK II/C340 IM brand injection molding machine with a 20-ton screw diameter of 36 mm and an L/D ratio of 23, after drying in the oven at 80 °C for 2 hours and dehumidifying. Injection molding parameters are given in Table 6.3.

Table 6.3 Injection molding parameters.

Parameters	**Values**
Zone 1 Temperature	160 °C
Zone 2 Temperature	165 °C
Zone 3 Temperature	175 °C
Zone 4 Temperature	175 °C
Zone 5 Temperature	170 °C
Mold Temperature	40 °C
Injection Pressure	95 Bar
Holding Pressure	65 Bar

6.3 Characterization of PLLA/PDLA Blends

6.3.1 Thermogravimetric Analysis (TGA)

Thermogravimetric analyses of the PLLA/PDLA blends were conducted by using thermogravimetric analyzer (TA Instruments, TGAQ500) at a heating rate of 10 °C/ min in the range of 30–600 °C under nitrogen atmosphere.

6.3.2 Differential Scanning Calorimeter (DSC) Analysis

The melting and crystallization behaviors of PLA and PLA-based composites were studied using differential scanning calorimetry (DSC) analysis (DSC Q2000; TA Instruments Inc., USA). Samples were heated from 20 °C to 250 °C at a rate of 10 °C/min in a nitrogen atmosphere to remove any thermal history from processing. The temperature was maintained for five minutes. The samples were then cooled to room temperature at a rate of 10°C/min while being kept in a nitrogen environment.

6.3.3 FTIR-ATR Analysis

FTIR-ATR analyses of the PLLA/PDLA blends were carried out by using Bruker Alpha spectrometer. The analyses were performed in the range of 400–4000 cm^{-1}, with a resolution of 4 cm^{-1} and with an accumulation of 16 scans.

6.3.4 Mechanical Analysis

Tensile tests were conducted in accordance with ASTM D638-10 standard, with specimen type IV. and the crosshead speed of 50 mm/min. Three-point bending test was performed by using ASTM D790 standard with a support span of 32 mm and a deformation rate of 1 mm/min. All tests were performed on universal testing machine having a 5 kN load cell (Shimadzu AGS-X).

6.3.5 Dynamic Mechanical Analysis (DMA)

Storage and loss modulus values of PLLA/PDLA blends were determined by using Dynamic Mechanical Analyzer (TA Instruments Inc., DMA Q800). Single cantilever clamp and multi frequency-strain modulus mode were utilized in DMA analyses which were made in the temperature range from 25 and 150 °C in air atmosphere.

6.4 Results and Discussions

6.4.1 Thermogravimetric Analysis (TGA)

The thermal stability of the PLLA and PLLA/PDLA blends were shown in Figure 6.1 and Table 6.4. While PLLA started to degrade at about 334 °C, PLLA/PDLA blends started to degrade at temperatures of 332.43, 331.95, 323.88 and 321.44 °C, respectively, depending on the increasing PDLA ratio. This indicated that the addition of PDLA in PLLA, which resulted in PLLA/PLDA blend, decreased its onset decomposition temperature and the slight decrease in the PLLA/PDLA blends' thermal stability could have been due to the poor PLLA and PDLA interaction. Particularly, the thermal stability decreased as the composition of PDLA increased, but without any significant changes [152,153].

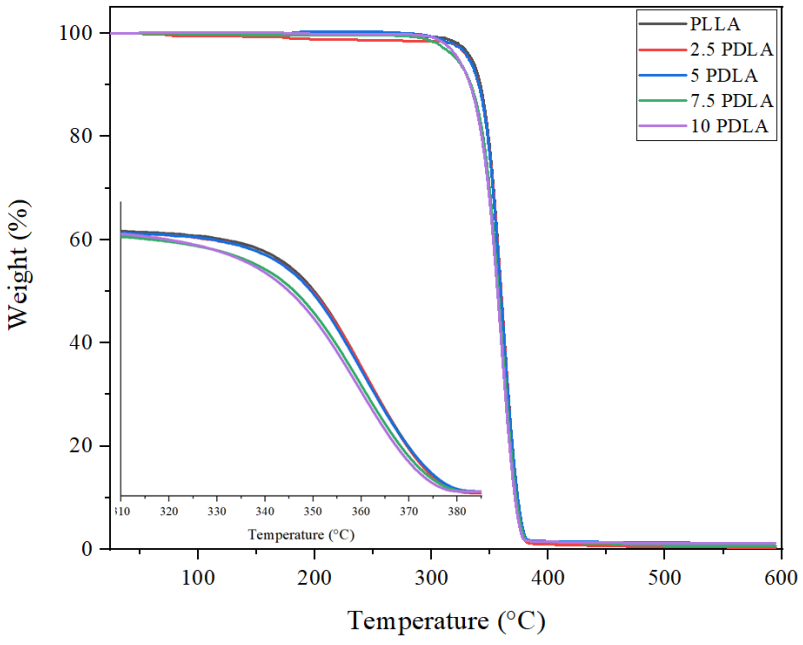

Figure 6.1: TGA graph of PLLA and PLLA/PDLA blends.

Table 6.4: TGA data of PLLA and PLLA/PDLA blends.

Samples	T_{onset} (at 5% degredation) (°C)	T_{max} (°C)	Degraded Weight (%)
PLLA	334.38	361.55	98.68
2.5 PDLA	332.43	360.28	98.70
5 PDLA	331.95	360.39	98.96
7.5 PDLA	323.88	359.89	98.99
10 PDLA	321.44	359.45	99.24

6.4.2 Differential Scanning Calorimeter (DSC) Analysis

DSC curves of PLLA and PLLA/PDLA blends were shown in Figure 6.2. DSC melting and crystallization parameters for PLLA and PLLA/PDLA blends, such as glass transition temperature (T_g), melting temperature (Tm), crystallization temperature (T_c), crystallization enthalpy (ΔH_c), and melting enthalpy (ΔH_m) are presented in Table 6.5. The degree of crystallinity (X_c) of materials was estimated using equation (1) [116].

$$\%Xc \frac{\Delta Hm/\phi PLA}{\Delta Hm^0} x\ 100 \quad (1)$$

where ΔHm^0 is the melting enthalpy of 100% crystalline PLLA assumed to be (93 J/g) and ϕPLA is PLLA weight fractions in the blends.

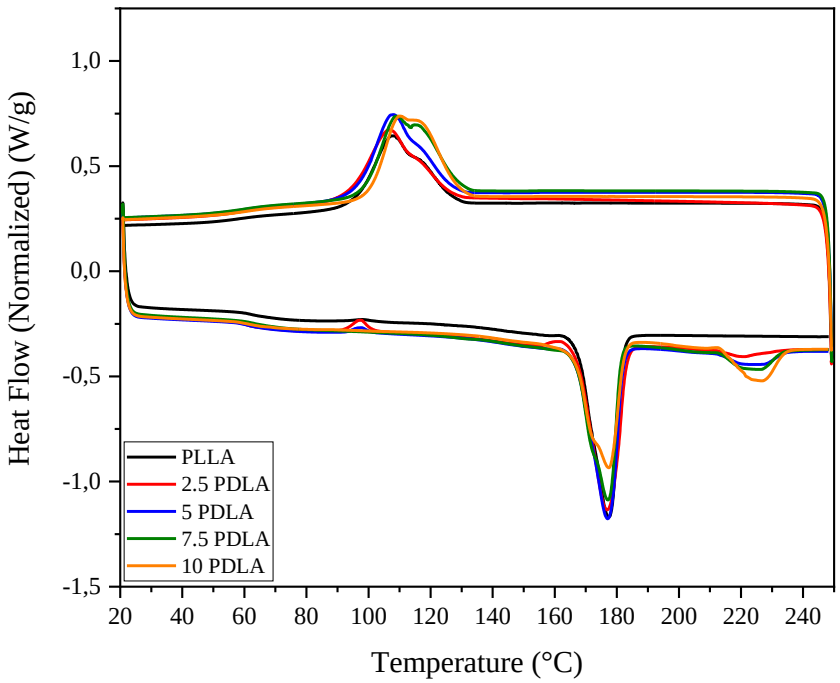

Figure 6.2: DSC curves of PLLA and PLLA/PDLA blends.

From the DSC curves in Figure 6.2, with the addition of PDLA, the crystallization peak temperatures of the blends shift to higher temperature, and these peaks become sharper compared with that of neat PLLA. The results manifest evidently that the formed SC (stereo complex) crystallites improve the crystallization rate of PLLA remarkably due to the heterogeneous nucleating effect of SC crystallites [154]. In addition, it was observed that the crystallinity of PLLA increased with increasing PDLA ratio.

Table 6.5: DSC data of PLLA and PLLA/PDLA blends.

Samples	**T_g (°C)**	**T_c (°C)**	**ΔH_c (j/g)**	**T_{m1} (°C)**	**ΔH_{m1} (j/g)**	**T_{m2} (°C)**	**ΔH_{m1} (j/g)**	**X_c (%)**
PLLA	65.19	107.52	39.86	177.17	46.16	-	-	49.63
2.5 PDLA	61.80	106.48	39.74	176.80	46.54	221.14	1.94	53.47
5 PDLA	61.46	107.90	43.34	177.03	43.11	226.44	5.47	54,98
7.5 PDLA	64.59	108.79	45.07	177.19	41.67	226.07	7.31	56,94
10 PDLA	63.57	109.94	46.68	178.12	38.67	226.49	12.04	60,59

The highest degree of crystallinity was obtained in 10PDLA with approximately 58%. When the effect of the added PDLA concentration on crystallization was examined in detail, it was observed that if the amount of PDLA was 0.3% or more by weight, it had a nucleating effect, but if it was below 0.1% by weight, it acted as an impurity and slowed down the crystallization [155].

6.4.3 FTIR-ATR Analysis

FTIR spectra of PLLA and PLLA/PDLA blends was shown in Figure 6.3. PLLA shows characteristic stretching frequencies for C=O, –CH3 asymmetric, –CH3 symmetric, and C–O, at 1746, 2995, 2946 and 1080 cm^{-1}, respectively [156]. Bending frequencies for –CH3 asymmetric and –CH3 symmetric have been identified at 1452 and 1361 cm^{-1}, respectively. The peaks at about 1750 and 1180 cm^{1}, which belong to the C=O stretching and the C–O–C stretching of PLA, are clearly visible in Figure 6.3. It is known that the PLA chain conformation in stereo complex crystals results in a distinctive vibrational band at 908 cm^{-1} [157,158].

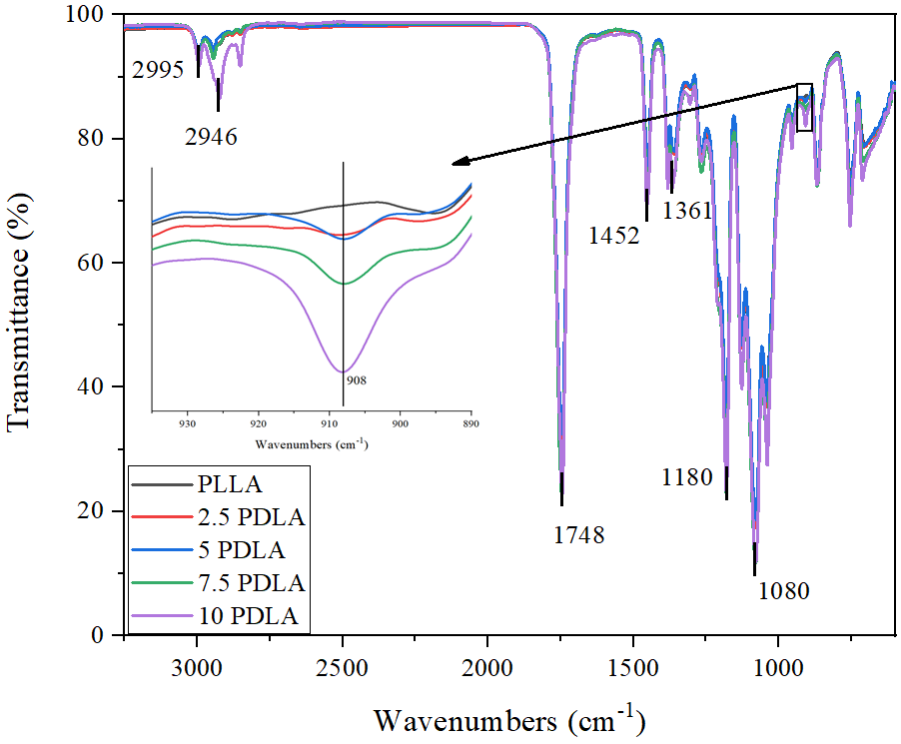

Figure 6.3: FTIR spectra of PLLA and PLLA/PDLA blends.

6.4.4 Mechanical Analysis

5.4.4.1 Tensile Test

Tensile testing results of PLLA and PLLA/PDLA blends were shown in Figure 6.4 and Figure 6.5. According the test results, tensile strengths (MPa) of pure PLLA, 2.5 PDLA, 5 PDLA, 7.5 PDLA, 10 PDLA were obtained to be 64.35, 68.83, 64.45, 61.95 and 56.65, respectively. It was observed that the tensile strength of PLLA increased slightly (approximately 5%) with the addition of 2.5% PDLA and decreased with increasing PDLA content. The mechanical properties of polylactides beyond the elastic region vary depending on both the amount and type of crystalline regions developed during the process. The ductility of pure polylactides may decrease due to the increasing degree of crystallinity, thus causing harder polylactides to form and not reaching high stress values during tensile tests due to lack of ductility [155,159]. This is thought to be an indication that the tensile strength of PLLA first increases up to 2.5% PDLA and then decreases slightly for higher crystallinity.

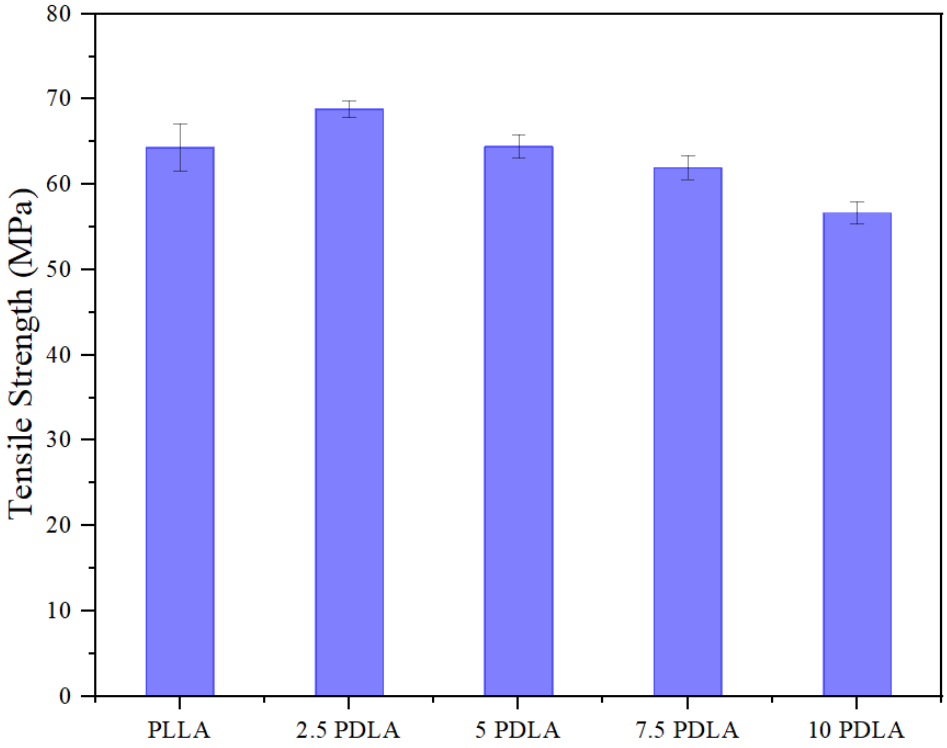

Figure 6.4: Tensile strength results of PLLA and PLLA/PDLA blends.

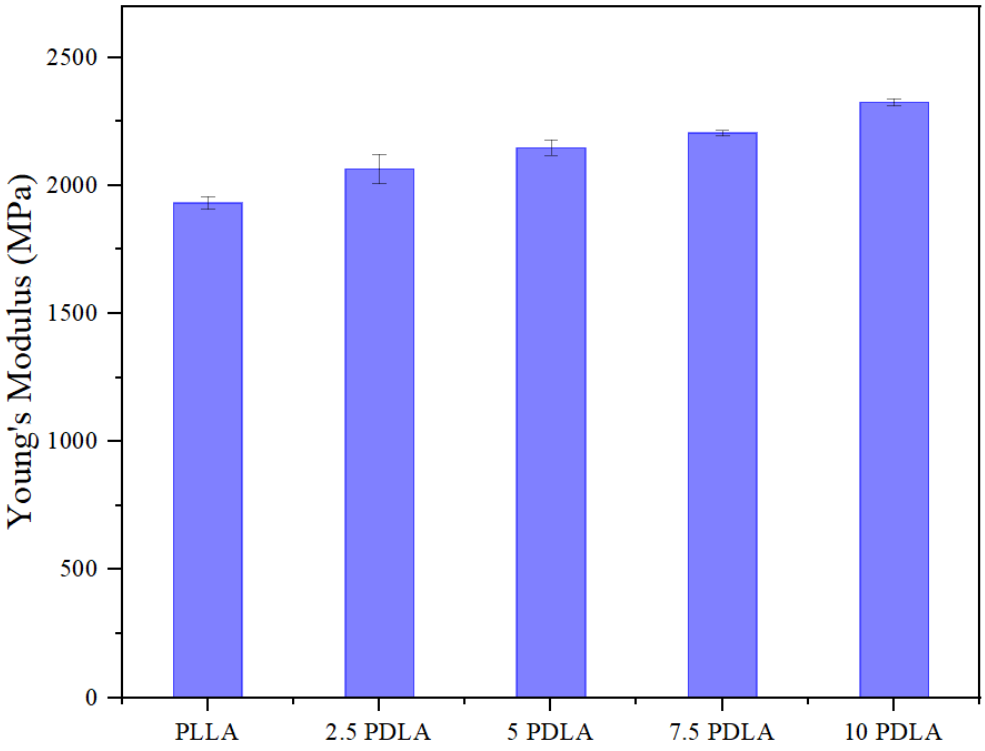

Figure 6.5: Young's modulus results of PLLA and PLLA/PDLA blends.

When the tensile test results are examined, it is seen that the Young's modulus of samples were increased with the increasing PDLA content. These results can be explained by two contributing factors that affect the compaction of polylactide

macromolecules in solid state: crystallinity amount and stereo complexation. As usually encountered in semi crystalline thermoplastics, a higher degree of crystallization means lower content of free volume and therefore an increase of stiffness generally follows [159].

5.4.4.2 Three Point Bending Test

Three-point bending test results of PLLA and PLLA/PDLA blends were shown in Figure 6.6 and Figure 6.7. Just like the tensile test results, the three-point bending results show that the flexural strength of PLLA increases with the addition of 2.5 wt. % PDLA and decreases with higher PDLA content.

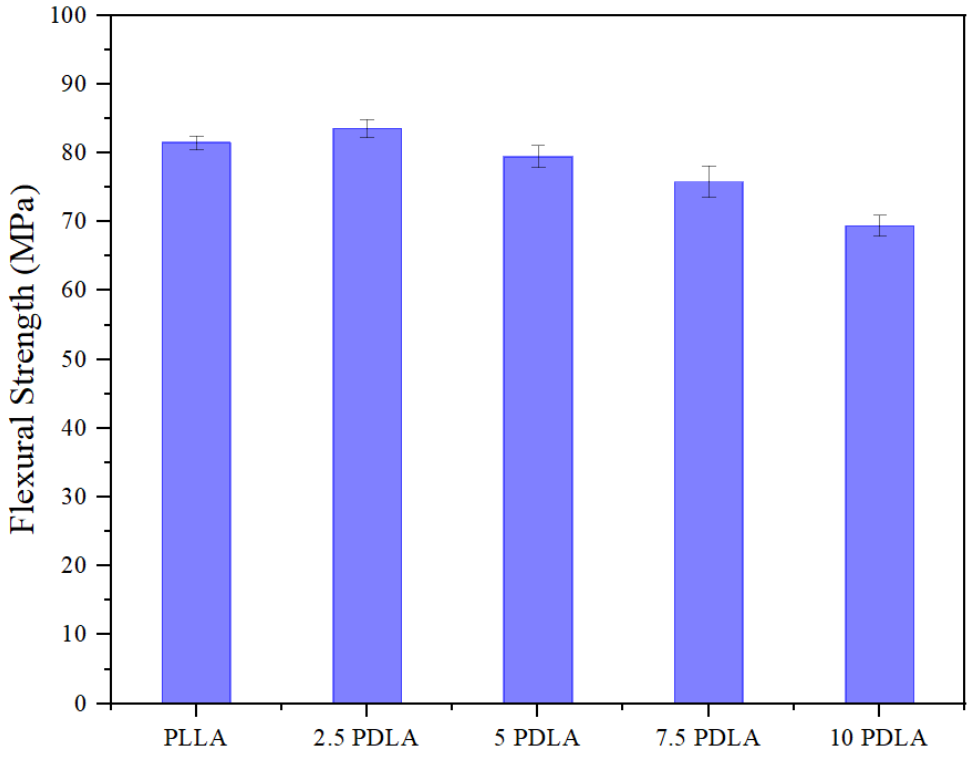

Figure 6.6: Flexural strength results of PLLA and PLLA/PDLA blends.

Similar to the Young's modulus results, it has been observed that the increasing PDLA content into PLLA enhanced the flexural modulus of the material because of stiffness due to the higher crystallinity value [159].

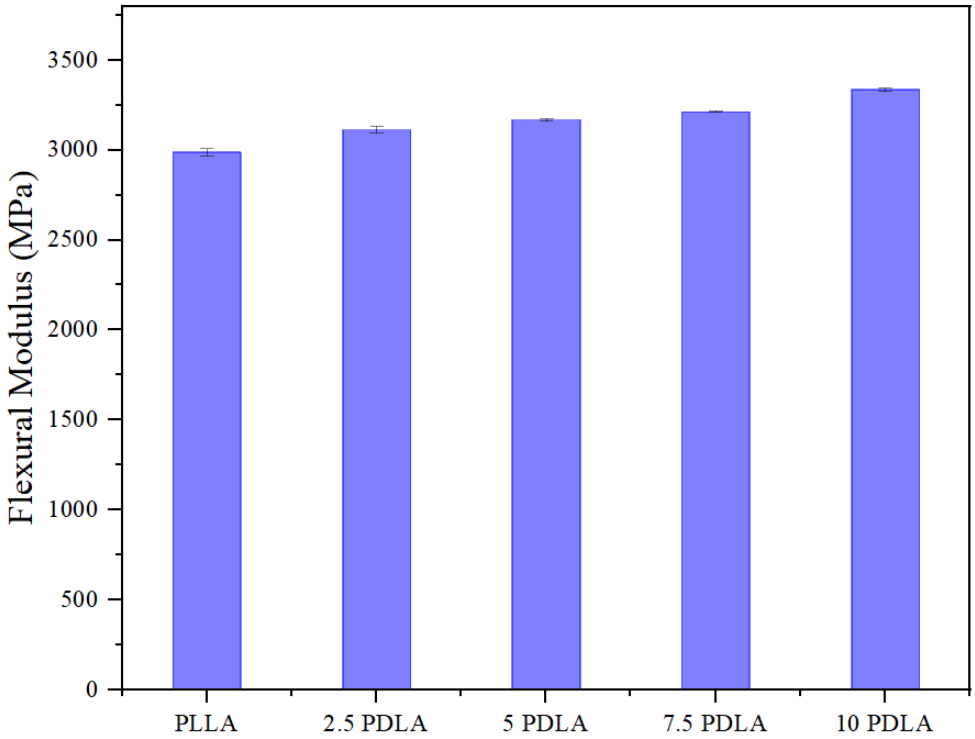

Figure 6.7: Flexural modulus results of PLLA and PLLA/PDLA blends.

6.4.5 Dynamic Mechanical Analysis (DMA)

Storage modulus curves of PLLA and PLLA/PDLA blends were showed in Figure 6.8. As can be seen from Figure 6.8 all the storage modulus curves first keep plateau and then started to decrease quickly because of the glass transition, followed by a slight increase again related to the cold crystallization after 100 °C. The increasing storage moduli at higher temperature is consistent with the above DSC results. In the glassy region, general increased storage moduli can be related to the increasing crystallinities [160]. As expected, the E' plot also highlights the fact that the PLLA/PDLA blends have a higher E' than PLLA at 40 °C, indicating an increased stiffness and the E' increased with an increase in the PDLA content. These results revealed that the intermolecular stereo complexation had cross-linking points and increased the storage modulus [160].

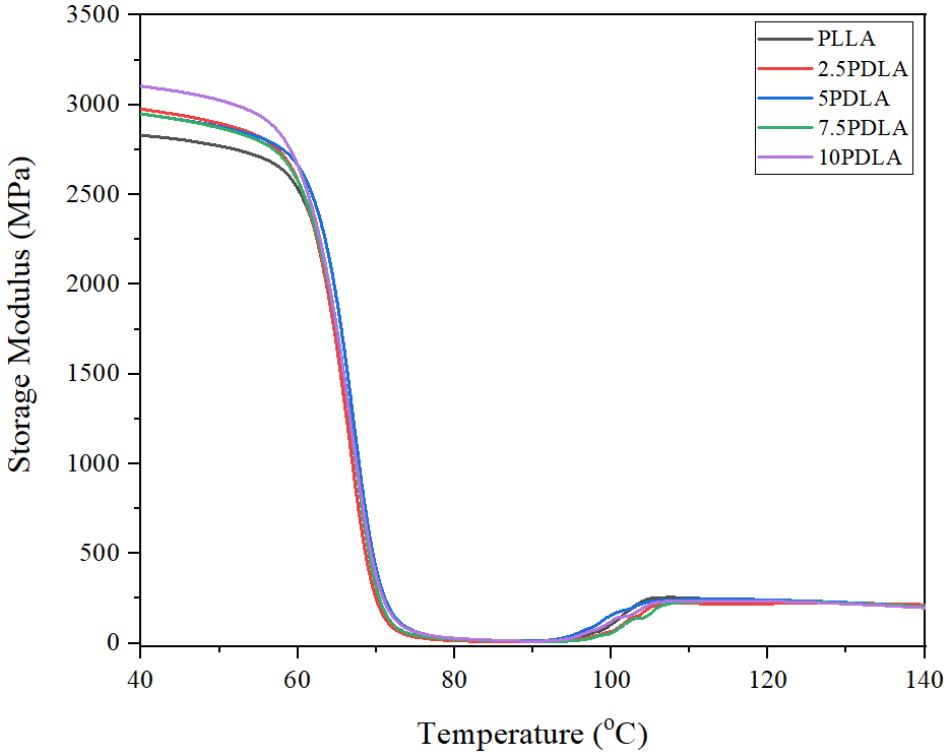

Figure 6.8: Storage modulus curves of PLLA and PLLA/PDLA blends.

Figure 6.9 shows the variation of the tan δ curves of PLLA and PLLA/PDLDA blends with temperature.

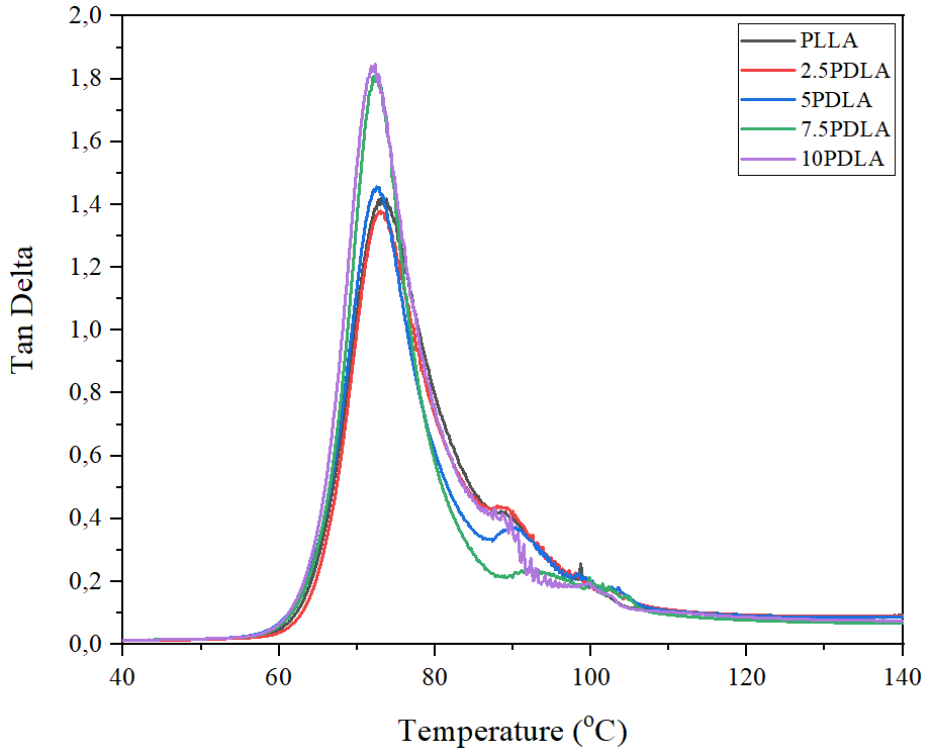

Figure 6.9: Tan δ curves of PLLA and PLLA/PDLA blends.

Similar to the literature [161], the peak at about 71 °C is considered to be the dynamic transition temperature (dynamic T_g) of pure PLLA. T_g (Tan δ peak) peak intensity increased as the crystallinity increased. Therefore, 10PDLA had the highest tan δ peak intensity [160]. This trend was similar to that of the DSC results, in which 10PDLA had the highest crystallinity.

6.5 Conclusion

The results obtained in this chapter where PLLA/PDLA Blend ratios are investigated and analyzed are given below.

- DSC results revealed that stereo complex crystallites significantly increased the crystallization rate of PLLA due to the heterogeneous nucleating action of SC crystallites. The highest degree of crystallinity was obtained in 10PDLA with approximately 58%.
- FTIR analysis results showed that PLLA/PDLA stereo complex structure was formed and increased with increasing PDLA ratio.
- In the DMA results, the highest tan δ peak intensity was obtained by 10 PDLA, this result was similar to the DSC results, in which 10 PDLA had the highest crystallinity.
- In the mechanical analysis results, it was observed that both tensile and flexural modulus values increased in direct proportion with increasing crystallinity. In the mechanical analysis results, it was observed that both tensile and flexural modulus values increased in direct proportion with increasing crystallinity. It was also observed that 2.5 PDLA increased the tensile strength of PLLA by about 5%. Similarly, the highest flexural strength was obtained in 2.5 PDLA.

Chapter 7

7 Production and Characterization of PLLA/PDLA Composite

7.1 Introduction

PLA is available in three enantiomeric forms: poly (L-lactic acid) (PLLA), poly (D-lactic acid) (PDLA), and poly (racemic-lactic acid), each with unique features [162]. By combining PLLA and PDLA, a specific crystalline structure known as a stereo complex may be generated, which is readily formed by melt blending, solution casting, or supercritical fluid processes when mixing two polymers with equal chemical content but differing steric structures [163,164]. This stereo complex-type poly (lactic acid) (sc-PLA) demonstrated a T_m at 230 °C that is approximately 50 °C higher than that of pure PLLA or PDLA, implying that sc-PLA may have superior thermal, mechanical, and hydrolytic stability than PLLA. Since the first publication, researchers have exhaustively investigated the impact of homopolymer molecular weight, blending condition, blending ratio, and optical purity on the formation and properties of stereo complexes [165–173]. Calcium phosphate (CaP) has mostly been employed in the creation of bone tissue scaffolds. Because of their biocompatibility and assistance for the bone healing process, hydroxyapatite and -tricalcium phosphate are becoming more relevant in the biomedical area among the available crystalline CaP. In addition, hydroxyapatite and -tricalcium phosphate are found in the mineral phase of bone [174]. When compared to pure polymer, the addition of CaP into the polymer can improve mechanical qualities. Researchers have been working intensively on HA and B-TCP added PLA composites in recent years [46,63,79,100,109]. It should be noted that Stereo Complex type PLLA/calcium phosphate composites have not yet received much attention.

In this chapter, Production and characterization of hybrid composites containing stereo complex type PLLA and HA and B-TCP were performed. Chemical structure, thermal, mechanical and morphological properties of PLLA/PDLA composite were investigated.

7.2 Materials and Methods

7.2.1 Materials

The specifications for polymers (PLLA and PDLA) and ceramic raw materials (HA and B-TCP) used in this section are given earlier in Chapter 4 and Chapter 5.

7.2.2 Methods

6.2.2.1 Production of Composite

Melt mixing method was used for the production of composite. Composite was prepared by using Lab tech corotating twin screw extruder with a screw speed of 100 rpm and barrel temperatures of about 170–190 °C. L/D ratio of the extruder is selected as 25:1. After passing through the extruder, the polymer strands (3 mm in diameter) entered a water bath and then a pelletizer that produced nominally 3 mm pellets. At the exit of the pelletizer, blend pellets produced had moist due to cooling process after extrusion. The oven was used to eliminate the moisture of the composite pellets. After extrusion, blend pellets were dried in oven for 1 hour at 80 °C. Sample codes of PLLA and composite were shown in Table 7.1.

Table 7.1: Sample codes of PLLA and composite.

Materials	**Sample Codes**
PLLA Extruded	PLLA
PLLA+2.5% PDLA+%5 HA+%5 B-TCP	2.5 PDLA-5HA-5TCP

6.2.2.2 Manufacturing of Composite Plates

The pellets obtained by the extrusion process were molded in a Bole 100 EK II/C340 IM brand injection molding machine with a 20-ton screw diameter of 36 mm and an

L/D ratio of 23, after drying in the oven at 80 °C for 2 hours and dehumidifying. Injection molding parameters are given in Table 7.2.

Table 7.2 Injection molding parameters.

Parameters	Values
Zone 1 Temperature	160 °C
Zone 2 Temperature	165 °C
Zone 3 Temperature	175 °C
Zone 4 Temperature	175 °C
Zone 5 Temperature	170 °C
Mold Temperature	40 °C
Injection Pressure	95 Bar
Holding Pressure	65 Bar

7.3 Characterization of PLLA/PDLA Composite

7.3.1 FTIR-ATR Analysis

FTIR-ATR analyses of the PLLA/PDLA blends were carried out by using Bruker Alpha spectrometer. The analyses were performed in the range of 400–4000 cm^{-1}, with a resolution of 4 cm^{-1} and with an accumulation of 16 scans.

7.3.2 Differential Scanning Calorimeter (DSC) Analysis

Thermal properties were studied by using a DSC (TA Instruments, DSCQ20). Specimens were heated from 20 °C to 250 °C at a rate of 10°C/min under a nitrogen atmosphere and held for 10 min to destroy any residual nuclei before cooling at 20 °C/min.

7.3.3 Mechanical Analysis

Tensile tests were conducted in accordance with ASTM D638-10 standard, with specimen type IV. and the crosshead speed of 50 mm/min. Three-point bending test was performed by using ASTM D790 standard with a support span of 32 mm and a deformation rate of 1 mm/min. All tests were performed on universal testing machine having a 5 kN load cell (Shimadzu AGS-X).

7.4 Results and Discussions

7.4.1 FTIR-ATR Analysis

FTIR spectra of PLLA, 2.5 PDLA, and 2.5 PDLA-5HA-5TCP was shown in Figure 7.1. PLLA has distinctive stretching frequencies of 1746, 2995, 2946, and 1080 cm^{-1} for C=O, -CH3 asymmetric, -CH3 symmetric, and C-O, respectively.

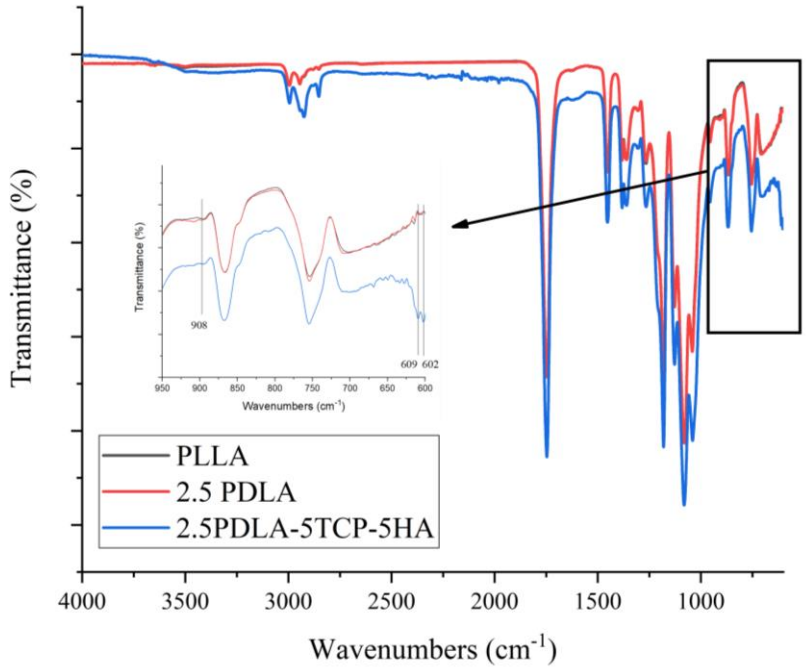

Figure 7.1: FTIR spectra of PLLA, 2.5 PDLA, and 2.5 PDLA-5HA-5TCP.

Bending frequencies for -CH3 asymmetric and -CH3 symmetric have been determined to be 1452 and 1361 cm^{-1}, respectively. Figure 7.1 clearly shows the peaks at roughly 1750 and 1180 cm^{-1} that correspond to the C=O stretching and the C-O-C stretching of PLA. The bands 600 cm^{-1} associated with the V4 vibration mode [46,114] emphasize the existence of phosphate group PO_4^{-3}, which is derived from HA and β-TCP.

7.4.2 Differential Scanning Calorimeter (DSC) Analysis

DSC curves of PLLA, 2.5 PDLA and 2.5PDLA-5HA-5TCP were shown in Figure 7.2. DSC melting and crystallization parameters for PLLA and PLLA/PDLA blends, such as glass transition temperature (T_g), melting temperature (T_m), crystallization

temperature (T_c), crystallization enthalpy (ΔH_c), and melting enthalpy (ΔH_m) are presented in Table 7.3. The degree of crystallinity (X_c) of materials was estimated using equation (1) [116].

$$\%Xc \frac{\Delta Hm/\phi PLA}{\Delta Hm^0} x\ 100 \quad (1)$$

where ΔHm^0 is the melting enthalpy of 100% crystalline PLLA assumed to be (93 J/g) and ϕPLA is PLLA weight fractions in the materials.

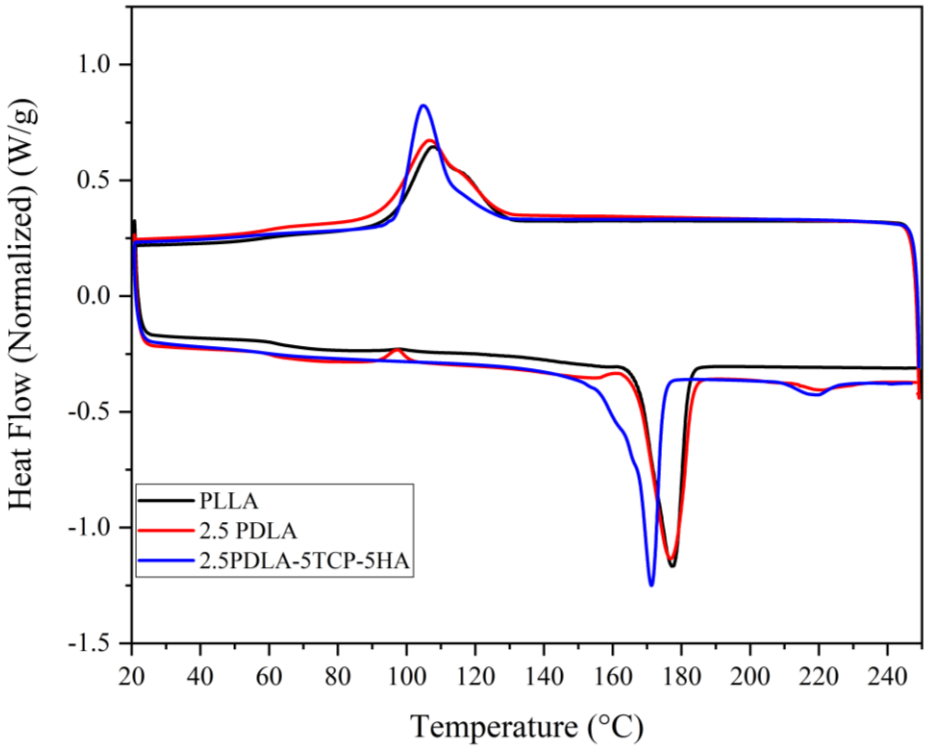

Figure 7.2: DSC curves of PLLA, 2.5 PDLA and 2.5PDLA-5HA-5TCP.

Addition of 5TCP-5HA decreased the T_c, Tm_1 and Tm_2 values by 2 to 5 °C. The reason for this decrease is thought to be due to the restriction of polymer chain movement by HA [99] and the hydrolysis of TCP to PLLA [175,176]. An increase in X_c value was observed because the addition of PDLA caused the formation of SC and the addition of HA and TCP had a nucleating effect [154].

Table 7.3: DSC data of PLLA, 2.5 PDLA and 2.5PDLA-5HA-5TCP.

Samples	**T_g (°C)**	**T_c (°C)**	**ΔH_c (j/g)**	**Tm_1 (°C)**	**ΔHm_1 (j/g)**	**Tm_2 (°C)**	**ΔHm_2 (j/g)**	**X_c (%)**
PLLA	65.19	107.52	39.86	177.17	46.16	-	-	49.63
2.5 PDLA	61.8	106.48	39.74	176.8	46.54	221.14	1.94	53.47
2.5 PDLA-5TCP-5HA	58.81	104.80	39.37	171.28	42.45	219.35	3.13	56.01

7.4.3 Mechanical Analysis

6.4.3.1 Tensile Test

Tensile testing results of PLLA, 2.5 PDLA, and 2.5 PDLA-5HA-5TCP were shown in Figure 7.3 and Figure 7.4. From the test results, tensile strengths (MPa) of PLLA, 2.5 PDLA, and 2.5 PDLA-5HA-5TCP were obtained to be 64.35, 68.83, and 81.80, respectively.

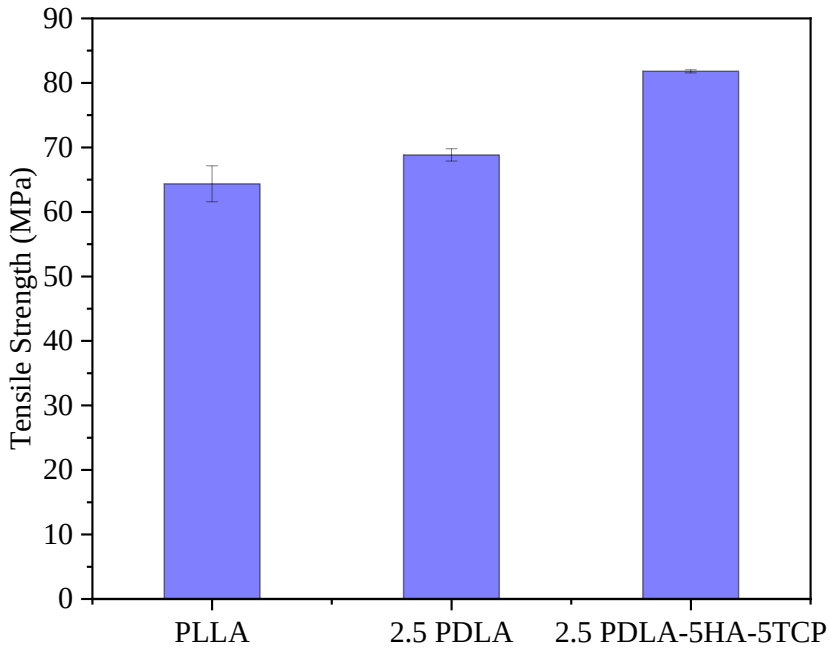

Figure 7.3: Tensile strength results of PLLA, 2.5 PDLA, and 2.5 PDLA-5HA-5TCP

When the test results were examined, it was observed that the highest tensile strength was obtained at 2.5PDLA-5HA-5TCP. An approximately 27% increase in tensile strength of PLLA was obtained with the final composition, 2.5PDLA-5HA-5TCP. The

reason for this increase is thought to be due to the homogeneous distribution of HA and TCP particles and the stereo complex structure formed as a result of the addition of PDLA with its high wettability, as explained in the previous sections [121,154,159].

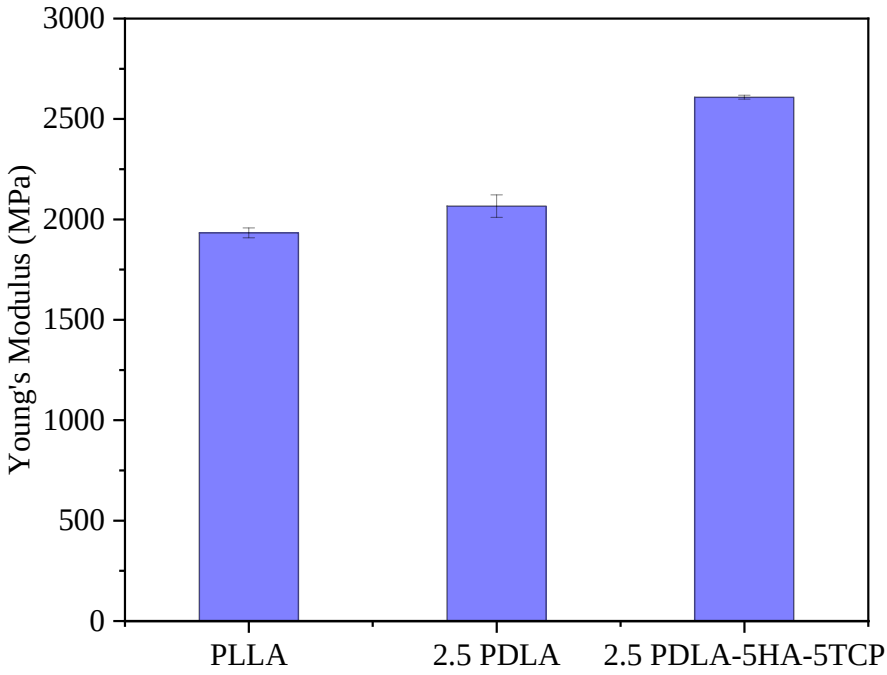

Figure 7.4: Young's modulus results of PLLA, 2.5 PDLA, and 2.5 PDLA-5HA-5TCP.

As can be seen from Figure 7.4, the highest modulus value of approximately 2600 MPa was obtained in the final composition 2.5 PDLA-5HA-5TCP. This increase is thought to be due to two main reasons. First, HA and β-TCP particles are more rigid than PLLA. The second is crystallinity, which increases with the formation of stereo complex structure [121,152,155,163].

6.4.3.2 Three Point Bending Test

Three-point bending testing results of PLLA, 2.5 PDLA, and 2.5 PDLA-5HA-5TCP were shown in Figure 7.5 and Figure 7.6. It can be seen from Figures that the best mechanical properties are obtained in 2.5PDLA-5HA-5TCP, similar to the tensile test results. It has been observed that blending with PDLA, adding HA and β-TCP particles produces an increase of approximately 20% in the bending strength of PLLA. The flexural modulus values were also obtained in a similar trend with the modulus values obtained in the tensile test.

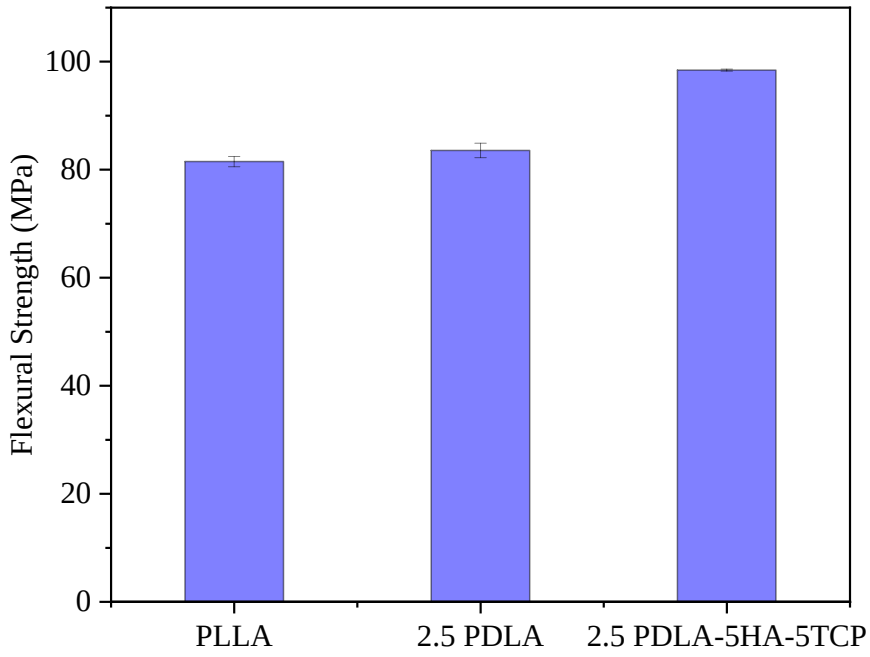

Figure 7.5: Flexural strength results of PLLA, 2.5 PDLA, and 2.5 PDLA-5HA-5TCP.

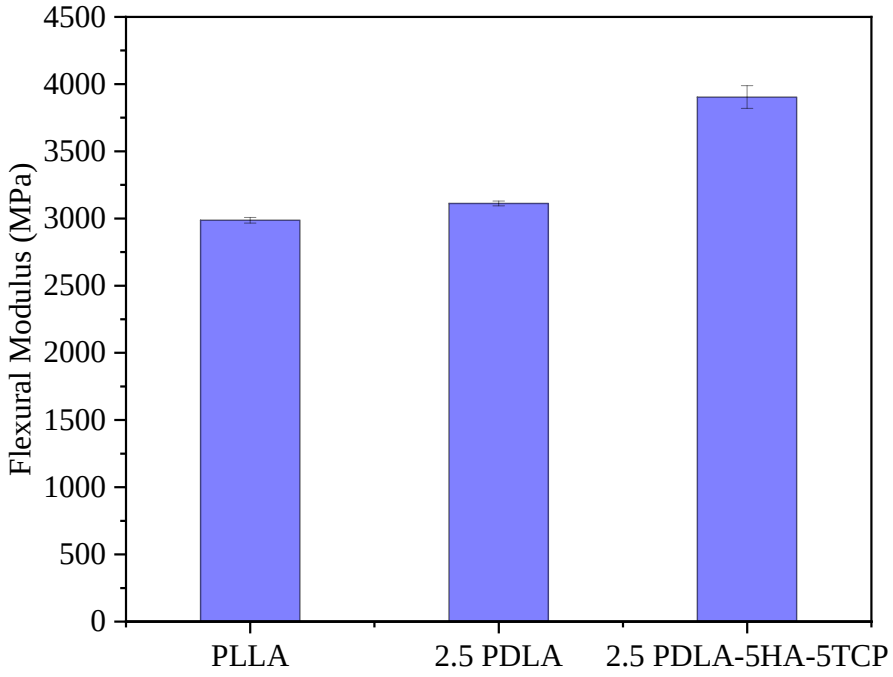

Figure 7.6: Flexural modulus results of PLLA, 2.5 PDLA, and 2.5 PDLA-5HA-5TCP.

7.5 Conclusion

As a result of the production of PLLA/PDLA composites, the aim of increasing the mechanical properties, which is the first of the two main objectives for the thesis study, was successfully achieved. As the first step of realizing the final composition obtained for use in the medical field, implant screw prototype productions were carried out using a plastic injection device. The different sizes of implant screw materials produced are shown in Figure 7.7.

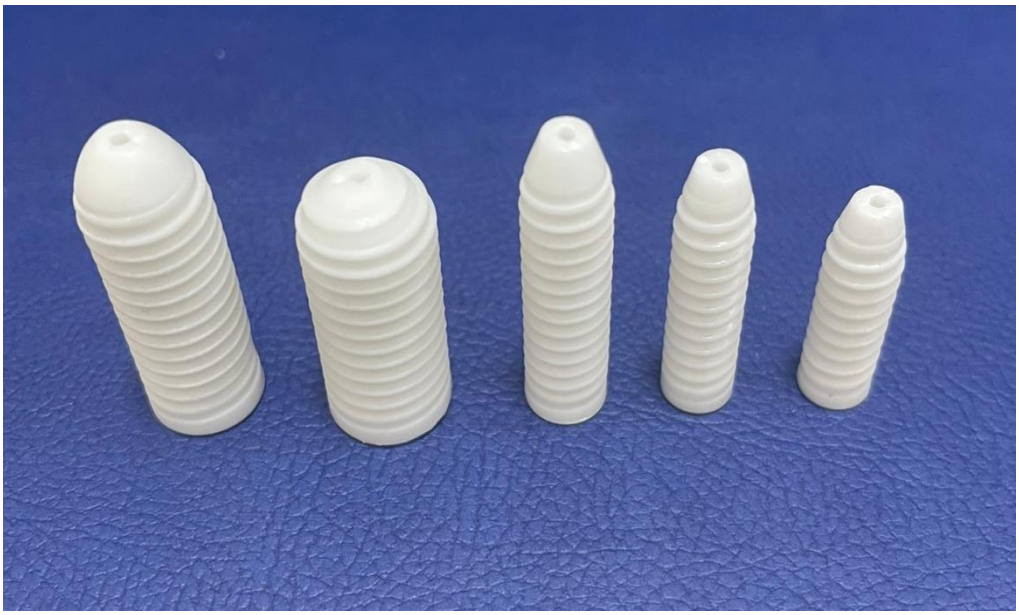

Figure 7.7: The different sizes of implant screw materials.

Chapter 8

8 Peptide Coating and Biomedical Characterization of PLLA/PDLA Composite

8.1 Introduction

Peptides are defined as the short chains of amino acids attached via peptide bonds. Apart from proteins, peptide molecules are crucial modifiers of polymer scaffolds. Peptide-modified biomaterials show structural and biological features similar to that of protein-modified scaffolds. However, peptides have a greater number of advantages than proteins [177]. For functionalization of biomaterial surfaces, utilization of peptides rather than native proteins possesses some advantageous features such as that they might be synthesized synthetically and this provides a certain control over chemical composition of them, thus prevents pathogenic contamination. Also, peptide molecules have more resistance to denaturation reasoned by pH or temperature changes. Furthermore, manipulation of peptides is easier throughout the grafting process [178].

When tissue engineering scaffolds are modified by using bioactive molecules like extracellular matrix (ECM) proteins or peptides, this type of modification might induce some intended signaling pathways in cells, and therefore increase the functionality of scaffold constructs [179]. Biomimetic peptides are promising molecules to develop bioactive material surfaces in tissue engineering field for repair and regeneration of tissues. Sequences derived from the active parts of soluble or ECM proteins might be utilized for modifying and functionalizing the biomaterials that are utilized as scaffold

constructs for the growth of new tissue in order for either directing the cell adhesion or being released like soluble ligands [180].

Modification of scaffold surfaces with bioactive and biomimetic peptides might ensure biological ligands which could increase attachment, reproduction, and differentiation of cells, and cell-scaffold interactions [179]. Although polymer scaffolds are usually non-toxic, in some situations, they might not ensure proper support for cells attachment, reproduction, and differentiation, and this decelerates regeneration of tissue. For enhancing biological features, scaffold constructs are augmented by bioactive molecules, ECM proteins, adhesive peptides, hormones, and etc. [177].

Bioactive molecules are the biological factors or signals which increase the features of scaffolds, assist the activities of cells, and thus causing to better and effective regeneration of certain type of tissue. As a result, augmenting polymer scaffolds by bioactive elements encourages biocompatibility, via causing to enhanced attachment, proliferation, and differentiation of cells [177]. Combining peptides which imitate the functions of ECM proteins with polymer scaffolds ends up with the enrichment of biomaterials with specific sequences, triggering cell adhesion or stimulating cell signaling pathways [177,181]. Furthermore, addition of proteins and/or peptides to polymer scaffolds influences the physicochemical properties such as surface wettability and charge, mechanical features, and degradability of them, and those properties closely affect the biomaterials biological activities [177].

It has been demonstrated that peptide-modified bone tissue materials could encourage new bone creation more influentially when compared to conventional types [178]. Onak et al. conjugated the aspartic acid (ASP) and glutamic acid (GLU) templated peptides on poly (lactic-co-glycolic acid) (PLGA) electrospun nanofibers, and investigated the effect of these scaffolds on human bone marrow-derived mesenchymal stem cells (hMSCs) osteogenic differentiation. It was reported that conjugation of biomimetic ASP templated peptide molecules showed enhanced alkaline phosphatase (ALP) activity, calcium content, and expression of key osteogenic markers such as collagen type I (Col-I), osteocalcin (OC), and osteopontin (OP) [179].

8.2 Materials and Methods

Cold Atmospheric Plasma (CAP) was applied on PLLA composite materials at 40 kV of output voltage and 20 kHz of frequency for 120 seconds with a fixed 2.5 mm discharge gap. For conjugating the peptide on PLLA composite materials, firstly we prepared a 0.1 M 2-Morpholinoethanesulfonic acid (MES) buffer at pH 6.5. 1-ethyl-3-(3- dimethylaminopropyl)-carbodiimide and N-hydroxy succinimide (EDC/ NHS) chemistry was used for surface modification. 2 mM EDC and 5 mM NHS were made prepared in 0.1 M MES buffer. PLLA materials were incubated in EDC/NHS solution in MES buffer during 40 minutes in the incubator at 37 °C. Later on, PLLA materials were washed with Phosphate Buffer Solution (PBS) for two times. Following this step, 1 mM peptide was dissolved in sterile PBS, and materials were incubated in this peptide solution at 4 °C for 24 hours. PLLA materials were washed with PBS before characterization steps.

8.3 Characterization of PLLA/PDLA Composite

8.3.1 Contact Angle Measurement

For assessing the effect of plasma treatment for 30 s, 45 s, 60 s, 90 s, 120 s, 150 s, and 180 s on hydrophilicity, we performed water contact angle measurements by utilizing KSV Attension Teta goniometer (Biolin Scientific, Stockholm, Sweden). In brief, we dropped 4 μL deionized water onto the plasma treated-PLLA material surface, photographed and then the contact angle (θ) was calculated

8.3.2 FTIR Analysis

For obtaining Fourier-Transform Infrared Spectroscopy (FTIR) spectra of PLLA materials, a Nicolet iS5 spectrometer (Termo Scientific, Madison, WI, USA) with a spectral resolution of 4 cm^{-1} was utilized. This spectrometer was equipped by an iD5 attenuated total refection (ATR) accessory having a diamond crystal, collecting 16 scans between 400–4000 cm^{-1}.

8.3.3 SEM Analysis

To image the PLLA-based materials, a Scanning Electron Microscope (SEM; Carl Zeiss Microscopy, Germany) was used at 3kV accelerating voltage following the coating with gold (QUORUM; Q150 RES; East Sussex; United Kingdom) at 20 mA during 60 seconds.

8.3.4 Immunofluorescent Staining

For immunofluorescence staining assay, first we washed the cell-seeded blend, composite, and composite-peptide samples in PBS for two times, and they are fixed with 4% paraformaldehyde (Sigma Aldrich, St. Louis, MO, USA) at 4 °C during 30 minutes. Then, all the samples were kept in 0.1% Triton X-100 in PBS for 1 hour and blocked with 1.5% bovine serum albumin (BSA) in PBS for 2 hours. In the next step, we incubated the samples with primary antibodies in PBS containing 1% BSA overnight at 4 °C based on the manufacturer's directives. Utilized primary antibodies (Santa Cruz Biotechnology Inc., Santa Cruz, California, USA) involved mouse monoclonal antibody against COL-1 (cat. no sc-59772; 1:50), mouse monoclonal against OP antibody (cat. no. sc-21742; 1:50), and mouse monoclonal antibody against OC (cat. no. sc-365797; 1:500). In the day after, fluorescence secondary antibody (Santa Cruz Biotechnology Inc., Santa Cruz, California, USA) which is m-IgG kappa BP-PE (cat. no. sc-21742; 1:200) was diluted with 1% BSA, and added on samples. It is important to note that each of the samples was stained by 4,6-diamidino-2-phenylindole (DAPI, Sigma Aldrich, St. Louis, MO, USA) for imaging the cell nuclei and one of the antibodies for COL-I, OC, and OP. Lastly, expression patterns of COL-1, OP, and OC with same exposure time and light intensity was observed by taking images with an inverted fluorescence microscope (Olympus CKX41, Tokyo, Japan).

8.3.5 Live and Dead Staining

To analyze the cell viability of hMSCs seeded on blend, composite, and composite-peptide materials, Live and Dead staining assay was performed on Day 7 of cell cultivation. Live and Dead staining assay was evaluated by using the Viability/Cytotoxicity Assay Kit for Animal Live and Dead Cells (Biotium, Inc.

Hayward, MN, USA) based on the instructions of manufacturer. First, the growth medium was removed from hMSC-seeded PLLA materials, and hMSCs were washed twice with PBS. Next, the viability/cytotoxicity assay solution, including 5 μL Calcein acetoxymethyl ester (Calcein AM; 4 mM) and 20 μL Ethidium homodimer III (EthD-III; 2 mM) in 10 mL PBS, was added on hMSCs in 96 well-plates. Then, cells were incubated in the incubator for 45 minutes. After incubation period, staining solution was removed from cells, and they were washed with PBS again for one time. For producing fluorescent images of stained hMSCs, a fluorescence microscope (Olympus CKX41, Tokyo, Japan) was used. Lastly, live cells (green) that are stained by Calcein AM and dead cells (red) that are stained by EthD-III, were imaged by the microscope.

8.3.6 Osteogenic Differentiation of hMSCs on PLLA-based Materials

At each time point (7, 14, and 21 days), hMSCs-seeded PLLA-based materials were rinsed with PBS, and lysed by 10 mM Tris supplemented with 0.2% Triton in PBS. These lysed samples were utilized for measuring the DNA content, and ALP activity. Double-stranded DNA content, and ALPase activity of the samples were measured with DNA Quantification Kit (Sigma Aldrich, St. Louis, MO, USA), and QuantiChrom ALPase assay (Bioassay Systems, Hayward, CA, USA), respectively based on the instructions of manufacturer as beforehand explained [182].

In brief, first we prepared bisbenzimide H 33258 Solution and added on lysed samples found in 96-well plate. Fluorescence (excited at a wavelength of 360 nm) was measured by utilizing a spectrophotometer (Bio Tek, Winooski, VT, USA) at an emission wavelength of 460 nm, at ambient temperature. Then, we assessed the ALP activity by p-nitrophenyl phosphate (pNPP) at 405 nm in alkaline solution by utilizing the ALP kit. At this stage, 50 μL of lysed sample to 200 μL of total reaction volume were utilized for starting the reaction with the addition of assay buffer, 5 mM magnesium acetate, and 10 mM pNPP in a 96-well plate. Optical density (OD) at 405 nm was measured at initial time (t=0) and after 4 min (t=4 min) on multiplate reader (bio Tek, Winooski, VT, USA). The measured ALP activities were normalized to cell numbers via division to DNA contents at every time point.

8.4 Results and Discussions

8.4.1 Contact Angle Measurement

The effect of CAP treatment for 0, 30, 45, 60, 90, 120, 150 and 180 s on hydrophilicity of the PLLA composite materials was evaluated by using water contact angle measurement as shown in Figure A-H.

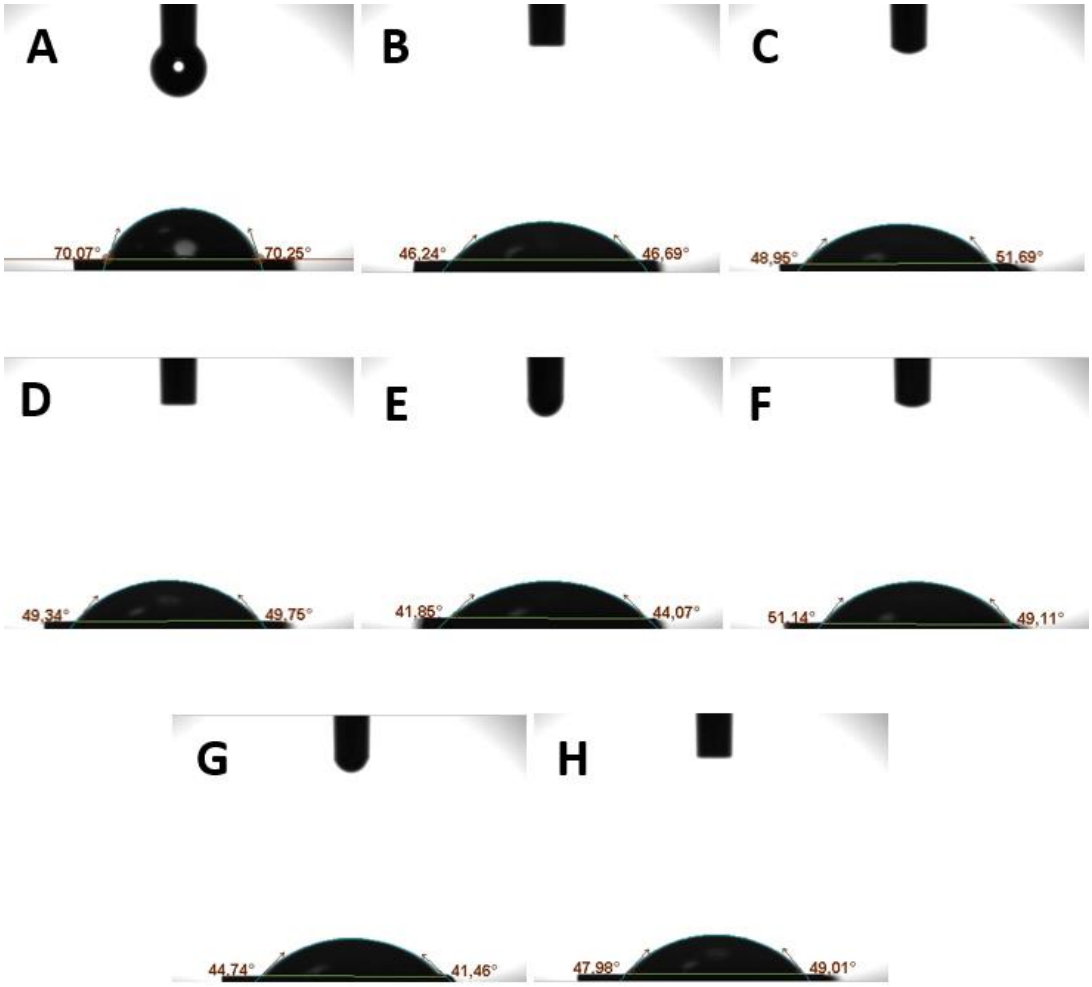

Figure 8.1:Water contact angles of plasma treated PLLA composite materials. A) 0 s, B) 30 s, C) 45 s, D) 60 s, E) 90 s, F) 120 s, G) 150 s, H) 180 s CAP treated PLLA composite materials.

In Figure 8.1 A, CAP treatment was not applied to the composite materials. After applying CAP treatment for 30 s, a decrease in water contact angle was observed. For increasing the peptide conjugation to composite material surface, maximizing and reproducing the -COOH groups introduction to PLLA composite materials with no loss of integrity is very crucial.

Also, when FTIR measurement was performed for 90 s and 120 s CAP treated composite materials, it was observed that the peaks corresponding to -COOH groups were clearer for 120 s. Therefore, 120 seconds was selected as the optimum CAP treatment duration in subsequent experiments.

8.4.2 FTIR Analysis

FTIR spectroscopy was utilized for confirming the surface functionalization by CAP treatment and after peptide conjugation. Figure 8.2 demonstrated the FTIR spectra of PLLA blend (Blend), PLLA composite (Composite), 120 s plasma treated composite (Composite-Plasma), and 120 s plasma treated GLU peptide conjugated composite (Composite-Peptide) materials.

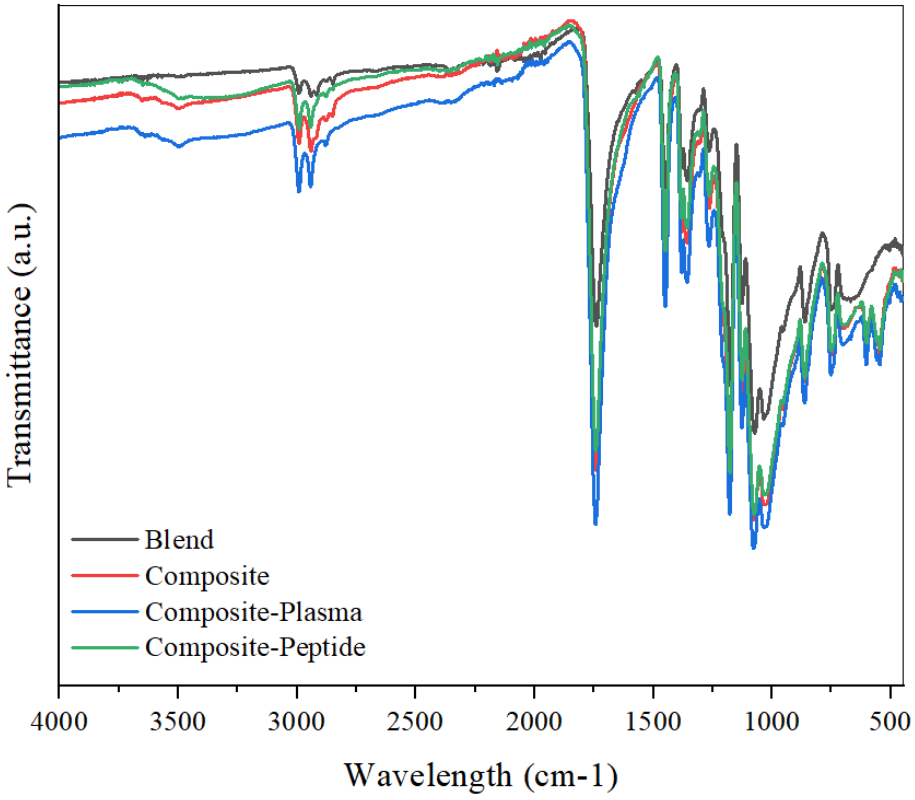

Figure 8.2: FTIR spectra for Blend, Composite, Composite-Plasma, and Composite-Peptide.

Broad band occurred at around 3600 and 3000 cm^{-1} because of the existence of hydroxyl and alkyl groups. Also, bands between 1420–1400 cm^{-1} and 900–690 cm^{-1} were assigned to the CH_2, CH_3, and CH bending vibrations. Moreover, strong stretching bands because of asymmetric and symmetric C-C(=O)-O vibrations were seen around 1200–1150 cm^{-1} [183].

Furthermore, C-O-C bending bands occurred at the 560–520 cm^{-1} area. As can be seen in Figure, transmittance intensity of composite material enhanced by expose to CAP, showing the incorporation of oxygen-containing groups like carbonyl and carboxyl groups on the surface of material [184,185]. Also, the similar situation was observed for CAP treated peptide conjugated composite material. For the peptide conjugated composite materials, in bands at 3600–3000 cm^{-1} and 1460–1240 cm^{-1}, a variation was appeared due to the nitrogen introduction following the peptide conjugation. Altogether, such functionalization of composite material surface indicates the favorable effect of CAP application on peptide conjugation.

8.4.3 SEM Analysis

SEM images of PLLA-based materials are given in Figure 8.3. As can be understood from these images, in Figure 8.3 A, a smooth surface of PLLA blend material was observed. On the other hand, in Figure 8.3 B, there are some small point particles on the surface, and these are because of the HA and TCP additive materials.

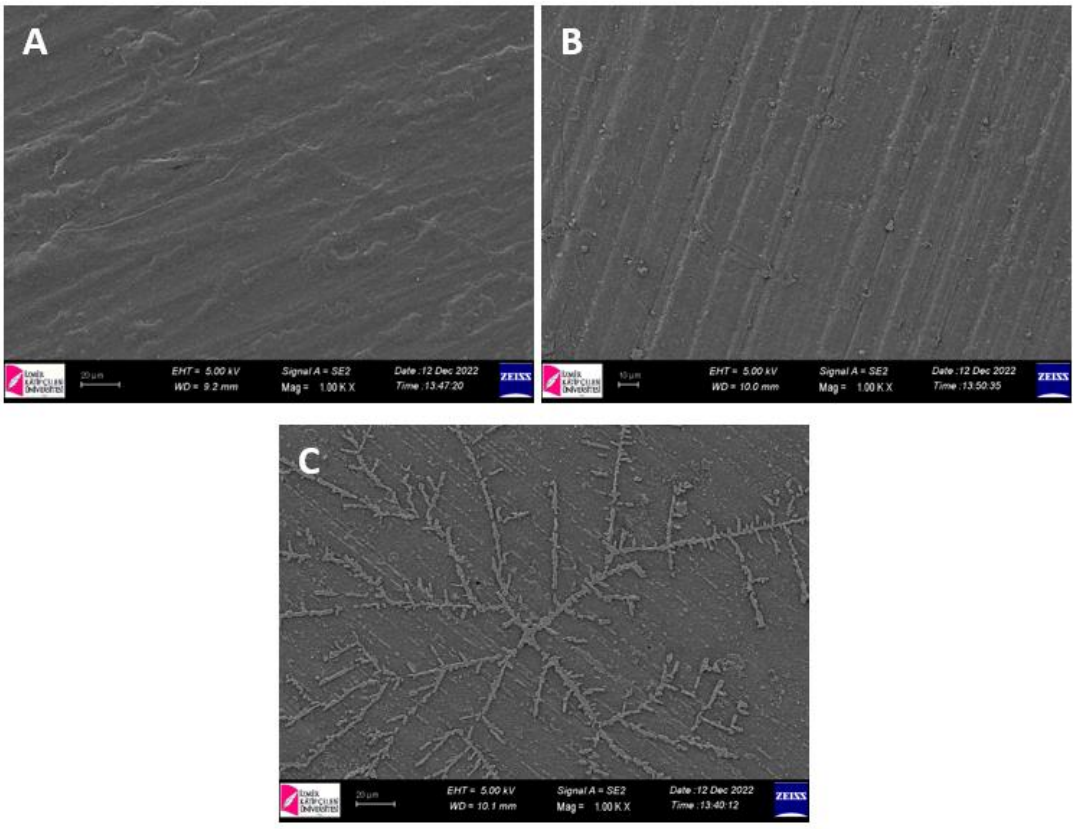

Figure 8.3: SEM images of A) Blend, B) Composite, C) Composite-Peptide materials.

Moreover, a SEM image of EEEEEE peptide conjugated-PLLA composite material was given in Figure 8.3 C, and it can be clearly observed that the PLLA composite material surface is covered with a thin layer of EEEEEE peptide material after peptide conjugation. Overall, as seen in these figures, the morphology of composite material was changed after peptide conjugation, and these SEM images show that EEEEEE peptide was successfully conjugated on the surface of PLLA composite material.

8.4.4 Immunofluorescent Staining

Throughout the osteogenic differentiation period, COL-I is known to mineralize in the existence of calcium ions into calcium phosphate, which forms nearly 70% of bone matrix, while enzyme ALP, OP, and OC proteins mediate nucleation and stabilization of calcium phosphate crystals [186]. In this study, hMSCs osteogenic differentiation was also assessed by characterizing the expression patterns of osteogenic markers such as COL-1, OP, and OC using immunofluorescent staining. Immunofluorescent staining images of hMSCs seeded on blend, composite, and composite-peptide samples are demonstrated in Figure 8.4.

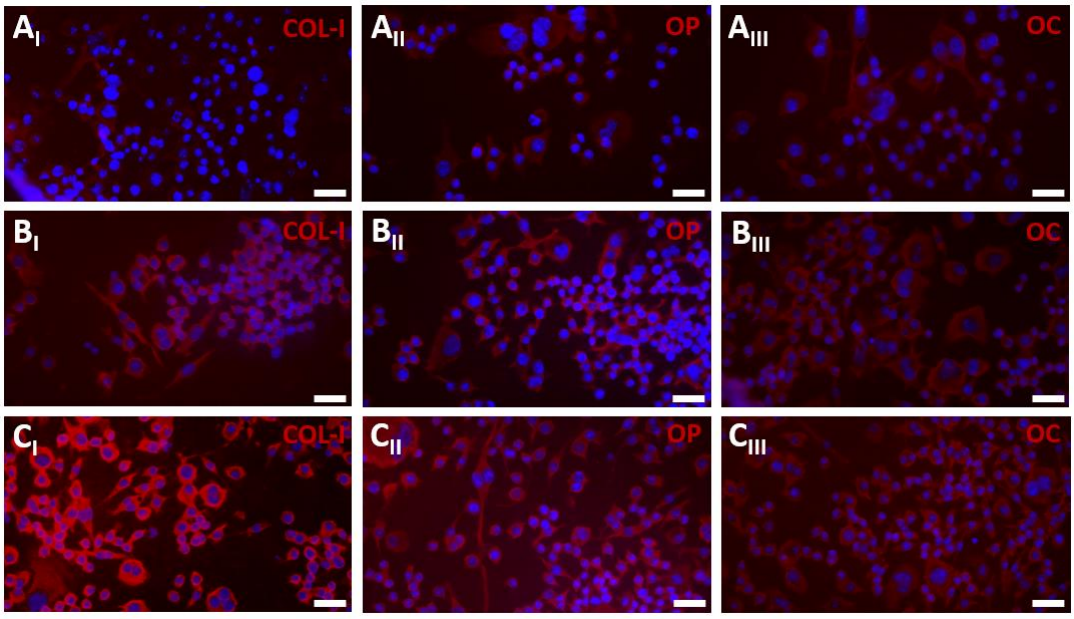

Figure 8.4: Expression patterns of osteogenic markers collagen type 1 (COL-I) (red, first column), osteopontin (OP) (red, second column), and osteocalcin (OC) (red, third column) for hMSCs seeded on blend (AI–III), composite (BI–III), and composite-peptide (CI–III) samples after 21 day of incubation in osteogenic culture medium. In those images, cell nuclei were stained with 4',6-diamidino-2-phenylindole (DAPI; blue) (scale bar represents 10 μm).

In brief, hMSCs were incubated in osteogenic medium for 21 days, and on Day 21 for immunostaining they were chemically fixed. Then, proteins first were stained by utilizing primary antibodies and then labelled by secondary antibody to be imaged utilizing an inverted fluorescence microscope. As shown in Figure, first column is COL-I (red), second column is OP (red), and third column is OC (red). Rows A_{I-III}, B_{I-III}, C_{I-III} represents the blend, composite, and composite-peptide, respectively. It can be seen that the expression of those osteogenic maturation-related proteins such as COL-I, OP, and OC was significantly higher for hMSCs on composite-peptide group than those on composite, and blend samples. While blend group demonstrated a weak staining for the markers of COL-I, OP, and OC, composite group demonstrated a moderate to strong staining for all three markers, and the composite-peptide group showed the strongest staining for these markers. Overall, hMSCs on GLU conjugated-composite group showed an elevated expression of markers when compared to cells on composite and blend group, and this indicates the osteogenic inductive impact of glutamic acid templated peptide. Onak et al. modified the self-assembling peptide KLD (KLDLKLDLKLDL) with short bioactive peptide motif O1 (EEGGC) and O2 (EEEEE), and aimed to increase osteogenesis [187]. It was reported that the osteogenic markers of ALP activity, COL-I, OP, and OC expression levels that are obtained via real-time polymerase chain reaction (PCR) and immunofluorescence staining assay were importantly enhanced with the incorporation of glutamic acid residues to KLD. Furthermore, KLD-EEEEE showed enhanced ALP activity, calcium content, and expression of osteogenic markers of ALP, COL-1, OP, and OC when compared to two glutamic acid templated peptide including KLD.

8.4.5 Live and Dead Staining

Cell viability was evaluated by performing Live/Dead staining assay. Figure 8.5 shows the fluorescent microscopy images of hMSCs seeded on blend, composite, and composite-peptide. In those images, green color represents the live cells, and red color represents the dead cells. For all types of PLLA-based materials, there are both live cells and dead cells on them.

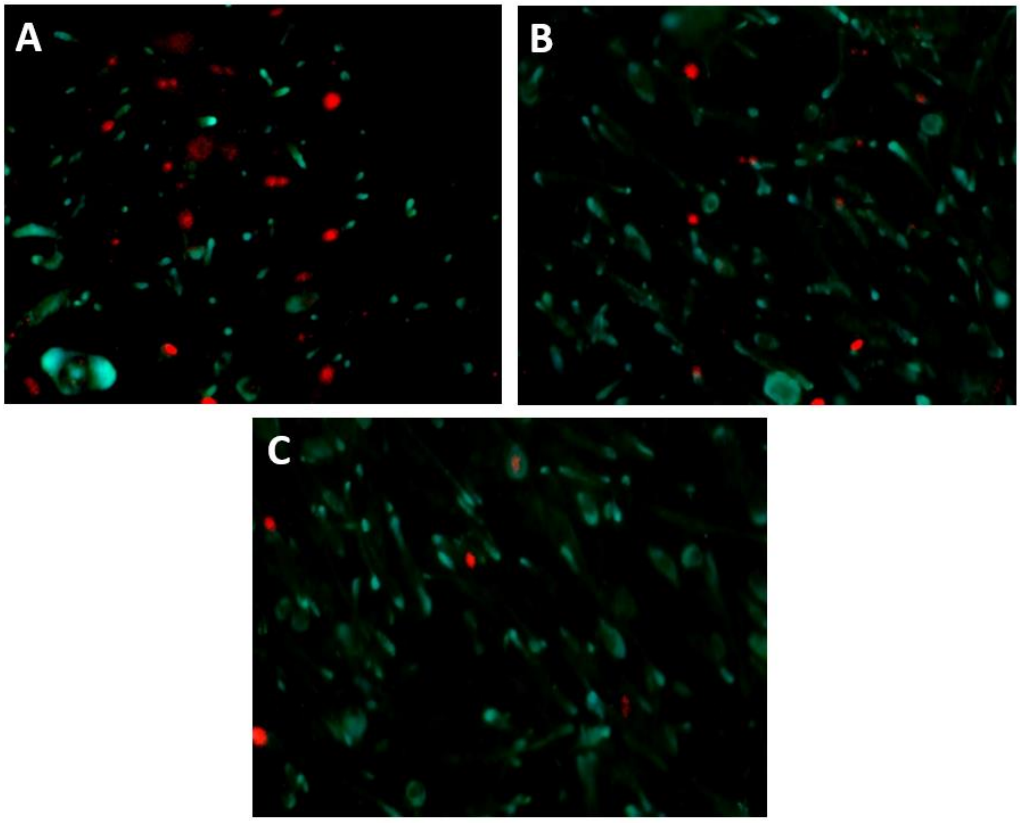

Figure 8.5: Live/Dead staining assay images of A) Blend, B) Composite, C) Composite-Peptide materials. Live cells are stained with Calcein-AM (green), and dead cells are stained with EthD-III (red) (scale bar represents 100 μm).

However, when compared with PLLA blend material, green color intensity was greater for PLLA composite and EEEEEE conjugated PLLA composite materials. This suggests that PLLA composite and EEEEEE conjugated PLLA composite materials possess higher number of viable cells, and less number of dead cells. These results indicated that composite and EEEEEE conjugated-composite materials had more appropriate cell compatibility, with being composite-peptide is the most.

It was previously distinguished that scaffolds surface features such as roughness, wettability, and chemical functionalities by biologically active molecules have a direct influence on the adhesion and reproduction of cell [188]. In this regard, functionalizing the surface of PLLA composite materials first with plasma treatment, and then modifying with EEEEEE peptide are expected to affect the attachment, proliferation, and differentiation of seeded hMSCs. Onak et al. treated the electrospun poly(lactide-co-glycolide) (PLGA) nanofibers (NFs) with non-thermal atmospheric plasma (NTAP), and then modified by glutamic acid (GLU) peptide which is followed with incubation in simulated body fluid for mineralization [189]. It was reported that

treatment with NTAP remarkably enhanced the GLU peptide conjugation which is resulted in increased mineralization and mechanical features of both NTAP treated and GLU conjugated NF (GLU-pNF) when compared with pure NF, NTAP treated NF (pNF) and GLU conjugated NF (GLU-NF). Moreover, in consistent with our results, their findings showed that cellular attachment and proliferation were notably greater for GLU-pNF compared to other groups.

8.4.6 Osteogenic Differentiation of hMSCs on PLLA-based Materials

hMSCs differentiation into osteoblastic lineage is known as a complicated procedure, including attachment, reproduction, differentiation, maturation, and mineralization of hMSCs [186,187]. Bone ECM-mimetic peptide sequences can be utilized to guide proliferation and osteogenic differentiation of cells, and with this way bioinert synthetic scaffolds might gain the ability of osteoinductivity [186,187]. In this regard, herein, we modified the synthetic PLLA composite materials with glutamic acid templated peptide sequence for enhancing the osteogenic differentiation.

Osteogenic differentiation ability of hMSCs seeded on blend, composite, and composite-peptide samples was evaluated. For this assay, hMSCs were seeded and incubated on blend, composite, and composite-peptide materials for 7, 14, and 21 days. DNA content, and ALP activity of cells over 21 days were quantified and showed in Figure 8.6.

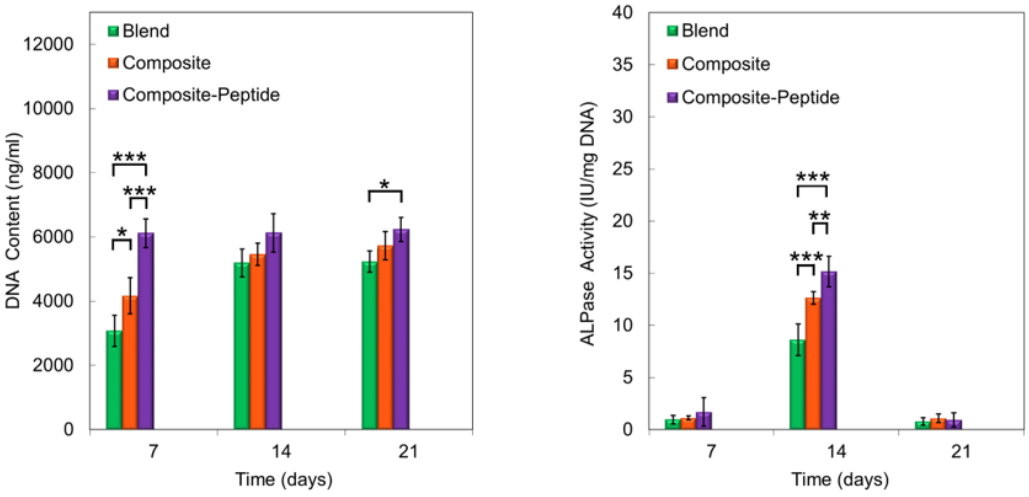

Figure 8.6: DNA content and ALP activity of blend, composite, and composite peptide materials for 7, 14, 21 days.

The measured ALP activities were normalized to cell numbers via dividing to DNA contents at every time point. The cell number was determined based on DNA content. At each time point, DNA content for all three groups were increased during 21 days of incubation. Also, at all-time points, cells on composite-peptide group have the highest DNA content, followed by pure composite and blend, respectively. DNA content measurement analysis results suggest that composite material which consists of six glutamic acid residues, made easy the hMSCs proliferation remarkably when compared to blend and composite materials during the 21 days of incubation period. These results also recommended that functionalization with glutamic acid induces the cell proliferation of hMSCs. Moreover, our findings are in consistence with previous reports demonstrating an increased proliferation of hMSCs that were seeded on glutamic acid modified synthetic nanofibers [179,182]. The positive effect and potential of glutamic acid in cellular proliferation might be associated with the existence and more effectual role of glutamic acid in integrin binding motif [187]. It is known that integrin molecules may recognize glutamic acid-based sequence motifs in structurally diverse ligands [190].

Adequate cellular growth, ALP activity, calcium deposition, and osteogenic markers expression are very crucial for assessing osteogenic differentiation [182,187]. In our study, measurement of ALP activity was evaluated via utilizing the time-dependent pNPP formation in alkaline solution. Consistent with the results of previous studies, the ALP activity of all three experimental groups incubated in osteogenic medium made a peak on Day 14 of cell culture, and then started to decrease with longer period of incubation [179,187]. It was observed that the ALP activity was the highest for cells seeded on glutamic acid templated peptide conjugated composite material on Day 14 when compared to blend and pure composite groups, and this indicates that hMSCs on composite-peptide group received more osteogenic induction. For instance, peak ALP activity of blend, and composite was enhanced to $8,62 \pm 1,51$, and $12,64 \pm 0,61$ IU/mg DNA, respectively, while the peak ALP activity of composite-peptide was enhanced to $15,17 \pm 1,46$ IU/mg DNA. These results suggest that functionalizing with glutamic acid templated peptide encouraged the ALP activity of cells on composite materials.

8.5 Conclusion

In this study, it was aimed to investigate the effect of glutamic acid templated peptide conjugation to PLLA composite materials on the viability and osteogenic differentiation of hMSCs. Herein, to increase the conjugation efficacy of glutamic acid peptide on composite materials, we functionalized the surface of composite materials with cold atmospheric plasma application. For this stage, PLLA composite materials were first treated with cold atmospheric plasma, and then conjugated with peptide.

In summary, glutamic acid templated peptide was successfully conjugated on PLLA composite materials following the cold atmospheric plasma treatment. Our results from Live/Dead staining assay demonstrated that peptide modified composite samples supported the viability of hMSCs, followed by composite, and blend, respectively. Furthermore, PLLA-based composite material containing six glutamic acid templated peptide showed significantly enhanced DNA content, ALP activity, and expression of key osteogenic markers of COL-1, OP, and OC when compared to blend and pure composite sample groups. Conjugation with glutamic acid templated peptide improved the osteoinductive capability of PLLA-based materials.

Our findings revealed that PLLA-based composite material functionalized with EEEEEE peptide possessed more potential on triggering osteogenesis of hMSCs. It is believed that these kinds of findings will contribute to the development of biomimetic peptide modified bioactive synthetic scaffold materials for supporting the effective repair and regeneration of bone tissue. Overall, the results of the current study suggest that conjugation of PLLA composite materials with biomimetic glutamic acid peptide might be a promising method to enhance the viability, proliferation, and osteogenesis of hMSCs for potentially use in diverse bone tissue engineering applications.

Chapter 9

9 General Conclusion

The results obtained as a result of the experiments and examinations carried out within the scope of the thesis are summarized in this section. Irregular shaped TCP and HA particles which met the requirements of ASTM F1088 – 18 were obtained. Incorporation of HA / TCP particles increased both the tensile and flexural strength of PLA composites and highest tensile/flexural modulus and strength values were obtained in case of 10 wt.% TCP incorporation. HA/TCP increased the amount of crystallinity and caused slight changes in crystallization and melting temperatures and the highest crystallinity value was obtained at 5 wt.% HA and 5wt.% TCP incorporation. Addition of TCP and HA increased the viability of PLA, and the highest cell viability was obtained at 5 wt.% HA and 5wt.% TCP incorporation. Stereo complex crystallites significantly increased the crystallization rate of PLLA due to the heterogeneous nucleating action of SC crystallites. The highest degree of crystallinity was obtained in 10PDLA with approximately 58%. PLLA/PDLA stereo complex structure was formed and increased with increasing PDLA ratio. It was also observed that 2.5 PDLA increased the tensile strength of PLLA by about 5%. Similarly, the highest flexural strength was obtained in 2.5 PDLA. Addition of 5TCP-5HA decreased the T_c, T_{m1} and T_{m2} values by 2 to 5 °C. Highest tensile strength was obtained at 2.5PDLA-5HA-5TCP. An approximately 27% increase in tensile strength of PLLA was obtained with the final composition, 2.5PDLA-5HA-5TCP. PLLA-based composite material functionalized with EEEEEE peptide possessed more potential on triggering osteogenesis of hMSCs.

References

[1] Williams DF. Materials in clinical dentistry / by D. F. Williams and J. Cunningham. Oxford ; New York: Oxford University Press; 1979.

[2] Park JB. Biomaterials science and engineering. Springer Science & Business Media; 2012.

[3] Patel NR, Gohil PP. A review on biomaterials: scope, applications & human anatomy significance. International Journal of Emerging Technology and Advanced Engineering 2012;2:91–101.

[4] Benčina M, Resnik M, Starič P, Junkar I. Use of Plasma Technologies for Antibacterial Surface Properties of Metals. Molecules 2021, Vol 26, Page 1418 2021;26:1418. https://doi.org/10.3390/MOLECULES26051418.

[5] Chan C-M, Wu J, Li J-X, Cheung Y-K. Polypropylene/calcium carbonate nanocomposites. Polymer (Guildf) 2002;43:2981–92. https://doi.org/https://doi.org/10.1016/S0032-3861(02)00120-9.

[6] Naik KS. Advanced bioceramics. Advances in Biological Science Research: A Practical Approach 2019:411–7. https://doi.org/10.1016/B978-0-12-817497-5.00025-2.

[7] Ratner BD, Hoffman AS, Schoen FJ, Lemons JE. Biomaterials science: an introduction to materials in medicine. Elsevier; 2004.

[8] Middleton JC, Tipton AJ. Synthetic biodegradable polymers as orthopedic devices. Biomaterials 2000;21:2335–46.

[9] Mooney DJ, Vandenburgh H. Cell delivery mechanisms for tissue repair. Cell Stem Cell 2008;2:205–13.

[10] Mondrinos MJ, Dembzynski R, Lu L, Byrapogu VKC, Wootton DM, Lelkes PI, et al. Porogen-based solid freeform fabrication of polycaprolactone–calcium phosphate scaffolds for tissue engineering. Biomaterials 2006;27:4399–408.

[11] Pego AP, Siebum B, van Luyn MJA, Gallego y Van Seijen XJ, Poot AA, Grijpma DW, et al. Preparation of degradable porous structures based on 1, 3-trimethylene carbonate and D, L-lactide (co) polymers for heart tissue engineering. Tissue Eng 2003;9:981–94.

[12] Doppalapudi S, Jain A, Khan W, Domb AJ. Biodegradable polymers—an overview. Polym Adv Technol 2014;25:427–35.

[13] Baek J, Chen X, Sovani S, Jin S, Grogan SP, D'Lima DD. Meniscus tissue engineering using a novel combination of electrospun scaffolds and human meniscus cells embedded within an extracellular matrix hydrogel. J Orthop Res 2015;33:572–83. https://doi.org/10.1002/JOR.22802.

[14] Ionescu LC, Mauck RL. Porosity and cell preseeding influence electrospun scaffold maturation and meniscus integration in vitro. Tissue Eng Part A 2012;19:538–47.

[15] How SLS Can be Used to 3D Print Bioresorbable Polymer Implants - BONEZONE n.d. https://bonezonepub.com/2022/04/13/how-sls-can-be-used-to-3d-print-bioresorbable-polymer-implants/ (accessed January 23, 2023).

[16] Schneider AK. Polymers of high melting lactide 1955.

[17] Majola A, Vainionpää S, Vihtonen K, Mero M, Vasenius J, Törmälä P, et al. Absorption, biocompatibility, and fixation properties of polylactic acid in bone tissue: an experimental study in rats. Clin Orthop Relat Res 1991:260–9.

[18] Nakamura T, Hitomi S, Watanabe S, Shimizu Y, Jamshidi K, Hyon S, et al. Bioabsorption of polylactides with different molecular properties. J Biomed Mater Res A 1989;23:1115–30.

[19] Zhang X, Hua H, Shen X, Yang Q. In vitro degradation and biocompatibility of poly (L-lactic acid)/chitosan fiber composites. Polymer (Guildf) 2007;48:1005–11.

[20] Lembeck B, Wülker N. Severe cartilage damage by broken poly–L–lactic acid (PLLA) interference screw after ACL reconstruction. Knee Surgery, Sports Traumatology, Arthroscopy 2005;13:283–6.

[21] Rossi F, Santoro M, Perale G. Polymeric scaffolds as stem cell carriers in bone repair. J Tissue Eng Regen Med 2015;9:1093–119.

[22] Wang J-L, Chen Q, Du B-B, Cao L, Lin H, Fan Z-Y, et al. Enhanced bone regeneration composite scaffolds of PLLA/β-TCP matrix grafted with gelatin and HAp. Materials Science and Engineering: C 2018.

[23] Yagihara K, Okabe S, Ishii J, Amagasa T, Yamashiro M, Yamaguchi S, et al. Mandibular reconstruction using a poly (L-lactide) mesh combined with autogenous particulate cancellous bone and marrow: a prospective clinical study. Int J Oral Maxillofac Surg 2013;42:962–9.

[24] Gao Y, Sun Y, Ren F, Gao S. PLGA–PEG–PLGA hydrogel for ocular drug delivery of dexamethasone acetate. Drug Dev Ind Pharm 2010;36:1131–8.

[25] Cao Y, Zhang C, Shen W, Cheng Z, Yu LL, Ping Q. Poly (N-isopropylacrylamide)–chitosan as thermosensitive in situ gel-forming system for ocular drug delivery. Journal of Controlled Release 2007;120:186–94.

[26] Cifuentes SC, Frutos E, González-Carrasco JL, Muñoz M, Multigner M, Chao J, et al. Novel PLLA/magnesium composite for orthopedic applications: A proof of concept. Mater Lett 2012;74:239–42.

[27] Lavik EB, Klassen H, Warfvinge K, Langer R, Young MJ. Fabrication of degradable polymer scaffolds to direct the integration and differentiation of retinal progenitors. Biomaterials 2005;26:3187–96.

[28] Pertici G, Rossi F, Casalini T, Perale G. Composite polymer-coated mineral grafts for bone regeneration: material characterisation and model study. Annals of Oral & Maxillofacial Surgery 2014;2.

[29] Sui G, Yang X, Mei F, Hu X, Chen G, Deng X, et al. Poly-L-lactic acid/hydroxyapatite hybrid membrane for bone tissue regeneration. J Biomed Mater Res A 2007;82:445–54.

[30] Hasegawa S, Neo M, Tamura J, Fujibayashi S, Takemoto M, Shikinami Y, et al. In vivo evaluation of a porous hydroxyapatite/poly-DL-lactide composite for bone tissue engineering. J Biomed Mater Res A 2007;81:930–8.

[31] Noh K-T, Lee H-Y, Shin U-S, Kim H-W. Composite nanofiber of bioactive glass nanofiller incorporated poly (lactic acid) for bone regeneration. Mater Lett 2010;64:802–5.

[32] McCullen SD, Zhu Y, Bernacki SH, Narayan RJ, Pourdeyhimi B, Gorga RE, et al. Electrospun composite poly (L-lactic acid)/tricalcium phosphate scaffolds induce proliferation and osteogenic differentiation of human adipose-derived stem cells. Biomedical Materials 2009;4:35002.

[33] Wang X, Song G, Lou T. Fabrication and characterization of nano composite scaffold of poly (l-lactic acid)/hydroxyapatite. J Mater Sci Mater Med 2010;21:183–8.

[34] El-Kady AM, Ali AF, Farag MM. Development, characterization, and in vitro bioactivity studies of sol–gel bioactive glass/poly (l-lactide) nanocomposite scaffolds. Materials Science and Engineering: C 2010;30:120–31.

[35] McManus AJ, Doremus RH, Siegel RW, Bizios R. Evaluation of cytocompatibility and bending modulus of nanoceramic/polymer composites. J Biomed Mater Res A 2005;72:98–106.

[36] Gerhardt L-C, Widdows KL, Erol MM, Burch CW, Sanz-Herrera JA, Ochoa I, et al. The pro-angiogenic properties of multi-functional bioactive glass composite scaffolds. Biomaterials 2011;32:4096–108.

[37] Serra T, Planell JA, Navarro M. High-resolution PLA-based composite scaffolds via 3-D printing technology. Acta Biomater 2013;9:5521–30.

[38] Karst D, Yang Y. Molecular modeling study of the resistance of PLA to hydrolysis based on the blending of PLLA and PDLA. Polymer (Guildf) 2006;47:4845–50. https://doi.org/10.1016/J.POLYMER.2006.05.002.

[39] Quynh TM, Mitomo H, Nagasawa N, Wada Y, Yoshii F, Tamada M. Properties of crosslinked polylactides (PLLA & PDLA) by radiation and its biodegradability. Eur Polym J 2007;43:1779–85. https://doi.org/10.1016/J.EURPOLYMJ.2007.03.007.

[40] Lin PL, Fang HW, Tseng T, Lee WH. Effects of hydroxyapatite dosage on mechanical and biological behaviors of polylactic acid composite materials. Mater Lett 2007;61:3009–13. https://doi.org/10.1016/J.MATLET.2006.10.064.

[41] Huang Z, Wan Y, Peng M, Yang Z, Luo H. Incorporating nanoplate-like hydroxyapatite into polylactide for biomimetic nanocomposites via direct melt intercalation. Compos Sci Technol 2020;185:107903. https://doi.org/10.1016/J.COMPSCITECH.2019.107903.

[42] Gendviliene I, Simoliunas E, Rekstyte S, Malinauskas M, Zaleckas L, Jegelevicius D, et al. Assessment of the morphology and dimensional accuracy of 3D printed PLA and PLA/HAp scaffolds. J Mech Behav Biomed Mater 2020;104:103616. https://doi.org/10.1016/J.JMBBM.2020.103616.

[43] Amnael Orozco-Díaz C, Moorehead R, Reilly GC, Gilchrist F, Miller C. Characterization of a composite polylactic acid-hydroxyapatite 3D-printing filament for bone-regeneration. Biomed Phys Eng Express 2020;6:025007. https://doi.org/10.1088/2057-1976/AB73F8.

[44] Liu S, Li Y, Sun H, Zhang S, Zeng X, Zong P, et al. Preparation and characterisation of a lamellar hydroxyapatite/polylactic acid composite. Https://DoiOrg/101080/1465801120181548191 2018;48:66–73. https://doi.org/10.1080/14658011.2018.1548191.

[45] Custodio CL, Broñola PJM, Cayabyab SR, Lagura VU, Celorico JR, Basilia BA. Powder Loading Effects on the Physicochemical and Mechanical Properties of 3D Printed Poly Lactic Acid/Hydroxyapatite Biocomposites. Int J Bioprint 2021;7:112–22. https://doi.org/10.18063/IJB.V7I1.326.

[46] Ferri JM, Jordá J, Montanes N, Fenollar O, Balart R. Manufacturing and characterization of poly(lactic acid) composites with hydroxyapatite. Journal of Thermoplastic Composite Materials 2017;31:865–81. https://doi.org/10.1177/0892705717729014.

[47] Im SH, Im DH, Park SJ, Chung JJ, Jung Y, Kim SH. Stereocomplex Polylactide for Drug Delivery and Biomedical Applications: A Review. Molecules 2021, Vol 26, Page 2846 2021;26:2846. https://doi.org/10.3390/MOLECULES26102846.

[48] Wei XF, Bao RY, Cao ZQ, Yang W, Xie BH, Yang MB. Stereocomplex crystallite network in asymmetric PLLA/PDLA blends: Formation, structure, and confining effect on the crystallization rate of homocrystallites. Macromolecules 2014;47:1439–48. https://doi.org/10.1021/MA402653A/ASSET/IMAGES/MEDIUM/MA-2013-02653A_0013.GIF.

[49] Park HS, Hong CK. Relationship between the Stereocomplex Crystallization Behavior and Mechanical Properties of PLLA/PDLA Blends. Polymers 2021, Vol 13, Page 1851 2021;13:1851. https://doi.org/10.3390/POLYM13111851.

[50] Yu B, Cao Y, Sun H, Han J. The Structure and Properties of Biodegradable PLLA/PDLA for Melt-Blown Nonwovens. J Polym Environ 2017;25:510–7. https://doi.org/10.1007/S10924-016-0827-Y/TABLES/3.

[51] Jumat MA, Chevallier P, Mantovani D, Copes F, Razak SIA, Saidin S. Three-dimensional printed biodegradable poly(l-lactic acid)/(poly(d-lactic acid) scaffold as an intervention of biomedical substitute. Https://DoiOrg/101080/2574088120211876879 2021;60:1005–15. https://doi.org/10.1080/25740881.2021.1876879.

[52] Saeidlou S, Huneault MA, Li H, Sammut P, Park CB. Evidence of a dual network/spherulitic crystalline morphology in PLA stereocomplexes. Polymer (Guildf) 2012;53:5816–24. https://doi.org/10.1016/J.POLYMER.2012.10.030.

[53] Okihara T, Tsuji M, Kawaguchi A, Katayama KI, Tsuji H, Hyon SH, et al. Crystal structure of stereocomplex of poly(L-lactide) and poly(D-lactide). Http://DxDoiOrg/101080/00222349108245788 2006;30:119–40. https://doi.org/10.1080/00222349108245788.

[54] Hoogsteen W, Postema AR, Pennings AJ, Brinke G ten, Zugenmaier P. Crystal Structure, Conformation, and Morphology of Solution-Spun Poly(L-Lactide) Fibers. Macromolecules 1990;23:634–42. https://doi.org/10.1021/MA00204A041/ASSET/MA00204A041.FP.PNG_V03 .

[55] Tsuji H. Autocatalytic hydrolysis of amorphous-made polylactides: effects of l-lactide content, tacticity, and enantiomeric polymer blending. Polymer (Guildf) 2002;43:1789–96. https://doi.org/10.1016/S0032-3861(01)00752-2.

[56] Tsuji H. In vitro hydrolysis of blends from enantiomeric poly(lactide)s. Part 4: Well-homo-crystallized blend and nonblended films. Biomaterials 2003;24:537–47. https://doi.org/10.1016/S0142-9612(02)00365-4.

[57] Xu S, Liu J, Zhang L, Yang F, Tang P, Wu D. Effects of HAp and TCP in constructing tissue engineering scaffolds for bone repair. J Mater Chem B 2017;5:6110–8. https://doi.org/10.1039/C7TB00790F.

[58] Yang Y, Zhao J, Zhao Y, Wen L, Yuan X, Fan Y. Formation of porous PLGA scaffolds by a combining method of thermally induced phase separation and porogen leaching. J Appl Polym Sci 2008;109:1232–41.

[59] Neuendorf RE, Saiz E, Tomsia AP, Ritchie RO. Adhesion between biodegradable polymers and hydroxyapatite: Relevance to synthetic bone-like materials and tissue engineering scaffolds. Acta Biomater 2008;4:1288–96. https://doi.org/10.1016/j.actbio.2008.04.006.

[60] Ciofani G, Ricotti L, Mattoli V. Preparation, characterization and in vitro testing of poly(lactic-co-glycolic) acid/barium titanate nanoparticle composites for enhanced cellular proliferation. Biomed Microdevices 2011;13:255–66. https://doi.org/10.1007/s10544-010-9490-6.

[61] Kothapalli CR, Shaw MT, Wei M. Biodegradable HA-PLA 3-D porous scaffolds: Effect of nano-sized filler content on scaffold properties. Acta Biomater 2005;1:653–62. https://doi.org/https://doi.org/10.1016/j.actbio.2005.06.005.

[62] Lee JB, Lee SH, Yu SM, Park J-C, Choi JB, Kim JK. PLGA scaffold incorporated with hydroxyapatite for cartilage regeneration. Surf Coat Technol 2008;202:5757–61.

[63] Deng X, Hao J, Wang C. Preparation and mechanical properties of nanocomposites of poly (D, L-lactide) with Ca-deficient hydroxyapatite nanocrystals. Biomaterials 2001;22:2867–73.

[64] Jeong SI, Ko EK, Yum J, Jung CH, Lee YM, Shin H. Nanofibrous Poly(lactic acid)/Hydroxyapatite Composite Scaffolds for Guided Tissue Regeneration. Macromol Biosci 2008;8:328–38. https://doi.org/doi:10.1002/mabi.200700107.

[65] Zhang R, Ma PX. Porous poly(L-lactic acid)/apatite composites created by biomimetic process. J Biomed Mater Res 1999;45:285–93. https://doi.org/doi:10.1002/(SICI)1097-4636(19990615)45:4<285::AID-JBM2>3.0.CO;2-2.

[66] Damadzadeh B, Jabari H, Skrifvars M, Airola K, Moritz N, Vallittu PK. Effect of ceramic filler content on the mechanical and thermal behaviour of poly-l-lactic acid and poly-l-lactic-co-glycolic acid composites for medical applications. J Mater Sci Mater Med 2010;21:2523–31. https://doi.org/10.1007/s10856-010-4110-9.

[67] Shikinami Y, Okuno M. Bioresorbable devices made of forged composites of hydroxyapatite (HA) particles and poly-L-lactide (PLLA): Part I. Basic

characteristics. Biomaterials 1999;20:859–77. https://doi.org/https://doi.org/10.1016/S0142-9612(98)00241-5.

[68] Kim S-S, Sun Park M, Jeon O, Yong Choi C, Kim B-S. Poly(lactide-co-glycolide)/hydroxyapatite composite scaffolds for bone tissue engineering. Biomaterials 2006;27:1399–409. https://doi.org/https://doi.org/10.1016/j.biomaterials.2005.08.016.

[69] Ignjatovic N, Uskokovic D. Synthesis and application of hydroxyapatite/polylactide composite biomaterial. Appl Surf Sci 2004;238:314–9. https://doi.org/https://doi.org/10.1016/j.apsusc.2004.05.227.

[70] Xiong Z, Yan Y, Wang S, Zhang R, Zhang C. Fabrication of porous scaffolds for bone tissue engineering via low-temperature deposition. Scr Mater 2002;46:771–6.

[71] Sherwood JK, Riley SL, Palazzolo R, Brown SC, Monkhouse DC, Coates M, et al. A three-dimensional osteochondral composite scaffold for articular cartilage repair. Biomaterials 2002;23:4739–51.

[72] Huang YX, Ren J, Chen C, Ren TB, Zhou XY. Preparation and Properties of Poly(lactide-co-glycolide) (PLGA)/ Nano-Hydroxyapatite (NHA) Scaffolds by Thermally Induced Phase Separation and Rabbit MSCs Culture on Scaffolds. J Biomater Appl 2008;22:409–32. https://doi.org/10.1177/0885328207077632.

[73] Haimi S, Suuriniemi N, Haaparanta A-M, Ellä V, Lindroos B, Huhtala H, et al. Growth and osteogenic differentiation of adipose stem cells on PLA/bioactive glass and PLA/β-TCP scaffolds. Tissue Eng Part A 2008;15:1473–80.

[74] Lv Q, Nair L, Laurencin CT. Fabrication, characterization, and in vitro evaluation of poly(lactic acid glycolic acid)/nano-hydroxyapatite composite microsphere-based scaffolds for bone tissue engineering in rotating bioreactors. J Biomed Mater Res A 2009;91A:679–91. https://doi.org/doi:10.1002/jbm.a.32302.

[75] Ajduković Z, Ignjatović N, Petrović D, Uskoković D. Substitution of Osteoporotic Alveolar Bone by Biphasic Calcium Phosphate/Poly-DL-lactide-

co-glycolide Biomaterials. J Biomater Appl 2007;21:317–28. https://doi.org/10.1177/0885328207073760.

[76] Lin LC, Chang SJ, Kuo SM, Niu GC-C, Keng HK, Tsai PH. Preparation and evaluation of β-TCP/polylactide microspheres as osteogenesis materials. J Appl Polym Sci 2008;108:3210–7. https://doi.org/doi:10.1002/app.27309.

[77] Schneider OD, Weber F, Brunner TJ, Loher S, Ehrbar M, Schmidlin PR, et al. In vivo and in vitro evaluation of flexible, cottonwool-like nanocomposites as bone substitute material for complex defects. Acta Biomater 2009;5:1775–84. https://doi.org/https://doi.org/10.1016/j.actbio.2008.11.030.

[78] van der Pol U, Mathieu L, Zeiter S, Bourban PE, Zambelli PY, Pearce SG, et al. Augmentation of bone defect healing using a new biocomposite scaffold: An in vivo study in sheep. Acta Biomater 2010;6:3755–62. https://doi.org/https://doi.org/10.1016/j.actbio.2010.03.028.

[79] Najman S, Savic V, Djordjevic L, Ignjatovic N, Uskokovic D. Biological evaluation of hydroxyapatite/poly-L-lactide (HAp/PLLA) composite biomaterials with poly-L-lactide of different molecular weights intraperitoneally implanted into mice. Biomed Mater Eng 2004;14:61–70.

[80] Keskin AO. Hidroksiapatit Seramiklerinin Mekanik Özelliklerinin Zirkonya İlavesiyle Geliştirilmesi 2015.

[81] Advancements in tissue engineered bone substitutes : Current Opinion in Orthopaedics n.d. https://journals.lww.com/co-ortho/Fulltext/1999/12000/Advancements_in_tissue_engineered_bone_substitutes.5.aspx (accessed November 29, 2022).

[82] Zhang X. UC San Diego UC San Diego Electronic Theses and Dissertations Title Preparation and characterization of calcium phosphate ceramics and Composites as bone substitutes 2007.

[83] Engin NÖ. Makro Gözenekli Kalsiyum Hidroksiapatit (HA) ve Trikalsiyum Fosfat (TCP) Bioseramiklerin Üretilmesi. ODTÜ, Ankara, Şubat 1999.

[84] Suchanek W, Yoshimura M. Processing and properties of hydroxyapatite-based biomaterials for use as hard tissue replacement implants. J Mater Res 1998;13:94–117. https://doi.org/10.1557/JMR.1998.0015.

[85] Ritter Stephen K. At the human body shop, bioceramics or biopolymers combined with bone cells and growth factors are likely to lead the parts list. Chemical & Engineering News Archive 1997;75:37. https://doi.org/10.1021/CEN-V075N034.P037.

[86] Weiner S, Wagner HD. The material bone: structure-mechanical function relations. Annual Review of Materials Science 1998;28:271–98.

[87] Brown PW, Constantz B. Hydroxyapatite and related materials. vol. 368. CRC press Boca Raton, FL, USA:; 1994.

[88] Peters F, Schwarz K, Epple M. The structure of bone studied with synchrotron X-ray diffraction, X-ray absorption spectroscopy and thermal analysis. Thermochim Acta 2000;361:131–8. https://doi.org/10.1016/S0040-6031(00)00554-2.

[89] Rajpoot K, Tekade RK. Microemulsion as drug and gene delivery vehicle: an inside story. Drug Delivery Systems 2019:455–520. https://doi.org/10.1016/B978-0-12-814487-9.00010-7.

[90] Hill AJ, Walton A, Mazzeo F. Suspension Stability ; Why Particle Size , Zeta Potential and Rheology are Important 2011.

[91] Nanotecnologia Molecular - Materiais e Dispositivos - Editora Blucher n.d. https://www.blucher.com.br/livro/detalhes/nanotecnologia-molecular-materiais-e-dispositivos-1158 (accessed May 31, 2021).

[92] Roy TD, Simon JL, Ricci JL, Rekow ED, Thompson VP, Parsons JR. Performance of degradable composite bone repair products made via three-dimensional fabrication techniques. J Biomed Mater Res A 2003;66A:283–91. https://doi.org/doi:10.1002/jbm.a.10582.

[93] GOPAL R, CALVO C. Structural Relationship of Whitlockite and βCa3(PO4)2. Nature Physical Science 1972;237:30–2. https://doi.org/10.1038/physci237030a0.

[94] Frondel C. Mineralogy of the calcium phosphates in insular phosphate rock. American Mineralogist: Journal of Earth and Planetary Materials 1943;28:215–32.

[95] Bakan F, Sezen M, Gecgin M, Goncu Y, Ay N. Structural and Chemical Analysis of Hydroxyapatite (HA)-Boron Nitride (BN) Nanocomposites Sintered Under Different Atmospheric Conditions. Microscopy and Microanalysis 2017;23:891–9. https://doi.org/DOI: 10.1017/S1431927617012405.

[96] Mallik PK, Swain PK, Patnaik SC. Characterisation of Suspension Precipitated Nanocrystalline Hydroxyapatite Powders. IOP Conf Ser Mater Sci Eng, vol. 115, IOP Publishing; 2016, p. 12025.

[97] Venkateswarlu K, Sreekanth D, Sandhyarani M, Muthupandi V, Bose AC, Rameshbabu N. X-ray peak profile analysis of nanostructured hydroxyapatite and fluorapatite. Int J Biosci Biochem Bioinforma 2012;2:389.

[98] Romanzini D, Lavoratti A, Ornaghi Jr HL, Amico SC, Zattera AJ. Influence of fiber content on the mechanical and dynamic mechanical properties of glass/ramie polymer composites. Mater Des 2013;47:9–15.

[99] Akindoyo JO, Beg MDH, Ghazali S, Heim HP, Feldmann M. Effects of surface modification on dispersion, mechanical, thermal and dynamic mechanical properties of injection molded PLA-hydroxyapatite composites. Compos Part A Appl Sci Manuf 2017;103:96–105. https://doi.org/10.1016/J.COMPOSITESA.2017.09.013.

[100] Huang B, Caetano G, Vyas C, Blaker JJ, Diver C, Bártolo P. Polymer-ceramic composite scaffolds: The effect of hydroxyapatite and β-tri-calcium phosphate. Materials 2018;11. https://doi.org/10.3390/ma11010129.

[101] ASTM F1088 - 18 Standard Specification for Beta-Tricalcium Phosphate for Surgical Implantation n.d. https://www.astm.org/Standards/F1088.htm (accessed May 31, 2021).

[102] Cheung HY, Lau KT, Tao XM, Hui D. A potential material for tissue engineering: Silkworm silk/PLA biocomposite. Compos B Eng 2008. https://doi.org/10.1016/j.compositesb.2007.11.009.

[103] Lee SK, Han CM, Park W, Kim IH, Joung YK, Han DK. Synergistically enhanced osteoconductivity and anti-inflammation of PLGA/β-TCP/Mg(OH)2 composite for orthopedic applications. Materials Science and Engineering C 2019. https://doi.org/10.1016/j.msec.2018.09.011.

[104] Chen CC, Chueh JY, Tseng H, Huang HM, Lee SY. Preparation and characterization of biodegradable PLA polymeric blends. Biomaterials 2003. https://doi.org/10.1016/S0142-9612(02)00466-0.

[105] Narayanan G, Vernekar VN, Kuyinu EL, Laurencin CT. Poly (lactic acid)-based biomaterials for orthopaedic regenerative engineering. Adv Drug Deliv Rev 2016;107:247–76. https://doi.org/10.1016/j.addr.2016.04.015.

[106] Li X, Liu H, Wang J, Li C. Preparation and characterization of PLLA/nHA nonwoven mats via laser melt electrospinning. Mater Lett 2012;73:103–6. https://doi.org/10.1016/j.matlet.2011.12.108.

[107] Lim LT, Auras R, Rubino M. Processing technologies for poly(lactic acid). Progress in Polymer Science (Oxford) 2008;33:820–52. https://doi.org/10.1016/j.progpolymsci.2008.05.004.

[108] Oh JK. Polylactide (PLA)-based amphiphilic block copolymers: synthesis, self-assembly, and biomedical applications. Soft Matter 2011;7:5096–108. https://doi.org/10.1039/C0SM01539C.

[109] Leksakul K, Phuendee M. Development of hydroxyapatite-polylactic acid composite bone fixation plate. IEEE Journal of Selected Topics in Quantum Electronics 2018;25:903–14. https://doi.org/10.1515/secm-2016-0359.

[110] Ferri JM, Motoc DL, Bou SF, Balart R. Thermal expansivity and degradation properties of PLA/HA and PLA/βTCP in vitro conditioned composites. J Therm Anal Calorim 2019;138:2691–702. https://doi.org/10.1007/s10973-019-08799-0.

[111] Carrasco F, Pagès P, Gámez-Pérez J, Santana OO, Maspoch ML. Processing of poly(lactic acid): Characterization of chemical structure, thermal stability and mechanical properties. Polym Degrad Stab 2010;95:116–25. https://doi.org/10.1016/J.POLYMDEGRADSTAB.2009.11.045.

[112] Mathew AP, Oksman K, Sain M. The effect of morphology and chemical characteristics of cellulose reinforcements on the crystallinity of polylactic acid. J Appl Polym Sci 2006;101:300–10. https://doi.org/10.1002/app.23346.

[113] Damadzadeh B, Jabari H. Biodegradable Composites: Processing of thermoplastic polymers for medical applications. 2009.

[114] Liu X, Wang T, Chow LC, Yang M, Mitchell JW. Effects of inorganic fillers on the thermal and mechanical properties of poly (lactic acid). Int J Polym Sci 2014;2014.

[115] Siqueira L, Passador FR, Costa MM, Lobo AO, Sousa E. Influence of the addition of β-TCP on the morphology, thermal properties and cell viability of poly (lactic acid) fibers obtained by electrospinning. Materials Science and Engineering: C 2015;52:135–43. https://doi.org/https://doi.org/10.1016/j.msec.2015.03.055.

[116] Cheewawuttipong W, Fuoka D, Tanoue S, Uematsu H, Iemoto Y. Thermal and Mechanical Properties of Polypropylene/Boron Nitride Composites. Energy Procedia 2013;34:808–17. https://doi.org/https://doi.org/10.1016/j.egypro.2013.06.817.

[117] Ferri JM, Jordá J, Montanes N, Fenollar O, Balart R. Manufacturing and characterization of poly(lactic acid) composites with hydroxyapatite. Https://DoiOrg/101177/0892705717729014 2017;31:865–81. https://doi.org/10.1177/0892705717729014.

[118] Damadzadeh B, Jabari H, Skrifvars M, Airola K, Moritz N, Vallittu PK. Effect of ceramic filler content on the mechanical and thermal behaviour of poly-L-lactic acid and poly-L-lactic-co-glycolic acid composites for medical applications. J Mater Sci Mater Med 2010;21:2523–31. https://doi.org/10.1007/S10856-010-4110-9.

[119] Morawska-Chochół A, Uszko P, Szaraniec B, Gryń K, Chłopek J. The influence of bioactive additives on polylactide accelerated degradation. E-Polymers 2016;16:475–80. https://doi.org/10.1515/EPOLY-2016-0227/MACHINEREADABLECITATION/RIS.

[120] Zenkiewicz M, Richert J, Rytlewski P, Moraczewski K, Stepczyńska M, Karasiewicz T. Characterisation of multi-extruded poly(lactic acid). Polym Test 2009;28:412–8. https://doi.org/10.1016/j.polymertesting.2009.01.012.

[121] Okulus Z, Voelkel A. Mechanical properties of experimental composites with different calcium phosphates fillers. Materials Science and Engineering C 2017;78:1101–8. https://doi.org/10.1016/j.msec.2017.04.158.

[122] Seki Y, Sever K, Sarikanat M, Sakarya A, Elik E. Effect of huntite mineral on mechanical, thermal and morphological properties of polyester matrix. Compos B Eng 2013;45:1534–40. https://doi.org/10.1016/J.COMPOSITESB.2012.09.083.

[123] Madugu IA, Abdulwahab M, Aigbodion VS. Effect of iron fillings on the properties and microstructure of cast fiber–polyester/iron filings particulate composite. J Alloys Compd 2009;476:807–11. https://doi.org/10.1016/J.JALLCOM.2008.09.165.

[124] Fu SY, Feng XQ, Lauke B, Mai YW. Effects of particle size, particle/matrix interface adhesion and particle loading on mechanical properties of particulate–polymer composites. Compos B Eng 2008;39:933–61. https://doi.org/10.1016/J.COMPOSITESB.2008.01.002.

[125] Erika P. Reyes J. Effect of Surface Treatment and Particle Loading on the Mechanical Properties of CFB Fly Ash Reinforced Thermoset Composite.

International Journal of Chemical Engineering and Applications 2015;6:6–11. https://doi.org/10.7763/IJCEA.2015.V6.441.

[126] Shumigin D, Tarasova E, Krumme A, Meier P. Rheological and mechanical properties of poly(lactic) acid/cellulose and LDPE/cellulose composites. Medziagotyra 2011;17:32–7. https://doi.org/10.5755/J01.MS.17.1.245.

[127] Sitticharoen W, Uthiyoung C, Passadee N, Wongprom C. Surface treated bagasse fiber ash on rheological, mechanical properties of PLA/BFA biocomposites. Polímeros 2018;28:187–95. https://doi.org/10.1590/0104-1428.0010.

[128] Sweeney M, Campbell LL, Hanson J, Pantoya ML, Christopher GF. Characterizing the feasibility of processing wet granular materials to improve rheology for 3D printing. J Mater Sci 2017;52:13040–53. https://doi.org/10.1007/S10853-017-1404-Z/FIGURES/7.

[129] Hausnerova B, Mukund BN, Sanetrnik D. Rheological properties of gas and water atomized 17-4PH stainless steel MIM feedstocks: Effect of powder shape and size. Powder Technol 2017;312:152–8. https://doi.org/10.1016/J.POWTEC.2017.02.023.

[130] Fu SY, Feng XQ, Lauke B, Mai YW. Effects of particle size, particle/matrix interface adhesion and particle loading on mechanical properties of particulate-polymer composites. Compos B Eng 2008;39:933–61. https://doi.org/10.1016/j.compositesb.2008.01.002.

[131] Kamalbabu P, Kumar GCM. Effects of Particle Size on Tensile Properties of Marine Coral Reinforced Polymer Composites. Procedia Materials Science 2014;5:802–8. https://doi.org/10.1016/j.mspro.2014.07.331.

[132] Designation: F1088 − 04a (Reapproved 2010) Standard Specification for Beta-Tricalcium Phosphate for Surgical Implantation 1 n.d. https://doi.org/10.1520/F1088-04AR10.

[133] Lee JTY, Leng Y, Chow KL, Ren F, Ge X, Wang K, et al. Cell culture medium as an alternative to conventional simulated body fluid. Acta Biomater 2011;7:2615–22.

[134] Bohner M, Lemaitre J. Can bioactivity be tested in vitro with SBF solution? Biomaterials 2009;30:2175–9. https://doi.org/10.1016/J.BIOMATERIALS.2009.01.008.

[135] Nair LS, Laurencin CT. Biodegradable polymers as biomaterials. Prog Polym Sci 2007;32:762–98. https://doi.org/10.1016/J.PROGPOLYMSCI.2007.05.017.

[136] Södergård A, Stolt M. Properties of lactic acid based polymers and their correlation with composition. Prog Polym Sci 2002;27:1123–63. https://doi.org/10.1016/S0079-6700(02)00012-6.

[137] Sun J, Yu H, Zhuang X, Chen X, Jing X. Crystallization behavior of asymmetric PLLA/PDLA blends. Journal of Physical Chemistry B 2011;115:2864–9. https://doi.org/10.1021/JP111894M/ASSET/IMAGES/MEDIUM/JP-2010-11894M_0006.GIF.

[138] Mano JF, Gómez Ribelles JL, Alves NM, Salmerón Sanchez M. Glass transition dynamics and structural relaxation of PLLA studied by DSC: Influence of crystallinity. Polymer (Guildf) 2005;46:8258–65. https://doi.org/10.1016/J.POLYMER.2005.06.096.

[139] Jung Y, Kim SS, Young HK, Kim SH, Kim BS, Kim S, et al. A poly(lactic acid)/calcium metaphosphate composite for bone tissue engineering. Biomaterials 2005;26:6314–22. https://doi.org/10.1016/J.BIOMATERIALS.2005.04.007.

[140] Mikos AG, Lyman MD, Freed LE, Langer R. Wetting of poly(l-lactic acid) and poly(dl-lactic-co-glycolic acid) foams for tissue culture. Biomaterials 1994;15:55–8. https://doi.org/10.1016/0142-9612(94)90197-X.

[141] Saini P, Arora M, Kumar MNVR. Poly(lactic acid) blends in biomedical applications. Adv Drug Deliv Rev 2016;107:47–59. https://doi.org/10.1016/J.ADDR.2016.06.014.

[142] Nofar M, Sacligil D, Carreau PJ, Kamal MR, Heuzey MC. Poly (lactic acid) blends: Processing, properties and applications. Int J Biol Macromol 2019;125:307–60. https://doi.org/10.1016/J.IJBIOMAC.2018.12.002.

[143] Cam D, Hyon S hyu, Ikada Y. Degradation of high molecular weight poly(l-lactide) in alkaline medium. Biomaterials 1995;16:833–43. https://doi.org/10.1016/0142-9612(95)94144-A.

[144] Ma P, Jiang L, Xu P, Dong W, Chen M, Lemstra PJ. Rapid Stereocomplexation between Enantiomeric Comb-Shaped Cellulose-g-poly(l-lactide) Nanohybrids and Poly(d-lactide) from the Melt. Biomacromolecules 2015;16:3723–9. https://doi.org/10.1021/ACS.BIOMAC.5B01135/SUPPL_FILE/BM5B01135_SI_001.PDF.

[145] Kawai T, Rahman N, Matsuba G, Nishida K, Kanaya T, Nakano M, et al. Crystallization and melting behavior of poly (L-lactic acid). Macromolecules 2007;40:9463–9. https://doi.org/10.1021/MA070082C/ASSET/IMAGES/MEDIUM/MA070082CN00001.GIF.

[146] Han L, Xie Q, Bao J, Shan G, Bao Y, Pan P. Click chemistry synthesis, stereocomplex formation, and enhanced thermal properties of well-defined poly(L-lactic acid)-b-poly(D-lactic acid) stereo diblock copolymers. Polym Chem 2017;8:1006–16. https://doi.org/10.1039/C6PY01989G.

[147] Hirata M, Kimura Y. Thermomechanical properties of stereoblock poly(lactic acid)s with different PLLA/PDLA block compositions. Polymer (Guildf) 2008;49:2656–61. https://doi.org/10.1016/J.POLYMER.2008.04.014.

[148] Oyama HT, Abe S. Stereocomplex Poly(lactic acid) Alloys with Superb Heat Resistance and Toughness. ACS Sustain Chem Eng 2015;3:3245–52. https://doi.org/10.1021/ACSSUSCHEMENG.5B00832/SUPPL_FILE/SC5B00832_SI_001.PDF.

[149] Tsuji H, Ikada Y. Stereocomplex formation between enantiomeric poly(lactic acid)s. XI. Mechanical properties and morphology of solution-cast films. Polymer (Guildf) 1999;40:6699–708. https://doi.org/10.1016/S0032-3861(99)00004-X.

[150] Tan BH, Muiruri JK, Li Z, He C. Recent Progress in Using Stereocomplexation for Enhancement of Thermal and Mechanical Property of Polylactide. ACS Sustain Chem Eng 2016;4:5370–91. https://doi.org/10.1021/ACSSUSCHEMENG.6B01713/ASSET/IMAGES/MEDIUM/SC-2016-01713V_0018.GIF.

[151] Ibrahim BA, M.Kadum K. Influence of Polymer Blending on Mechanical and Thermal Properties. Mod Appl Sci 2010;4:p157. https://doi.org/10.5539/MAS.V4N9P157.

[152] Tsuji H. Poly(lactide) Stereocomplexes: Formation, Structure, Properties, Degradation, and Applications. Macromol Biosci 2005;5:569–97. https://doi.org/10.1002/MABI.200500062.

[153] Fukushima K, Kimura Y. Stereocomplexed polylactides (Neo-PLA) as high-performance bio-based polymers: their formation, properties, and application. Polym Int 2006;55:626–42. https://doi.org/10.1002/PI.2010.

[154] Wei XF, Bao RY, Cao ZQ, Yang W, Xie BH, Yang MB. Stereocomplex Crystallite Network in Asymmetric PLLA/PDLA Blends: Formation, Structure, and Confining Effect on the Crystallization Rate of Homocrystallites. Macromolecules 2014;47:1439–48. https://doi.org/10.1021/MA402653A.

[155] Tsuji H. Poly(lactic acid) stereocomplexes: A decade of progress. Adv Drug Deliv Rev 2016;107:97–135. https://doi.org/10.1016/J.ADDR.2016.04.017.

[156] Hoidy WH, Al-Mulla EAJ, Al-Janabi KW. Mechanical and Thermal Properties of PLLA/PCL Modified Clay Nanocomposites. J Polym Environ 2010;18:608–16. https://doi.org/10.1007/S10924-010-0240-X/FIGURES/15.

[157] Pan P, Yang J, Shan G, Bao Y, Weng Z, Cao A, et al. Temperature-variable FTIR and solid-state 13C NMR investigations on crystalline structure and

molecular dynamics of polymorphic poly(l -lactide) and poly(l -lactide)/poly(d -lactide) stereocomplex. Macromolecules 2012;45:189–97. https://doi.org/10.1021/MA201906A/SUPPL_FILE/MA201906A_SI_001.PDF.

[158] Zhang J, Tashiro K, Tsuji H, Domb AJ. Disorder-to-Order Phase Transition and Multiple Melting Behavior of Poly(l-lactide) Investigated by Simultaneous Measurements of WAXD and DSC. Macromolecules 2008;41:1352–7. https://doi.org/10.1021/MA0706071.

[159] Sarasua JR, Arraiza AL, Balerdi P, Maiza I. Crystallinity and mechanical properties of optically pure polylactides and their blends. Polym Eng Sci 2005;45:745–53. https://doi.org/10.1002/PEN.20331.

[160] Park HS, Hong CK. Relationship between the Stereocomplex Crystallization Behavior and Mechanical Properties of PLLA/PDLA Blends. Polymers 2021, Vol 13, Page 1851 2021;13:1851. https://doi.org/10.3390/POLYM13111851.

[161] Yeh JT, Tsou CH, Huang CY, Chen KN, Wu CS, Chai WL. Compatible and crystallization properties of poly(lactic acid)/poly(butylene adipate-co-terephthalate) blends. J Appl Polym Sci 2010;116:680–7. https://doi.org/10.1002/APP.30907.

[162] Södergård A, Stolt M. Properties of lactic acid based polymers and their correlation with composition. Prog Polym Sci 2002;27:1123–63. https://doi.org/10.1016/S0079-6700(02)00012-6.

[163] Tsuji H. Poly(lactide) Stereocomplexes: Formation, Structure, Properties, Degradation, and Applications. Macromol Biosci 2007;7:1299–1299. https://doi.org/10.1002/MABI.200700275.

[164] Ikada Y, Jamshidi K, Tsuji H, Hyon SH. Stereocomplex Formation between Enantiomeric Poly(lactides). Macromolecules 1987;20:904–6. https://doi.org/10.1021/MA00170A034/ASSET/MA00170A034.FP.PNG_V03.

[165] Zhang J, Tashiro K, Tsuji H, Domb AJ. Investigation of phase transitional behavior of poly(L-lactide)/ poly(D-lactide) blend used to prepare the highly-oriented stereocomplex. Macromolecules 2007;40:1049–54. https://doi.org/10.1021/MA061693S/ASSET/IMAGES/MEDIUM/MA061693SN00001.GIF.

[166] Yamane H, Sasai K. Effect of the addition of poly(d-lactic acid) on the thermal property of poly(l-lactic acid). Polymer (Guildf) 2003;44:2569–75. https://doi.org/10.1016/S0032-3861(03)00092-2.

[167] Rahman N, Kawai T, Matsuba G, Kanaya T, Watanabe H, Okamoto H, et al. Effect of polylactide stereocomplex on the crystallization behavior of poly(L-lactic acid). Macromolecules 2009;42:4739–45. https://doi.org/10.1021/MA900004D/ASSET/IMAGES/MEDIUM/MA-2009-00004D_0009.GIF.

[168] Urayama H, Kanamori T, Fukushima K, Kimura Y. Controlled crystal nucleation in the melt-crystallization of poly(l-lactide) and poly(l-lactide)/poly(d-lactide) stereocomplex. Polymer (Guildf) 2003;44:5635–41. https://doi.org/10.1016/S0032-3861(03)00583-4.

[169] Andersson SR, Hakkarainen M, Inkinen S, Södergård A, Albertsson AC. Polylactide Stereocomplexation Leads to Higher Hydrolytic Stability but More Acidic Hydrolysis Product Pattern. Biomacromolecules 2010;11:1067–73. https://doi.org/10.1021/BM100029T/ASSET/IMAGES/MEDIUM/BM-2010-00029T_0001.GIF.

[170] Saeidlou S, Huneault MA, Li H, Sammut P, Park CB. Evidence of a dual network/spherulitic crystalline morphology in PLA stereocomplexes. Polymer (Guildf) 2012;53:5816–24. https://doi.org/10.1016/J.POLYMER.2012.10.030.

[171] Brochu S, Prud'homme RE, Barakat I, Jérôme R. Stereocomplexation and Morphology of Polylactides. Macromolecules 1995;28:5230–9. https://doi.org/10.1021/MA00119A010/ASSET/MA00119A010.FP.PNG_V03.

[172] Sun Y, He C. Synthesis and stereocomplex crystallization of poly(lactide)-graphene oxide nanocomposites. ACS Macro Lett 2012;1:709–13. https://doi.org/10.1021/MZ300131U/ASSET/IMAGES/MEDIUM/MZ-2012-00131U_0004.GIF.

[173] Schmidt SC, Hillmyer MA. Polylactide Stereocomplex Crystallites as Nucleating Agents for Isotactic Polylactide. J Polym Sci B: Polym Phys 2001;39:300–13. https://doi.org/10.1002/1099-0488.

[174] Petit C, Tulliani JM, Tadier S, Meille S, Chevalier J, Palmero P. Novel calcium phosphate/PCL graded samples: Design and development in view of biomedical applications. Materials Science and Engineering: C 2019;97:336–46. https://doi.org/10.1016/J.MSEC.2018.12.044.

[175] Ferri JM, Gisbert I, García-Sanoguera D, Reig MJ, Balart R. The effect of beta-tricalcium phosphate on mechanical and thermal performances of poly (lactic acid). J Compos Mater 2016;50:4189–98.

[176] Ferri JM, Jordá J, Montanes N, Fenollar O, Balart R. Manufacturing and characterization of poly (lactic acid) composites with hydroxyapatite. Journal of Thermoplastic Composite Materials 2018;31:865–81.

[177] Klimek K, Ginalska G. Proteins and Peptides as Important Modifiers of the Polymer Scaffolds for Tissue Engineering Applications-A Review. Polymers (Basel) 2020;12. https://doi.org/10.3390/POLYM12040844.

[178] Wang C, Liu Y, Fan Y, Li X. The use of bioactive peptides to modify materials for bone tissue repair. Regen Biomater 2017;4:191–206. https://doi.org/10.1093/RB/RBX011.

[179] Onak G, Şen M, Horzum N, Ercan UK, Yaralı ZB, Garipcan B, et al. Aspartic and Glutamic Acid Templated Peptides Conjugation on Plasma Modified Nanofibers for Osteogenic Differentiation of Human Mesenchymal Stem Cells: A Comparative Study. Scientific Reports 2018 8:1 2018;8:1–15. https://doi.org/10.1038/s41598-018-36109-5.

[180] Visser R, Rico-Llanos GA, Pulkkinen H, Becerra J. Peptides for bone tissue engineering. J Control Release 2016;244:122–35. https://doi.org/10.1016/J.JCONREL.2016.10.024.

[181] Hosoyama K, Lazurko C, Muñoz M, McTiernan CD, Alarcon EI. Peptide-Based Functional Biomaterials for Soft-Tissue Repair. Front Bioeng Biotechnol 2019;7:205. https://doi.org/10.3389/FBIOE.2019.00205.

[182] Karaman O, Kumar A, Moeinzadeh S, He X, Cui T, Jabbari E. Effect of surface modification of nanofibres with glutamic acid peptide on calcium phosphate nucleation and osteogenic differentiation of marrow stromal cells. J Tissue Eng Regen Med 2016;10:E132–46. https://doi.org/10.1002/TERM.1775.

[183] Erbetta CDC, Alves RJ, Resende JM, Freitas RF de S, Sousa RG de, Erbetta CDC, et al. Synthesis and Characterization of Poly(D,L-Lactide-co-Glycolide) Copolymer. J Biomater Nanobiotechnol 2012;3:208–25. https://doi.org/10.4236/JBNB.2012.32027.

[184] Mandracci P, Mussano F, Rivolo P, Carossa S. Surface Treatments and Functional Coatings for Biocompatibility Improvement and Bacterial Adhesion Reduction in Dental Implantology. Coatings 2016, Vol 6, Page 7 2016;6:7. https://doi.org/10.3390/COATINGS6010007.

[185] Kim HJ, Bae IS, Cho SJ, Boo JH, Lee BC, Heo J, et al. Synthesis and characteristics of NH2-functionalized polymer films to align and immobilize DNA molecules. Nanoscale Res Lett 2012;7:1–7. https://doi.org/10.1186/1556-276X-7-30/FIGURES/4.

[186] Marie PJ, Fromigué O. Osteogenic differentiation of human marrow-derived mesenchymal stem cells. Regenerative Med 2006;1:539–48. https://doi.org/10.2217/17460751.1.4.539.

[187] Onak G, Gökmen O, Yaralı ZB, Karaman O. Enhanced osteogenesis of human mesenchymal stem cells by self-assembled peptide hydrogel functionalized with glutamic acid templated peptides. J Tissue Eng Regen Med 2020;14:1236–49. https://doi.org/10.1002/TERM.3095.

[188] Siddiqa AJ, Maji S, Chaudhury K, Adhikari B. A facile route to develop hydrophilicity on the polyolefin surface for biomedical applications. Advances in Polymer Technology 2018;37:1410–9. https://doi.org/10.1002/ADV.21800.

[189] Onak G, Karaman O. Accelerated mineralization on nanofibers via non-thermal atmospheric plasma assisted glutamic acid templated peptide conjugation. Regen Biomater 2019;6:231–40. https://doi.org/10.1093/RB/RBZ014.

[190] Arnaout MA, Goodman SL, Xiong JP. Coming to grips with integrin binding to ligands: Opinion. Curr Opin Cell Biol 2002;14:641–52. https://doi.org/10.1016/S0955-0674(02)00371-X.

Curriculum Vitae

Metehan ATAGUR

EDUCATIONAL INFORMATION

Educational Period	Degree	University	Field of Education
2016-2023	PhD	Izmir Katip Celebi University	Materials Science and Engineering
2012- 2016	MSc	Dokuz Eylul University (DEU)	Metallurgical and Materials Engineering
2007-2012	Undergraduate	Anadolu University	Business Administration
2006-2011	Undergraduate	Dokuz Eylül University (DEU)	Metallurgical and Materials Engineering

Thesis Studies

Undergraduate Thesis: " Bachelor Thesis: Development of Coatings with High Oxidation Resistance for High Temperature Materials Dokuz Eylül University (DEU), Faculty of Engineering, 2011, Supervisor: Assoc.

Master's Thesis: "Production and Characterization of Polymer Matrix Composite Materials Using Different Structures of Clay Minerals and TPU (Thermoplastic Poiurethane)", DEU, Institute of Science, 2016, Supervisor: Assoc. Dr. Ugur MALAYOGLU

PhD Thesis: “Manufacturing and characterization of peptide coated polylactic acid based composites for various medical applications”, IKCU Institute of Science, 2023, Supervisor: Prof. Dr. M. Ozgur SEYDIBEYOGLU

RESEARCH AND PROJECTS WITH FINANCIAL SUPPORT

1. IKCU- "Central Research Laboratory Infrastructure Project", SPO project no 2014K120490, Researcher: Res. See. Metehan ATAGUR, Project Coordinator: Prof. Dr. Galip AKHAN, Project Start Date: 2014, Project Budget: 12.000.000 TL

2. "Artificial Bone Design for the Treatment of Orthopedic Bone Disorders" 2013-2-FMBP-42 İKCU BAP Project Assistant, Project Coordinator: Assist. Assoc. Dr. M. Özgür SEYDIBEYOGLU, Project Start Date: 01.09.2013, Project Budget: 61.620 TL

3. "Production of Electrically Conductive Biopolymer Nanocomposites and Investigation of Electrical, Mechanical and Viscoelastic Properties", 2013-2-FMBP-50 İKCU BAP Project Coordinator: Assist. Assoc. Dr. Kutlay SEVER, Project Start Date: 01.09.2013, Project Budget: 69.240 TL

4. "Production and Improvement of Properties of Vine stem and Pomace Wastes and Additive Polymer-Based Composites", TUBITAK 3001 Project No. 214M350, Scholar: Res. See. Metehan ATAGUR, Project Start Date: 15.01.2015, Project Budget: 60.000 TL

5. SANTEZ, "Hybrid Nanocomposite Flame Retardant Resin and Paint Production without Halogenated Compounds", Ministry of Industry

6. SANTEZ, "Development of Antimicrobial Washing Machine Detergent Drawer and Box", Ministry of Industry

7. BAP, "Production of Polypropylene Sutures with Antimicrobial Properties for Surgical Applications", IKCU

8. Production and Characterization of Carbon-Based Fillers and Thermal Conductive Polypropylene Composites", 2016-GAP-MUMF-0030, İKCU BAP Project Assistant, Project Coordinator: Assoc. Kutlay SEVER, Project Start Date: 17/08/2016, Project Budget: 39,985.48 TL

9. "Production of Mineral Additive Thermoplastic Composite Materials and Investigation of Their Properties", 2015-ÖDL-MUMF-0002, İKCU BAP Project

Assistant, Project Coordinator: Assoc. Kutlay SEVER, Project Start Date: 28/07/2015, Project Budget: 16,213 TL

10. Investigation of Flame-Retardant Properties of Nature-Friendly Additives in Different Paint Resins, 2016-ÖDL-MUMF-0007 İKCU BAP Project Assistant, Project Coordinator: Assist. Assoc. Dr. M. Ozgur SEYDIBEYOGLU, Project Start Date: 09.12.2016, Project Budget: 21,971.6 TL

11. Production of Hybrid Nanocomposite Flame Retardant Resin and Paint Without Halogenated Compounds, Ministry of Industry (SAN-TEZ) PROJECT, Researcher: ATAGUR METEHAN, Scholar: Sibel Demiroglu mustafov, Director: SEYDIBEYOGLU MEHMET ÖZGÜR, Researcher: Selmin Yanar Ocaktan, 2018.

PUBLICATIONS

Articles published in international peer-reviewed journals (in journals within the scope of SCI and SCI-E):

1. Seki, Y., Selli, F., Erdoğan, Ü. H., Atagür, M., & Seydibeyoğlu, M. Ö. (2022). A review on alternative raw materials for sustainable production: novel plant fibers. Cellulose, 1-42.
2. Atagur, M., Kaya, N., Uysalman, T., Durmuşkahya, C., Sarikanat, M., Sever, K., & Seki, Y. (2020). A detailed characterization of sandalwood-filled high-density polyethylene composites. Journal of Thermoplastic Composite Materials, 0892705720939157.
3. Atagur, M., Seki, Y., Oncu, O., Sever, K., Seki, Y., Sarikanat, M., & Altay, L. (2020). Evaluating of reinforcing effect of Ceratonia Siliqua for polypropylene: Tensile, flexural and other properties. Polymer Testing, 106607.
4. Atagur, M., Seki, Y., Pasaoglu, Y., Sever, K., Seki, Y., Sarikanat, M., & Altay, L. (2020). Mechanical and thermal properties of Carpinas betulus fiber filled polypropylene composites. Polymer Composites, 41(5), 1925-1935.
5. Altay, L., Atagur, M., Sever, K., Sen, I., Uysalman, T., Seki, Y., & Sarikanat, M. (2019). Synergistic effects of graphene nanoplatelets in thermally conductive synthetic graphite filled polypropylene composite. Polymer Composites, 40(1), 277-287.

6. Seki, Y., Avci, B., Uzun, S., Kaya, N., Atagur, M., Sever, K., & Sarikanat, M. (2019). The Using of Graphene Nano-Platelets for a Better through-Plane Thermal Conductivity for Polypropylene. Polymer Composites, 40(S2), E1320-E1328.
7. Atagur, M., Akyuz, O., Sever, K., Seki, Y., Seydibeyoglu, O., Isbilir, A., ... & Altay, L. (2019). Investigation of thermal and mechanical properties of synthetic graphite and recycled carbon fiber filled polypropylene composites. Materials Research Express, 6(6), 065312.
8. Altay, L., Bozaci, E., Atagur, M., Sever, K., Tantug, G. S., Sarikanat, M., & Seki, Y. (2019). The effect of atmospheric plasma treatment of recycled carbon fiber at different plasma powers on recycled carbon fiber and its polypropylene composites. Journal of Applied Polymer Science, 136(9), 47131.
9. Sarikanat, M., Seçgin, A., Uysalman, T., Tantug, G. S., Ozkaya, M., Atagur, M., ... & Seki, Y. (2019). The Effect of Various Minerals on Sound Transmission Loss and Mechanical Properties of Polypropylene. Acta Physica Polonica, A., 135(5).
10. Altay, L., Guven, A., Atagur, M., Uysalman, T., Tantug, G. S., Ozkaya, M., ... & Seki, Y. (2019). Linear Low-Density Polyethylene Filled with Almond Shells Particles: Mechanical and Thermal Properties. Acta Physica Polonica, A., 135(5).
11. Sever, K., Atagur, M., Tunçalp, M., Altay, L., Seki, Y., & Sarıkanat, M. (2019). The effect of pumice powder on mechanical and thermal properties of polypropylene. Journal of Thermoplastic Composite Materials, 32(8), 1092-1106.
12. Altay Lütfiye, Atagur Metehan, Akyüz Orhan, Seki Yoldaş, Sen Ibrahim, Sarikanat Mehmet, Sever Kutlay (2018). Manufacturing of Recycled Carbon Fiber Reinforced Polypropylene Composites by High Speed Thermo-Kinetic Mixing for Lightweight Applications. Polymer Composites, 39(10), 3656-3665., Doi: 10.1002/Pc.24394 (Publication No: 4629857)
13. Kaya Nusret, Atagur Metehan, Akyüz Orhan, Seki Yoldaş, Sarikanat Mehmet, Sütçü Mücahit, Seydibeyoğlu Mehmet Özgür, Sever Kutlay (2018). Fabrication And Characterization of Olive Pomace Filled PP Composites. Composites Part B-Engineering, 150, 277-283., Doi: 10.1016/J.Compositesb.2017.08.017 (Publication No: 4386003)
14. Sever Kutlay, Atagur Metehan, Altay Lütfiye, Seki Yoldaş, Uysalman Tuğçe, Sen Ibrahim, Kaya Nusret, Akın Güven, Sarikanat Mehmet (2018). Effect of Diatomite Weight Fraction On Morphology, Thermal And Physical Properties Of Diatomite

Filled High Density Polyethylene Composites. Acta Physica Polonica A, 134(1), 281-284., Doi: 10.12693/Aphyspola.134.281 (Publication No: 4630223)

15. Altay Lütfiye, Seki Yoldaş, Sever Kutlay, Sen Ibrahim, Uysalman Tuğçe, Atagur Metehan, Sarikanat Mehmet (2018). Thermal, Electrical, And Mechanical Properties of Various Thermal Conductive Powder Filled Polyamide 6 Composite Materials For Thermal Management Applications. Acta Physica Polonica A, 134(1), 200-203., Doi: 10.12693/Aphyspola.134.200 (Publication No: 4634040)
16. Altay Lütfiye, Seki Yoldaş, Sever Kutlay, Sen Ibrahim, Uysalman Tuğçe, Atagur Metehan, Seydibeyoğlu Mehmet Özgür, Sarikanat Mehmet (2018). Effect Of Compatibilizer On Morphology, Thermal And Mechanical Properties Of Recycled Carbon Fiber Reinforced Polypropylene Composites. Acta Physica Polonica A, 134(1), 196-199., Doi: 10.12693/Aphyspola.134.196 (Publication No: 4620872)
17. Seki Yasemin, Kilinç Ahmet Çağri, Dalmiş Ramazan, Atagur Metehan, Köktaş Serhan, Göktaş Ali Aydin, Çelik Erdal, Seydibeyoğlu Mehmet Özgür, Önay Ali Bülent (2018). Surface Modification Of New Cellulose Fiber Extracted From Conium Maculatum Plant: A Comparative Study. Cellulose, 25(6), 3267-3280., Doi: 10.1007/S10570-018-1797-0 (Publication No: 4635062)
18. Kilinç Ahmet Çağri, Köktaş Serhan, Seki Yasemin, Atagur Metehan, Dalmiş Ramazan, Erdoğan Ümit Halis, Göktaş Ali Aydin, Seydibeyoğlu Mehmet Özgür (2018). Extraction And Investigation Of Lightweight And Porous Natural Fiber From Conium Maculatum As A Potential Reinforcement For Composite Materials In Transportation. Composites Part B-Engineering, 140, 1-8., Doi: 10.1016/J.Compositesb.2017.11.059 (Publication No: 4634674)
19. Kilinç Ahmet Çağri, Köktaş Serhan, Atagur Metehan, Seydibeyoğlu Mehmet Özgür (2018). Effect Of Extraction Methods On The Properties Of althea Officinalis L./I Fibers/Title. Journal Of Natural Fibers, 15(3), 325-336., Doi: 10.1080/15440478.2017.1325813 (Publication No: 4266177)
20. Atagur Metehan, Sarikanat Mehmet, Uysalman Tuğçe, Polat Ozan, Elbeyli Yakar Iffet, Seki Yoldaş, Sever Kutlay (2018). Mechanical, Thermal, And Viscoelastic Investigations On Expanded Perlite–Filled High-Density Polyethylene Composite. Journal Of Elastomers Plastics, 50(8), 747-761., Doi: 10.1177/0095244318765045 (Publication No: 4256859)

21. Seydibeyoglu, M., Demiroglu, S., Atagur, M. and Ocaktan, S. (2017) Modification of Clay Crystal Structure with Different Alcohols. Natural Resources, 8, 709-715. doi: 10.4236/nr.2017.811044.
22. A.C. Kılınc, M. Atagur, O. Ozdemir, I. Sen, N. Kucukdogan, K. Sever, O. Seydibeyoglu, M. Sarikanat, Y. Seki, Manufacturing and characterization of vine stem reinforced high density polyethylene composites, Composites Part B: Engineering, Volume 91, 15 April 2016, Pages 267-274, ISSN 1359-8368, http://dx.doi.org/10.1016/j.compositesb.2016.01.033.

International books or chapters in books written:

1. Metehan Atagur and M. Özgür Seydibeyoglu, 11 - The use of biotechnology for green composites, In Woodhead Publishing Series in Composites Science and Engineering, Woodhead Publishing, 2017, Pages 237-250, Fiber Technology for Fiber-Reinforced Composites, ISBN 9780081018712, https://doi.org/10.1016/B978-0-08-101871-2.00011-4.

2. Metehan Atagur, Sibel Demiroglu and M. Özgür Seydibeyoglu, Chapter 17 - Flame Retardancy of Composites and Nanocomposites Based on PU Polymers, In Polyurethane Polymers, edited by Sabu Thomas, Janusz Datta, Józef T. Haponiuk and Arunima Reghunadhan, Elsevier, Amsterdam, 2017, Pages 499-524, ISBN 9780128040652, https://doi.org/10.1016/B978-0-12-804065-2.00017-6.

Articles published in national peer-reviewed journals:

1. Seydibeyoğlu Mehmet Özgür, Uysalman Tuğçe, Yakkan Ece, Atagur Metehan, Sever Kutlay (2018). The Influence of Coupling Agents on Mechanical Properties of Lignin-Filled Polypropylene Composites. Turkish Journal Of Forestry Türkiye Ormancılık Dergisi, 19(3), 308-316., Doi: 10.18182/Tjf.399787 (Publication No: 4629699)

2. Yakkan, E, Uysalman, T, Atagur M, Sever, K, Seydibeyoğlu, M. (2018). Nanocellulose-Polypropylene Nanocomposites Enhanced With Coupling Agent. Journal of Bartin Faculty of Forestry, 20 (3), 491-502. Retrieved from http://dergipark.gov.tr/barofd/issue/38873/455202

3. Lütfiye Altay, Metehan Atagur, Müslüm Erbektaş, Mehmet Sarıkanat (2019). Graphene Nanoplate Reinforced Ultra High Molecular Weight Polyethylene Based Nano-Composite Material Development and Characterization, Dokuz Eylul University Faculty of Engineering Science and Engineering Journal, Vol 21, No 62, Pg. 323-330.

Proceedings

International Research Proceedings

1. M. Atagur, U. Malayoglu, K. C. Tekin, S. Shrestha, "Electrochemical Behaviour Of Plasma Electrolytic Oxidized WE43 and E21 Magnesium Alloys" EUROCORR 2012 (The European Corrosion Congress) (2012).

2. Savaş Öztürk, Metehan Atagur, Tuncay Dikici, Serdar Yildirim, Mücahit Sütcü, Erdal Çelik, "Microstructure and Electrical Properties of Ce2O and TiO2 Doped ZnO Varistor Ceramics", PPM 2013, 3-6 September 2013.

3. Metehan Atagur, Savaş Öztürk, Tuncay Dikici, Serdar Yildirim, Mücahit Sütcü, Erdal Çelik, "Microstructure and Electrical Properties of Al2O3, Fe2O3 and Ce2O Doped ZnO Varistor Ceramics", PPM 2013, 3-6 September 2013.

4. Tuncay Dikici, Metehan Atagur, Savaş Öztürk, Serdar Yildirim, Mücahit Sütcü, Erdal Çelik, "Microstructure and Electrical Properties of CuO Doped ZnO Varistor Ceramics", PPM 2013, 3-6 September 2013.

5. Metehan Atagur, Tuğçe Uysalman, Hilal Kara, Ece Yakkan, M. Özgür Seydibeyoğlu, Uğur Malayoğlu, "Productıon And Characterızatıon Of TPU Nanocomposıtes Reınforced Wıth Clay Mınerals Whıch Have Dıfferent Mıcrostructures", IV th Internatıonal Polymerıc Composıtes Symposıum, Exhıbıtıon And Brokerage Event, 7-9 May 2015.

6. Tuğçe Uysalman, Ece Yakkan, Metehan Atagur, Hilal Kara, Altan Yıldırım, Burcu Girginer, M. Özgür Seydibeyoğlu, Kutlay Sever," The Effect Of Two Dıfferent Couplıng Agents On Thermal And Mechanıcal Properties Of Lıgnın Reınforced Polypropylene / Composıtes", IV th Internatıonal Polymerıc Composıtes Symposıum, Exhıbıtıon And Brokerage Event, 7-9 May 2015.

7. Ece Yakkan, Tuğçe Uysalman, Metehan Atagur, Hilal Kara, Altan Yıldırım, Burcu Girginer, M. Özgür Seydibeyoğlu, Kutlay Sever," Interfacıal Adhesıon And Mechanıcal Propertıes Of Nanocellulose–Polypropylene Composıtes Reınforced MAPP And Fusabond®E265", IV th Internatıonal Polymerıc Composıtes Symposıum, Exhıbıtıon And Brokerage Event, 7-9 May 2015.

8. Y. Seki, A. Ç. Kılıç, M. Atagur, O. Özdemir, İ. Şen, K. Sever, Ö. Seydibeyoğlu, M. Sarikanat, N. Küçükdoğan, "Evaluation of Vine Stem Waste as a Filler Material for High Density Polyethylene", ICCM 2015, International Conference on Composite Materials, 6-7 August 2015.

9. Kutlay Sever, Orhan Akyüz, Metehan ATAGUR, Nusret Kaya, Yoldaş Seki, Mehmet Sarıkanat, Investigation of Mechanical Properties of Diatomite Filled Polypropylene Composites, 6th International Conference on Materials Science and Technologies – RoMat 2016, Bükreş, ROMANIA.

10. Nusret Kaya, Metehan Atagur, Orhan Akyüz, Yoldaş Seki, Mehmet Sarikanat, Özgür Seydibeyoğlu, Mücahit Sütçü and Kutlay Sever, Viscoelastic and mechanical properties of olive pomace filled Polypropylene (PP) composites THERMAM 2016 - 3rd Thermophysical and Mechanical Properties of Advanced Materials 1-3 September 2016, IZMIR, TURKEY.

11. Nusret KAYA, Metehan ATAGUR, Orhan AKYÜZ, Mehmet SARIKANAT, Yoldaş SEKİ, Kutlay SEVER, Mechanıcal And Thermal Analysıs Of Dıfferent Ratıos of Vermıculıte-Pp Composıtes, 16th International Materials Symposium IMSP'2016 12-14 Oct 2016, Pamukkale University – Denizli - Turkey.

12. Ahmet Çağrı Kılınç, Serhan Köktaş, Metehan Atagur, Mehmet Özgür Seydibeyoğlu, Production and Characterization of Althea Officinalis L. Fiber Reinforced Polyester Composites, IMMC 2016| 18th International Metallurgy & Materials Congress, Istanbul- TURKEY.

13. ORAN Serhat, AKIN Ecem, TAŞDELEN M. Atilla, SEVER Kutlay, ATAGUR Metehan, SEYDİBEYOĞLU M. Özgür (2017). Preparation Of Recycled Pp/Reclaimed Epdm Composites Reinforcement Nut Cob As Filler. 5th International Polymeric Composites Symposium And Workshops, 317-319.

14. DEMİRCİ E. Afra, ATAGUR Metehan, KARAMAN Ozan (2017). Development of β-TCP Block Grafts withTunable Porosity and Mechanical Properties. Tıp Teknolojileri Kongresi TIPTEKNO2017 (Full Text Paper/Oral Presentation) (Publication No: 4045039).

15. DEMİRCİ E. Afra, ATAGUR Metehan, KARAMAN Ozan (2017). Development and Characterization of InjectableBone Substitutes. Tıp Teknolojileri Kongresi TIPTEKNO 2017 (Full Text Paper/Oral Presentation) (Publication No: 4041441).

16. ALTAY Lütfiye, BOZACI Ebru, ATAGUR Metehan, SEVER Kutlay, SEKİ Yoldaş, SEVİĞ Gözde, SARIKANAT Mehmet (2017). The Effect of Atmospheric Plasma Treatments on Mechanical Properties of Recycled Carbon Fiber Reinforced Polypropylene Composites. The 25th annual international conference on composites/nanoengineering (ICCE-25) (Summary Paper/Oral Presentation) (Publication No: 3787821).

17. SEVER Kutlay, ATAGUR Metehan, TUNÇALP Melike, SEKİ Yoldaş, ALTAY Lütfiye, SARIKANAT Mehmet (2017). Investigation of Mechanical and Thermal Properties of Pumice Powder Filled Polypropylene Composites. The 25th annual international conference on composites/nanoengineering (ICCE-25) (Summary Paper/Oral Presentation) (Publication No: 3787784).

18. SEKİ Yoldaş, AVCI Beliz, UZUN Seçil, KAYA Nusret, ATAGUR Metehan, SEVER Kutlay, ALTAY Lütfiye, SARIKANAT Mehmet (2017). The Effect of Modified Graphene on Thermal Properties of Polypropylene. The 25th annual international conference on composites/nanoengineering (ICCE-25) (Summary Paper/Oral Presentation) (Publication No: 3787912).

19. SEKİ Yasemin, DALMIŞ Ramazan, ATAGUR Metehan, KILINÇ A. Çağrı, KÖKTAŞ Serhan (2017). An alternative cellulose based natural fiber as a reinforcement material for polymeric composites. The 25th annual international conference on composites/nanoengineering ICCE-25 (Summary Paper/Oral Presentation) (Publication No:3976915).

20. SARIKANAT Mehmet, ALTAY Lütfiye, ATAGUR Metehan, AKYÜZ Orhan, SEKİ Yoldaş, AYCAN Yaşar, TOZOĞLU Haluk, SEVER Kutlay (2017). Utilization of agricultural waste fillers in polypropylene based composites. The 25th annual international conference on composites/nanoengineering (ICCE-25) (Summary Paper/Oral Presentation) (Publication No: 3787850).

21. ATAGUR Metehan, AKYÜZ Orhan, SEVER Kutlay, SEKİ Yoldaş, ALTAY Lütfiye, SEYDİBEYOĞLU M. Özgür, İŞBİLİR Akın, SARIKANAT Mehmet (2017). The Effect of Hybrid Carbon Fillers on Thermal and Mechanical Properties of PP Based Composites. The 25th annual international conference on composites/nanoengineering (ICCE-25) (Summary Paper/Oral Presentation) (Publication No: 3787870).

22. SEKİ Yasemin, KILINÇ A. Çağrı, DALMIŞ Ramazan, ATAGUR Metehan, KÖKTAŞ Serhan (2017). Kompozit Malzeme Üretiminde Destek Materyali Olarak Kullanılabilecek Yeni Selüloz Esaslı Conium Maculatum Liflerinin Karakterizasyonu ve Modifikasyonu. 2. Uluslararası Lif ve Polimer Araştırmaları Sempozyumu (Full Text Paper/Oral Presentation) (Publication No: 3879103).

23. ALTAY Lütfiye, ATAGUR Metehan, SEKİ Yoldaş, SEN İbrahim, SARIKANAT Mehmet, SEVER Kutlay (2017). Effect of Compatibilizer on Morphology, Thermal and Mechanical Properties of Recycled Carbon Fiber Reinforced Polypropylene Composites. 7th International Advances in Applied Physics and Materials Science Congress Exhibition (Summary Paper/Oral Presentation) (Publication No: 3787430).

24. ALTAY Lütfiye, ATAGUR Metehan, SEKİ Yoldaş, SEN İbrahim, SARIKANAT Mehmet, SEVER Kutlay, UYSALMAN Tuğçe, SEYDİBEYOĞLU M. ÖZGÜR (2017). Thermal, Electrical and Mechanical Properties of various Thermal Conductive Powder Filled Polyamide Composite Materials for Thermal Management Applications. 7th International Advances in Applied Physics and Materials Science Congress Exhibition (Summary Paper/Oral Presentation) (Publication No: 3787491)

25. ATAGUR Metehan, SEVER Kutlay, ALTAY Lütfiye, SEKİ Yoldaş, UYSALMAN Tuğçe, SEN İbrahim, GÜVEN Aysun, SARIKANAT Mehmet (2017). Effect of Diatomite Weight Fraction on Morphology, Thermal and Physical Properties of Diatomite Filled High Density Polyethylene Composites. 7th International

Advances in Applied Physics and Materials Science Congress Exhibition (Summary Paper/Poster) (Publication No: 3787660)

26. Atagur Metehan, Sever Kutlay, Altay Lütfiye, Seki Yoldaş,Seydibeyoğlu Mehmet Özgür, Sarikanat Mehmet (2018). Investigation On Mechanical, Viscoelastic, Andthermal Properties Of Ternary Carbon (Carbonfiber/Graphite/ Multiwalled Carbon Nanotubes) Filled Polypropylene Composites. Iv. International Ege Composite Materials Symposiumkompege 2018 (Summary Paper/Oral Presentation) (Publication No: 4444370)

27. Güven Aysun, Atagur Metehan, Altay Lütfiye, Seki Yoldaş, Uysalman Tugce, Seviğ Tantuğ Gözde, Sarikanat Mehmet, Sever Kutlay (2018). Polyethylene Filled With Almond Shells Particles: Mechanical And Thermal Properties. 8th International Advances In Applied Physics And Materials Science Congress Exhibition, 142-142. (Summary Paper/Oral Presentation) (Publication No: 4444338)

28. Sarikanat Mehmet, Seçgin Abdullah, Uysalman Tugce, Seviğ Tantuğ Gözde, Özkaya Melis, Atagur Metehan, Altay Lütfiye, Seki Yoldaş (2018). The Effect Of Various Minerals On Sound Absorption And Other Properties Of Polypropylene. 8th International Advances In Applied Physics And Materials Science Congress Exhibition, 145-145. (Summary Paper/Oral Presentation) (Publication No: 4444342)

29. Aysun GUVEN, Özay AKDEMIR, M. Turhan ÇOBAN, Metehan ATAGUR, Yoldaş SEKI, Kutlay SEVER, Lütfiye ALTAY, Mehmet SARIKANAT. Determination of Thermal Conductivity of Carbon Filled Polymeric Composite Plates for Compact Plate Heat Exchangers. 6th International Conference on Thermophysical and Mechanical Properties of Advanced Materials & 8th Rostocker Symposium on Thermophysical Properties for Technical Thermodynamics 22-24 September 2019.

National Research Proceedings

1. Tuğçe Uysalman, Metehan Atagur, Hilal Kara, Altan Yıldırım, M. Özgür Seydibeyoğlu, Kutlay Sever, Investigation The Effect Of Two Different Type Of Coupling Agents To Thermo mechanical Properties Of Lignin Reinforced Bio composites, KOMPEGE 2015, Uluslararası Katılımlı III. Ege Kompozit Malzemeler Sempozyumu, 05-07 KASIM 2015